Online ISSN : 2249-4626
Print ISSN : 0975-5896
DOI : 10.17406/GJSFR

Global Journal

of Science Frontier Research: A

Physics and Space Science

The Physics of Hadrons

Electroform Generator Mende

Highlights

Unification of Gravitational

Disordered Semiconductor Structures

Discovering Thoughts, Inventing Future

VOLUME 20 ISSUE 13 VERSION 1.0

Global Journal of Science Frontier Research: A
Physics & Space Science

Global Journal of Science Frontier Research: A
Physics & Space Science

Volume 20 Issue 13 (Ver. 1.0)

Open Association of Research Society

Incorporation No.: 0423089
License No.: 42125/022010/1186
Registration No.: 430374
Import-Export Code: 1109007027
Employer Identification Number (EIN):
USA Tax ID: 98-0673427

Global Journals Inc.

*(A Delaware USA Incorporation with "Good Standing"; **Reg. Number: 0423089**)*
Sponsors: Open Association of Research Society
Open Scientific Standards

Publisher's Headquarters office

Global Journals® Headquarters
945th Concord Streets,
Framingham Massachusetts Pin: 01701,
United States of America
USA Toll Free: +001-888-839-7392
USA Toll Free Fax: +001-888-839-7392

Offset Typesetting

Global Journals Incorporated
2nd, Lansdowne, Lansdowne Rd., Croydon-Surrey,
Pin: CR9 2ER, United Kingdom

Packaging & Continental Dispatching

Global Journals Pvt Ltd
E-3130 Sudama Nagar, Near Gopur Square,
Indore, M.P., Pin:452009, India

Find a correspondence nodal officer near you

To find nodal officer of your country, please email us at *local@globaljournals.org*

eContacts

Press Inquiries: *press@globaljournals.org*
Investor Inquiries: *investors@globaljournals.org*
Technical Support: *technology@globaljournals.org*
Media & Releases: *media@globaljournals.org*

Pricing (Excluding Air Parcel Charges):

Yearly Subscription (Personal & Institutional)
250 USD (B/W) & 350 USD (Color)

Editorial Board

Global Journal of Science Frontier Research

Contents of the Issue

Global Journal of Science Frontier Research: a
Physics and Space Science
Volume 20 Issue 13 Version 1.0 Year 2020
Type : Double Blind Peer Reviewed International Research Journal
Publisher: Global Journals
Online ISSN: 2249-4626 & Print ISSN: 0975-5896

Ether Dynamics and Unification of Gravitational and Electromagnetic Forces

By Ling Jun Wang
University of Tennessee at Chattanooga

Abstract- Recently we have presented a theory of unification of gravitational and electromagnetic fields based on the generalization of Newton's law to include a dynamic term similar to the Lorentz force of electrodynamics[1]. The unification is convincing. The generalization based on similarity of Newton's law and Coulomb's law, however, is speculative although reasonable and compelling. In this article, we have presented a derivation of the dynamic term of gravitation based on our newly proposed ether dynamics, which removes the speculative nature of dynamic term and perfects the unification theory. It turns out that the gravitational interaction is transmitted through the space medium ether. An object in ether is in direct contact with the ether, causing it to move like a highly viscous and incompressible fluid. The movement of ether propagates thorough space like a continuous medium, exerting a force on any object in ether.

Keywords: unification of gravitational and electromagnetic forces, ether dynamics, gravitation, biot-savart law, lorentz force.

GJSFR-A Classification: FOR Code: 260203

Strictly as per the compliance and regulations of:

Ether Dynamics and Unification of Gravitational and Electromagnetic Forces

Ling Jun Wang

Abstract- Recently we have presented a theory of unification of gravitational and electromagnetic fields based on the generalization of Newton's law to include a dynamic term similar to the Lorentz force of electrodynamics[1]. The unification is convincing. The generalization based on similarity of Newton's law and Coulomb's law, however, is speculative although reasonable and compelling. In this article, we have presented a derivation of the dynamic term of gravitation based on our newly proposed ether dynamics, which removes the speculative nature of dynamic term and perfects the unification theory. It turns out that the gravitational interaction is transmitted through the space medium ether. An object in ether is in direct contact with the ether, causing it to move like a highly viscous and incompressible fluid. The movement of ether propagates thorough space like a continuous medium, exerting a force on any object in ether.

Not only neutral objects can disturb the fluid ether, the charged objects can also disturb the ether as well. Applying the fluid dynamics of ether on charged particles, we have derived the empirical Biot-Savart law and Lorentz force of electrodynamics. The significance of theoretic derivation of these empirical and fundamental laws is similar to the derivation of the empirical Kepler's laws by Newton's theory of gravitation. It turns out that a moving charged particle would disturb the fluid ether. The disturbance spreads into the space as a continuous medium, causing local vorticity. The magnetic field is linearly proportional to the local vorticity of ether, exerting a force on another moving particle in space. The vorticity of ether is responsible for the dynamic gravitation and Lorentz force of electrodynamics.

The Ether Dynamics consummates our theory of unification of gravitational and electromagnetic forces.

Keywords: unification of gravitational and electromagnetic forces, ether dynamics, gravitation, biot-savart law, lorentz force.

I. Introduction

Recently, we have developed a unification theory of gravitational and electromagnetic fields based on generalization of Newton's Law of gravitation to include a dynamic term similar to the Lorentz force of electromagnetism:[1,2]

$$\mathbf{F}_2 = -G\frac{mm'}{r^2}\frac{1}{c^2}\mathbf{v}'\times\left(\mathbf{v}\times\hat{r}\right) \qquad (1)$$

where v and v' are the velocities of the masses m and m', r the distance between the two masses, $\hat{r}$ the unit vector from mass m to mass m', G the gravitational constant and c the speed of light. Without a dynamic term, there is no way one can explain the propagation of gravitational interaction, and the spooky action-at-distance is inevitable. The fact that Eq(1) alone is sufficient to yield a complete theory of field equations and the gravitational wave equation lends us confidence in such generalization. However, a generalization based on mathematical similarity between Newton's law of gravitation and Coulomb's law of electrostatics is speculative without theoretical foundation of physics. In this article, we will provide a theoretical derivation of the dynamic term, Eq(1), based on the fluid dynamics of ether. It turns out that the space medium ether is a highly viscous incompressible fluid. An object, be it neutral or charged, will disturb the fluid ether in contact with it, causing fluid-dynamic movement. The dynamic movement of ether then propagates into the space, exerting a force on objects is space near and far. We will produce the mathematic details of such fluid-dynamic movements, and derive the empirical Biot-Savart law and Lorentz force that govern both gravitational and electromagnetic interactions.

Before starting the mathematics, we must first justify the concept of ether. Physicists believed that the electromagnetic waves were propagating through a medium ether before Einstein proposed his theory of relativity in 1905.It was unimaginable that any interaction could propagate without a medium. Einstein believed that the propagation of a electromagnetic wave was realized through field instead of ether. Physics community was then lead to believed that the field is matter. However, Einstein never disproved, scientifically or philosophically, the existence of a universal medium ether. His believing of field as matter was merely a subjective opinion. It is now a common knowledge that the space is filled with interstellar and intergalactic materials. The cosmic microwave background is the experimental evidence of the existence of the interstellar and intergalactic materials. The author would like to distant himself from the concept of omnipresent dark matter or dark energy. Our point is simply that space is filled with an interstellar and intergalactic material that is historically called ether.

We do challenge the concept that the field is matter. What is field? The gravitational field is the force felt by unit mass, which is acceleration. To say that field is matter is to say that acceleration is matter, which is absurd. There are many other fields, such as velocity

Author: University of Tennessee at Chattanooga, 615 McCallie Av., Chattanooga, TN 37403. e-mail: Lingjun-wang@utc.edu

field or temperature field. If field is matter, then the velocity and the temperature would also be matter. Moreover, if field is matter, are the gravitational field and the electromagnetic field the same matter or different matters?

A mistake the early physicists made is to assume that ether was an absolutely static medium at rest, without regarding the possibility of ether being a fluid capable of local movement. The concept of an absolutely static ether run into a conflict with the null result of the famous Michelson-Morley's ether drift experiment. Wang [3] has pointed out that if the local ether is rotating with the solar system, the null result of both the first order ether drift experiment of Wang and the second order ether drift experiment of Michelson-Morley are naturally explained.

In this article, we will assume ether to be a highly viscous incompressible fluid, and derive the dynamic gravitation, the Biot-Savart Law and the Lorentz force based on fluid dynamics of ether.

II. Viscous Incompressible Fluid Moving around a Solid Sphere

The equation of motion of a fluid is described by the Navier-Stokes equation [4]. For an incompressible fluid, the continuity equation is:

$$\nabla \cdot \mathbf{v} = \mathbf{0} \tag{2}$$

where $\mathbf{v}$ is the velocity. The Navier-Stokes equation for incompressible fluid reduces to [4]

$$\frac{\partial \mathbf{v}}{\partial t} + (\mathbf{v} \cdot \nabla)\mathbf{v} = \mathbf{X} - \frac{\nabla p}{\rho} + \frac{\mu}{\rho}\nabla^2 \mathbf{v} \tag{3}$$

where ρ is the mass density, μ the viscosity coefficient, p the pressure, and $\mathbf{X}$ the external body force per unit mass. For fluids of high viscosity or flowing at very slow speeds (Reynolds number $<< 1$) the inertia-force terms on the left-hand side of Eq(3) can be neglected in comparison with the friction-force terms. The body force $\mathbf{X}$ external to the ether is non-existent. Eq(3) then reduces to [4]

$$\nabla p = \mu \nabla^2 \mathbf{v} \tag{4}$$

Taking divergence of both sides of Eq(4), we have

$$\nabla^2 p = \mu \nabla \cdot (\nabla^2 \mathbf{v}) = \mu \nabla^2 (\nabla \cdot \mathbf{v}) = 0 \tag{5}$$

Eq(2) is applied in the last step in yielding Eq(5). Eq(5) indicates that the pressure p satisfies the Laplace equation, hence, for a very slow motion the pressure is a harmonic function.

Equations (2), (4) and (5) can be applied to the problem of a steady uniform flow around a sphere at rest. This problem was first solved by Stokes and is often referred to as Stokes' Law [4,5]. Referring to Fig.1, the origin is chosen at the center of the sphere, the z axis in the direction opposite to a uniform flow velocity U far away from the sphere. At the spherical surface $r=R$, the velocity of the fluid must be zero due to high viscosity:

$$v_x = v_y = v_z = 0 \quad (r = R) \tag{6}$$

$$v_z = -V\,,\ v_x = v_y = 0\,,\ p = p_0\ (r \to \infty) \tag{7}$$

where R is the radius of the sphere. V and p_o are the velocity and the pressure far away from the sphere.

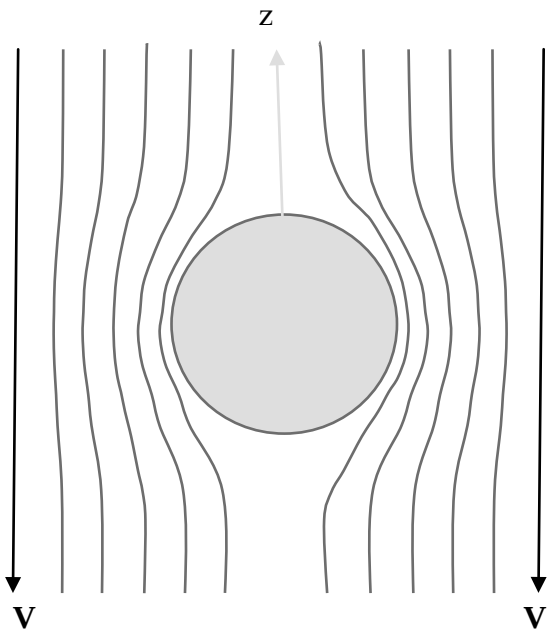

Figure 1: A fluid moving with a uniform velocity V opposite the z-axis against a solid sphere

The solution to Eq(5) is the first order spherical harmonics (Legendre polynomial):

$$p = p_0 - \frac{A\cos\theta}{r^2} = p_0 - \frac{Az}{r^3} \tag{8}$$

Substituting Eq (8) into Eq (4), we obtain

$$\begin{cases} \nabla^2 v_x = \dfrac{A}{\mu}\dfrac{3zx}{r^5} \\ \nabla^2 v_y = \dfrac{A}{\mu}\dfrac{3zy}{r^5} \\ \nabla^2 v_z = \dfrac{A}{\mu}\left(\dfrac{3z^2}{r^5} - \dfrac{1}{r^3}\right) \end{cases} \tag{9}$$

The solution to Eq (9) is [4-6]:

$$\begin{cases} v_x = -V\left[\frac{3}{4}\frac{Rzx}{r^3}\left(\frac{R^2}{r^2}-1\right)\right] \\ v_y = -V\left[\frac{3}{4}\frac{Rzy}{r^3}\left(\frac{R^2}{r^2}-1\right)\right] \\ v_z = -V\left[\frac{3}{4}\frac{Rz^2}{r^3}\left(\frac{R^2}{r^2}-1\right)+1-\frac{3}{4}\frac{R}{r}-\frac{1}{4}\frac{R^3}{r^3}\right] \end{cases} \quad (10)$$

The pressure is

$$p = p_o + \frac{3}{2}\mu VR\frac{z}{r^3} \quad (11)$$

It can be readily verified that the velocity components in Eq(10) satisfy Eq(9) and the boundary condition Eqs(6) and (7). Translating Eq(10) into the spherical coordinate system, the velocity components are:

$$\begin{cases} v_r = -V\cos\theta\left(1-\frac{3}{2}\frac{R}{r}+\frac{1}{2}\frac{R^3}{r^3}\right) \\ v_\theta = V\sin\theta\left(1-\frac{3}{4}\frac{R}{r}-\frac{1}{4}\frac{R^3}{r^3}\right) \\ v_\varphi = 0 \end{cases} \quad (12)$$

III. A Solid Sphere Moving in Viscous Uncompressible Fluid

Eq(12) gives the velocity of a fluid moving against a solid sphere at rest with the velocity V in the direction of negative *z*-axis. If a velocity of $\mathbf{V}_0 = \mathbf{0}V\hat{\mathbf{k}} = V\cos\theta\hat{\mathbf{r}} - V\sin\theta\hat{}$ is added to Eq(12), as shown in Fig.(2), it gives the velocities of a fluid ether at rest disturbed by a solid sphere moving with of a velocity of $\mathbf{v} = V\hat{\mathbf{k}}$ in the positive *z*-direction:

$$\begin{cases} v_r = V\cos\theta\left(\frac{3}{2}\frac{R}{r}-\frac{1}{2}\frac{R^3}{r^3}\right) \\ v_\theta = -V\sin\theta\left(\frac{3}{4}\frac{R}{r}+\frac{1}{4}\frac{R^3}{r^3}\right) \\ v_\varphi = 0 \end{cases} \quad (13)$$

The radius *R* in Eq (14) should be understood as the *effective radius* to be determined later. It may or may not be equal to the actual radius of the sphere. We do not know if a "solid" would remain "solid" with respect to the fluid ether. A solid to the air might well be "porous" with respect to ether. As a matter of fact, the solutionsEq(10) and (13) are obtained for the field satisfying condition Eq(6). The radius *R* is the radius of a sphere on the surface of which the velocity is zero. This sphere may or may not have the same radius of the particle.

The stream function ψ can be calculated according to reference[4]:

$$\begin{cases} v_r = \frac{1}{r^2\sin\theta}\frac{\partial\psi}{\partial\theta} \\ v_\theta = -\frac{1}{r\sin\theta}\frac{\partial\psi}{\partial r} \end{cases} \quad (14)$$

Integrating the second equation of Eq(14) yields

$$\psi = -\int v_\theta r\sin\theta dr = \frac{V\sin^2\theta}{4}\left(3Rr-\frac{R^3}{r}\right)+f(\theta) \quad (15)$$

Taking partial differentiation of Eq(15) with respect to θ, we obtain

$$\frac{\partial\psi}{\partial\theta} = \frac{V\sin\theta\cos\theta}{2}\left(3Rr-\frac{R^3}{r}\right)+\frac{df}{d\theta}$$

$$v_r = \frac{1}{r^2\sin\theta}\left[\frac{V\sin\theta\cos\theta}{2}\left(3Rr-\frac{R^3}{r}\right)+\frac{df}{d\theta}\right]$$

$$v_r = V\cos\theta\left(\frac{3R}{2r}-\frac{R^3}{2r^3}\right)+\frac{1}{r^2\sin\theta}\left[\frac{df}{d\theta}\right] \quad (16)$$

Comparing Eq(16) to the first equation of Eq(13), we have $\frac{df}{d\theta}=0$, *f* is a constant. We conveniently choose *f* = 0, and obtain:

$$v_r = V\cos\theta\left(\frac{3R}{2r}-\frac{R^3}{2r^3}\right) \quad (17)$$

Figure 2 shows a plot of the stream lines of the ether disturbed by a sphere moving with velocity v.

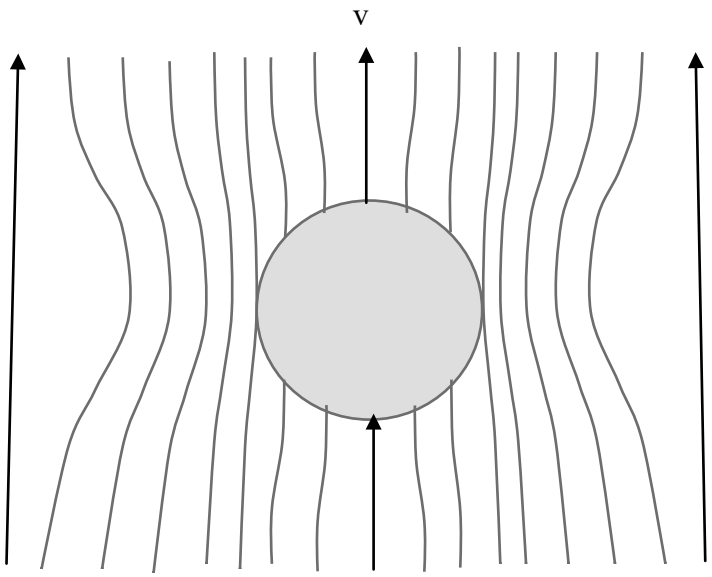

Figure 2: The stream lines of ether disturbed by a solid sphere moving with velocity v

Now let us consider the situations when $R \ll r$. Such would be the case either the radius *R* is very small for the electrical charges, or the distance *r* is very great for the astronomical movements of heavenly bodies. Under such condition, the last term in Eq(13) is negligibly small and can be dropped. We then have

$$\begin{cases} v_r = \dfrac{3}{2}\dfrac{R}{r}V\cos\theta \\ v_\theta = -\dfrac{3}{4}\dfrac{R}{r}V\sin\theta \\ v_\varphi = 0 \end{cases} \tag{18}$$

IV. Vorticity and Dynamic Field

The vorticity Ω can be easily calculated [4]:

$$\Omega = \nabla \times \mathbf{v}$$

$$= \frac{1}{r\sin\theta}\left(\frac{\partial\left(v_\varphi \sin\theta\right)}{\partial\theta} - \frac{\partial v_\theta}{\partial\varphi}\right)\hat{r} + \frac{1}{r}\left(\frac{1}{\sin\theta}\frac{\partial v_r}{\partial\varphi} - \frac{\partial\left(rv_\varphi\right)}{\partial r}\right)\hat{\theta} + \frac{1}{r}\left(\frac{\partial\left(rv_\theta\right)}{\partial r} - \frac{\partial v_r}{\partial\theta}\right)\hat{\varphi} \tag{19}$$

$$\boldsymbol{\Omega} = \frac{3}{2}\frac{RV}{r^2}\sin\theta\hat{\varphi} = \frac{3}{2}\frac{R}{r^2}\mathbf{v}\times\hat{r} \tag{20}$$

The vorticity Ω causes the local fluid to rotate. The angular velocity is related to the vorticity. Referring to Fig. 3,suppose a fluid is rotating with angular velocity ω, the linear velocity v at the radius *r* is

$$v = r\omega \tag{21}$$

The vorticity Ω is

$$\Omega = \left|\nabla\times\mathbf{v}\right| = \lim_{r\to 0}\frac{\left|\oint\mathbf{v}\cdot\mathbf{dl}\right|}{\pi r^2} = \lim_{r\to 0}\frac{v2\pi r}{\pi r^2} = 2\omega \tag{22}$$

Using Eq(20),

$$\boldsymbol{\omega} = \frac{\boldsymbol{\Omega}}{2} = \frac{3}{4}\frac{RV}{r^2}\sin\theta\hat{\varphi} = \frac{3}{4}\frac{R}{r^2}\mathbf{v}\times\hat{r} \tag{23}$$

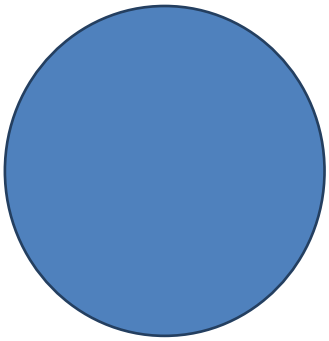

Figure 3: Relationship between vorticity and angular velocity

V. The Force of Ether on a Moving Body

Referring to Fig.4, if a mass *m'* is moving with velocity v' in a rotating fluid with angular velocity ω, its velocity would change due to rotation. The component of v' parallel to ω will not change. The component of v' perpendicular to ω will change. Suppose the angle between ω and v' is θ, the change in velocity (the acceleration a) caused by the rotation is

$$a = \frac{d}{dt}\left(\alpha\theta v' \sin\theta\right) = \alpha\omega v' \sin\theta \qquad (24)$$

where α is the *dragging coefficient* dependent on the friction between the ether and the moving object with which the ether is dragging the object:

$$0 < \alpha \le 1 \qquad (25)$$

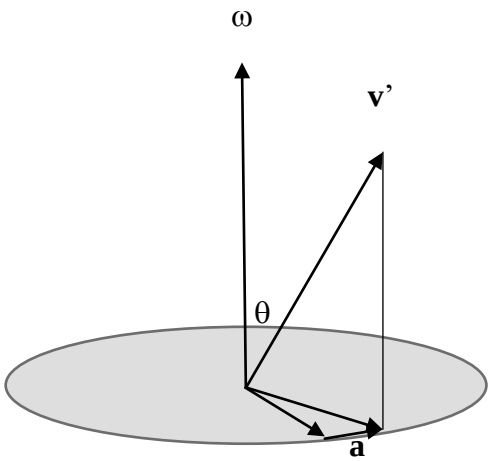

Figure 4: Acceleration of a moving object due to local rotation of fluid

In vector form

$$\mathbf{a} = \frac{d\mathbf{v}'}{dt} = \alpha\boldsymbol{\omega} \times \mathbf{v}' \qquad (26)$$

The force exerted on the mass *m'* is

$$\mathbf{F} = m'\mathbf{a} = m'\alpha\boldsymbol{\omega} \times \mathbf{v}' = -\frac{3\alpha R m'}{4r^2}\mathbf{v}' \times \left(\mathbf{v} \times \hat{r}\right) \qquad (27)$$

This is exactly the dynamic gravitational force given by Wang [1,2]:

$$\mathbf{F} = -\frac{Gmm'}{c^2 r^2}\mathbf{v}' \times \left(\mathbf{v} \times \hat{\mathbf{r}}\right) \qquad (28)$$

Comparing Eqs(27) and (28) gives

$$\alpha \cdot R = \frac{4Gm}{3c^2} \qquad (29)$$

The product of the two constants α and *R* are determined by *G* and *m*. However, we could not naively assume that the effective radius *R* is radius of mass *m* only. Qualitatively, we can see that both α and *R* could be dependent on the mass as well as the nature of the interaction.

The dynamic field (or, rotational field) h given by Wang [2] is:

$$\mathbf{h} = -\frac{Gm}{cr^2}\mathbf{v} \times \hat{\mathbf{r}} \qquad (30)$$

Comparing to Eq(23) and (29), we have

$$\mathbf{h} = -c\alpha\boldsymbol{\omega} = -\frac{c\alpha}{2}\boldsymbol{\Omega} \qquad (31)$$

Eq(31) says that the dynamic field h is essentially the measure of the local vorticity of the ether.

VI. The Origin of Lorentz Force and Biot-Savart Law

If a charged particle is moving in ether, it will disturb the ether in the same way that a mass does, because any charged particle has a mass and volume. The only difference is that the effective radius is going to be different, and the local angular velocity $\boldsymbol{\Omega}_{em}$ is given by:

$$\boldsymbol{\Omega}_{em} = \frac{3}{2}\frac{R_{em}V}{r^2}\sin\theta\hat{\varphi} = \frac{3}{2}\frac{R_{em}}{r^2}\mathbf{v} \times \hat{r} = 2\boldsymbol{\omega}_{em} \qquad (32)$$

where R_{em} is the *electromagnetic effective radius* of the charged particle. The change in velocity (the acceleration a_{em}) of a moving charge *q'* caused by the local rotation of ether is

$$a_{em} = \frac{d}{dt}\left(\alpha_{em}\theta v'\sin\theta\right) = \alpha_{em}\omega_{em}v'\sin\theta \tag{33}$$

The force exerted on the charge *q'* is

$$\mathbf{F}_{em} = m'\mathbf{a}_{em} = m'\alpha_{em}\boldsymbol{\omega}_{em}\times\mathbf{v}' = -\frac{3\alpha_{em}R_{em}m'}{4r^2}\mathbf{v}'\times\left(\mathbf{v}\times\hat{r}\right) \tag{34}$$

Comparing Eq(34) to the Lorentz force of electrodynamics:

$$\mathbf{F}_{em} = q'\mathbf{v}\times\mathbf{B} = \frac{k_1 q'q}{c^2r^2}\mathbf{v}'\times\left(\mathbf{v}\times\hat{r}\right) \tag{35}$$

We have

$$\alpha_{em}\cdot R_{em} = -\frac{4k_1 q}{3c^2}\frac{q'}{m'} \tag{36}$$

Comparing Eqs (29) and (36), we notice two differences: 1) There is a negative sign in Eq(36), which reflects the fact that the same mass attract while the same charge repel. 2) In Eq(36) there is a factor of specific charge (*q'/m'*), simply because Newton's second law describes the linear relation between the force and the mass, not the force and the charge. But the essence of Eq(36) basically says that the product of the *dragging coefficient* and the *effective radius* $\left(\alpha_{em}\cdot R_{em}\right)$ is determined by the source *q* and the nature of electromagnetic interaction represented by the Coulomb constant k_1 and the specific charge (*q'/m'*).

The Biot-Savart law of electrodynamics is

$$\mathbf{B} = \frac{k_1 q}{c^2r^2}\mathbf{v}\times\hat{r} \tag{37}$$

Comparing Eq(37) with Eq(32), using Eq(36), we have

$$\mathbf{B} = \frac{\alpha_{em}}{2}\frac{m'}{q'}\boldsymbol{\Omega}_{em} \tag{38}$$

Eq(38) states that the magnetic field is a measure of the local ether vorticity, just like the dynamic gravitational field is as expressed in Eq(31).

VII. Dynamic Gravitation

Eqs.(1) and (28) obtained above is the dynamic gravitational force that should be added to the static gravitational force in Newton's law, giving a complete description of gravitation:

$$\mathbf{F} = -G\frac{mm'}{r^2}\left[\hat{r} + \frac{1}{c^2}\mathbf{v}'\times\left(\mathbf{v}\times\hat{r}\right)\right] \tag{39}$$

where v and v' are the velocities of the masses *m* and *m'*, respectively. The constant *c* is the speed of gravitational wave. It must be noted that the theoretical development does not depend on the particular value of the speed of gravitational wave. Later on we will show that Eq(39) alone is sufficient to yield a complete theory of gravitational wave propagation, which further justifies and strengthens our confidence in the dynamic theory of gravitation.

The first term of the gravitational force is static:

$$\mathbf{F}_1 = -G\frac{mm'}{r^2}\hat{r} \tag{40}$$

We can define a static field:

$$\mathbf{g} = \frac{\mathbf{F}_1}{m'} = -G\frac{m}{r^2}\hat{r} \tag{41}$$

The second term can be written as

$$\mathbf{F}_2 = -G\frac{mm'}{r^2}\frac{1}{c^2}\mathbf{v}'\times\left(\mathbf{v}\times\hat{r}\right) = -G\frac{mm'}{r^2}\left[\left(\boldsymbol{\beta}'\cdot\hat{r}\right)\boldsymbol{\beta} - \left(\boldsymbol{\beta}'\cdot\boldsymbol{\beta}\right)\hat{r}\right] = \mathbf{M}\cdot m'\boldsymbol{\beta}' \tag{42}$$

where β and β' are the ratios of velocities over the speed *c* of gravitational wave in vacuum, The tensor M is a second rank anti symmetric tensor constructed by the usual rule of dyadic of two vectors:

$$\mathbf{M} = \frac{Gm}{cr^3}\left(\vec{r}\mathbf{v} - \mathbf{v}\vec{r}\right) = \frac{Gm}{cr^3}\begin{pmatrix} 0 & v_y x - v_x y & v_z x - v_x z \\ v_x y - v_y x & 0 & v_z y - v_y z \\ v_x z - v_z x & v_y z - v_z y & 0 \end{pmatrix} \tag{43}$$

Since the angular momentum

$$\mathbf{L} = \mathbf{r}\times\mathbf{p} = m\mathbf{r}\times\mathbf{v} \tag{44}$$

We have

$$\mathbf{M} = \frac{G}{cr^3}\begin{pmatrix} 0 & L_z & -L_y \\ -L_z & 0 & L_x \\ L_y & -L_x & 0 \end{pmatrix} \tag{45}$$

Define a vector h:

$$\mathbf{h} = \frac{G}{cr^3}\mathbf{L} = \frac{Gm}{cr^2}\hat{r}\times\mathbf{v} = -\mathbf{g}\times\boldsymbol{\beta} \qquad (46)$$

We have

$$\mathbf{M} = \begin{pmatrix} 0 & h_z & -h_y \\ -h_z & 0 & h_x \\ h_y & -h_x & 0 \end{pmatrix} \qquad (47)$$

Since L is proportional to *r*, Eqs (46) and (47) manifest inverse square law of h and M. We will call h the *rotational field*, and M the *dynamic field tensor*.

The physical meaning of the vector h can be appreciated if we recall the magnetic field B in *Biot-Savart* law:

$$\mathbf{B} = \frac{\mu_0 q}{4\pi r^2}\mathbf{v}\times\hat{r} = \frac{k_1 q}{c^2 r^2}\mathbf{v}\times\hat{r} \qquad (48)$$

There are two differences between the magnetic field B and the gravitational rotational field h:1) There is a difference of a factor of *c* due to the definition of M in Eq (43); 2) There is a difference of a negative sign due to the fact that the gravitational force between two masses is attractive while the electric force between two charges of the same sign is repulsive. The advantage of our definition of h is that M and h have the same dimension as that of the static field g.

It must be noted that the sign in the definition of h and B is arbitrary. Either sign can be adopted in the definition without affecting the force that acts on the mass *m'* or the charge *q'*. The essential framework of electromagnetic and the gravitational theory would remain intact. The direction of the force is physical and uniquely determined no matter what sign is adopted in the definition of h and B. The arbitrariness simply manifests that h and B are merely intermediate quantities that provide convenience in mathematical presentation. Historically, the magnetic field B was defined according to the conventional right-hand rule. It was used by engineers and scientists for centuries. We will stick with this convention.

The gravitational force can be expressed as

$$\mathbf{F} = m'\left[\mathbf{g} + \mathbf{M}\cdot\boldsymbol{\beta}'\right] = m'\left[\mathbf{g} + \boldsymbol{\beta}'\times\mathbf{h}\right] \qquad (49)$$

The total gravitational field f is defined as the total gravitational force per unit mass

$$\mathbf{f} = \mathbf{g} + \mathbf{M}\cdot\boldsymbol{\beta}' = \mathbf{g} + \boldsymbol{\beta}'\times\mathbf{h} \qquad (50)$$

VIII. Field Equations and Wang's Law

It is amazing that with the dynamic term included in the force law of gravitation we can develop a whole dynamic theory without any additional hypothesis. Let us derive the field equations from the complete force law.

a) Gauss' Law and Wang's Law

Consider the closed surface integral of the static field g over a spherical surface *s* with radius *r*:

$$\iint_s \mathbf{g}\,d\boldsymbol{\sigma} = -\iint_s \frac{Gm}{r^2}\hat{r}\,d\boldsymbol{\sigma} = -\iint_s Gm\,d\Omega = -4\pi Gm \qquad (51)$$

This is the Gauss' law of the static field. If we allow the radius of the spherical surface approaching zero, we obtain the differential form of Gauss' Law:

$$\nabla\cdot\mathbf{g} = -4\pi G\rho \qquad (52)$$

where

$$\rho = \frac{dm}{dV} \qquad (53)$$

is the local mass density. *V* is the volume.

The similar closed surface integral of the dynamic field tensor M is

$$\iint_s \mathbf{M}\cdot d\boldsymbol{\sigma} = \iint_s \mathbf{M}\cdot\hat{r}\,d\sigma \qquad (54)$$

From Eq (43) we have

$$\iint_s \mathbf{M}\boldsymbol{\sigma}\,d = \frac{Gm}{c}\iint \frac{1}{r^2}\begin{bmatrix} v_y xy + v_z xz - v_x y^2 - v_x z^2 \\ v_x xy + v_z yz - v_y x^2 - v_y z^2 \\ v_x xz + v_y yz - v_z y^2 - v_z x^2 \end{bmatrix} d\Omega \qquad (55)$$

where Ω is the solid angle. Note that the velocity of the mass is constant with respect to the integration. The integration (55) involves integrals like

$$\iint \frac{x^2}{r^2}d\Omega = \iint \left(\sin^3\theta\cos^2\varphi\right)d\theta d\varphi = \frac{4\pi}{3} \qquad (56)$$

$$\iint \frac{y^2}{r^2}d\Omega = \iint \left(\sin^3\theta\sin^2\varphi\right)d\theta d\varphi = \frac{4\pi}{3}$$

$$\iint \frac{z^2}{r^2}d\Omega = \iint \left(\cos^2\theta\sin\theta\right)d\theta d\varphi = \frac{4\pi}{3}$$

and

$$\iint \frac{xy}{r^2}d\Omega = \iint \frac{xz}{r^2}d\Omega = \iint \frac{yz}{r^2}d\Omega = 0$$

Substituting these integrals into Eq(55) we have

$$\iint_s \mathbf{M}\cdot d\boldsymbol{\sigma} = -\frac{8\pi Gm}{3c}\begin{pmatrix} v_x \\ v_y \\ v_z \end{pmatrix} = -\frac{8\pi G}{3c}m\mathbf{v} = -\frac{8\pi G}{3c}\mathbf{p} \qquad (60)$$

where p = *m*v is the linear momentum of the mass *m*. Eq(60) is the dynamic counterpart of the static Gauss' Law of (51). The Gauss' Law is well known, but the dynamic counterpart was not known to the physics community before the publication of reference 1 in 2018. Eq (60) is called *Wang's Law*[1]. It says that the closed integration of the dynamic field tensor M is a constant proportional to the linear momentum of the moving mass. Wang's Law is therefore a statement that the total linear momentum transmitted through the gravitational field is conserved. The constant $-4\pi Gm$ in Gauss' Law will be called the *total statics flux*. The constant $\frac{-8\pi G}{3c}m\mathbf{v}$ will be called the *total dynamic flux.* We can then speak of *conservation of the total static and dynamic fluxes* of the gravitational field.

Wang's Law revels that the total linear momentum transmitted into the space through ether is conserved. It is a hint that the Gauss' Law must also be a manifestation of conservation of a physical quantity. As a matter of fact, the Gauss's law can be written, according to Eq(51), as

$$\iint_s \mathbf{g}\cdot d\,\boldsymbol{\sigma} = -4\pi Gm \tag{61}$$

Eq(61) simply says that the total mass is conserved.

The conservation of the total static and dynamic fluxes reveals how the gravitational interaction is transmitted. Thus, a mass *m* at rest in space causes stress to the ether. The total stress flux is equal to $-4\pi Gm$. If the mass is moving with velocity v, it will cause additional dynamic stress to the ether. The total dynamic stress flux is $-\frac{8\pi}{3c}Gm\mathbf{v}$. The stress of the ether will then propagate into the space, with the total static and dynamic fluxes conserved and distributed over the whole solid angle. The static and the dynamic fields are simply the stress fluxes per unit area and therefore inversely proportional to the distance squared. It naturally explains the inverse square law of the electromagnetic and the gravitational forces because the total area of a spherical surface is inversely proportional to the radius (distance). Up to now, the inverse square law is an empirical law deducted from experimental observations. We know that the gravitational force gets weaker as the distance increases. We then assume the force to be proportional to r^s and determine the parameter *s* such that the theory produces Kepler's third law. It turns out that *s* must be equal to 2 to do just right. Since Kepler's laws are all empirical laws, we then could not say that the inverse square law is absolutely accurate. The discovery of Wang's Law together with Gauss' law show that the inverse square law is as accurate as the surface area of a sphere is proportional to the square of its radius.

The differential form of Wang's law, Eq(60), is

$$\nabla\cdot\mathbf{M} = -\frac{8\pi G}{3c}\mathbf{j} \tag{62}$$

where

$$\mathbf{j} = \rho\mathbf{v} = \frac{\mathbf{p}}{V} \tag{63}$$

is the *momentum density*, i.e., the momentum per unit volume. p is the total momentum of the mass contained in the volume *V*. j is also the current density (current per unit area).

Since $\nabla\cdot\mathbf{M} = -\nabla\times\mathbf{h}$, we have

$$\nabla\times\mathbf{h} = \frac{8\pi G}{3c}\mathbf{j} \tag{64}$$

It is straightforward to check that the divergence of h is zero:

$$\nabla\cdot\mathbf{h} = -\nabla\cdot\left(\frac{Gm}{cr^2}\mathbf{v}\times\hat{r}\right) = 0 \tag{65}$$

Substituting Eqs (52), (64) and (65) into Eq(50), we have

$$\nabla\cdot\mathbf{f} = \nabla\cdot\mathbf{g} + \nabla\cdot(\boldsymbol{\beta}'\times\mathbf{h}) = \nabla\cdot\mathbf{g} + \mathbf{h}\cdot(\nabla\times\boldsymbol{\beta}') - \boldsymbol{\beta}'\cdot(\nabla\times\mathbf{h}) \tag{66}$$

Since $\boldsymbol{\beta}'$ is a constant, $\nabla\times\boldsymbol{\beta}' = 0$. Using Eqs(52) and (64), we have

$$\nabla\cdot\mathbf{f} = \nabla\cdot\mathbf{g} - \boldsymbol{\beta}'\cdot(\nabla\times\mathbf{h}) = -4\pi G\left(\rho + \frac{2}{3c}\boldsymbol{\beta}'\cdot\mathbf{j}\right) \tag{67}$$

b) Divergence of M and Curl of h in vacuum

From Eqs(43) and (47) we have

$$\nabla\cdot\mathbf{M} = -\nabla\times\mathbf{h} = \frac{Gm}{c}\nabla\times\left(\frac{\mathbf{v}\times\mathbf{r}}{r^3}\right) \tag{68}$$

But

$$\nabla\times\left(\frac{\mathbf{v}\times\mathbf{r}}{r^3}\right) = -\frac{\mathbf{r}}{r^3}(\nabla\cdot\mathbf{v}) + \mathbf{v}\left(\nabla\cdot\left(\frac{\mathbf{r}}{r^3}\right)\right) - (\mathbf{v}\cdot\nabla)\frac{\mathbf{r}}{r^3} + \left(\frac{\mathbf{r}}{r^3}\cdot\nabla\right)\mathbf{v}$$

The velocity v of the source is a constant with respect to the differential operation:

$$\nabla \cdot \mathbf{v} = 0 \text{ and } \left(\frac{\mathbf{r}}{r^3} \cdot \nabla\right)\mathbf{v} = 0 \tag{69}$$

Also, if $r \neq 0$, $\nabla \cdot \left(\frac{\mathbf{r}}{r^3}\right) = 0$,

Therefore,

$$\nabla \cdot \mathbf{M} = -\nabla \times \mathbf{h} = \frac{Gm}{c}\nabla \times \left(\frac{\mathbf{v} \times \mathbf{r}}{r^3}\right) = -\frac{Gm}{c}(\mathbf{v} \cdot \nabla)\frac{\mathbf{r}}{r^3} \tag{70}$$

Now let us examine the static field defined in Eq(41)

$$\mathbf{g} = \frac{\mathbf{F}_1}{m'} = -\frac{Gm}{r^2}\hat{r} = -Gm\frac{\mathbf{i}(x-x_1)+\mathbf{j}(y-y_1)+\mathbf{k}(z-z_1)}{\left((x-x_1)^2+(y-y_1)^2+(z-z_1)^2\right)^{3/2}} \tag{71}$$

The difference between (71) and (41) is that we now place the mass m at a more general point (x_1,y_1,z_1) instead of the origin, and allow the mass m to move. Namely, its coordinates are functions of time t. To an observer at the point (x,y,z), the field g is a time-varying function $g(x,y,z,t)$, where the time dependence is caused by the change in the coordinates (x_1,y_1,z_1) of the mass m. We can calculate this time derivative:

$$\frac{\partial \mathbf{g}}{\partial t} = -Gm\left[\frac{\partial}{\partial x_1}\left(\frac{\mathbf{r}}{r^3}\right)\frac{dx_1}{dt} + \frac{\partial}{\partial y_1}\left(\frac{\mathbf{r}}{r^3}\right)\frac{dy_1}{dt} + \frac{\partial}{\partial z_1}\left(\frac{\mathbf{r}}{r^3}\right)\frac{dz_1}{dt}\right]$$

But $\frac{\partial}{\partial x_1}\left(\frac{\mathbf{r}}{r^3}\right) = -\frac{\partial}{\partial x}\left(\frac{\mathbf{r}}{r^3}\right)$ and so on, we have

$$\frac{\partial \mathbf{g}}{\partial t} = Gm\left[\frac{\partial}{\partial x}\left(\frac{\mathbf{r}}{r^3}\right)\frac{dx_1}{dt} + \frac{\partial}{\partial y}\left(\frac{\mathbf{r}}{r^3}\right)\frac{dy_1}{dt} + \frac{\partial}{\partial z}\left(\frac{\mathbf{r}}{r^3}\right)\frac{dz_1}{dt}\right] = Gm(\mathbf{v} \cdot \nabla)\left(\frac{\mathbf{r}}{r^3}\right) \tag{72}$$

Comparing Eq(70) and (72), we arrive at

$$\nabla \cdot \mathbf{M} = -\nabla \times \mathbf{h} = -\frac{1}{c}\frac{\partial \mathbf{g}}{\partial t} \tag{73}$$

Eq(73) gives the divergence of M when the point of interest is not at the origin, namely, $r \neq 0$.

At the origin where the source of gravitation m is located, $r = 0$, the divergence of M is given by Eqs(62) and (63). Combining Eq(62) and Eq(73), we have a general formula for the divergence of M (or curl of h):

$$-\nabla \cdot \mathbf{M} = \nabla \times \mathbf{h} = \frac{1}{c}\frac{\partial \mathbf{g}}{\partial t} + \frac{8\pi G}{3c}\mathbf{j} \tag{74}$$

where j is the current density as defined in Eq(63).

The total gravitational field f is related to the static field g by Eqs(41), (46) and (50):

$$\mathbf{g} = \frac{\mathbf{F}_1}{m'} = -G\frac{m}{r^2}\hat{r} \tag{41}$$

$$\mathbf{h} = \frac{G}{cr^3}\mathbf{L} = \frac{Gm}{cr^2}\hat{r} \times \mathbf{v} = -\mathbf{g} \times \boldsymbol{\beta} \tag{46}$$

$$\mathbf{f} = \mathbf{g} + \mathbf{M} \cdot \boldsymbol{\beta}' = \mathbf{g} + \boldsymbol{\beta}' \times \mathbf{h} = \mathbf{g} + \boldsymbol{\beta}' \times (\boldsymbol{\beta} \times \mathbf{g}) \tag{50}$$

We have the relation of time derivatives

$$\frac{\partial \mathbf{f}}{\partial t} = \frac{\partial \mathbf{g}}{\partial t} + \boldsymbol{\beta}' \times \left(\boldsymbol{\beta} \times \frac{\partial \mathbf{g}}{\partial t}\right) \tag{75}$$

For most heavenly bodies and the objects on the earth, both $\boldsymbol{\beta}'$ and $\boldsymbol{\beta}$ are negligibly small, the second term of Eq(75) can be dropped. Namely,

$$\frac{\partial \mathbf{f}}{\partial t} = \frac{\partial \mathbf{g}}{\partial t} \tag{76}$$

We therefore have from Eq(76):

$$\nabla \times \mathbf{h} = \frac{1}{c}\frac{\partial \mathbf{f}}{\partial t} + \frac{8\pi G}{3c}\mathbf{j} \tag{77}$$

Eq(77) is to be compared to Ampere's law in electrodynamics:

$$\nabla \times \mathbf{B} = \frac{1}{c^2}\frac{\partial \mathbf{E}}{\partial t} + \mu_0 \mathbf{j} \tag{78}$$

Since $\mu_0\varepsilon_0 = \frac{1}{c^2}$ and $\varepsilon_0 = \frac{1}{4\pi k_1}$

We have $$\mu_0 = \frac{4\pi k_1}{c^2} \tag{79}$$

Substituting (79) into (78), we obtain

$$\nabla \times \mathbf{B} = \frac{1}{c^2}\frac{\partial \mathbf{E}}{\partial t} + \frac{4\pi k_1 \mathbf{j}}{c^2} \tag{80}$$

Comparing (77) and (80), we see two differences: 1) The difference of a factor of c is due to our definition h of Eq(46) so that h, M and g all have the same dimension, while the magnetic field B and the electric field E differ in dimension by a speed. 2) The more significant difference between (77) and (80) is the

difference in the coefficient of the current density j in the second term of the right hand of the two equations. The difference can be traced to the derivation of Ampere's law. We know that the magnetic field of an infinitely long straight current is given by

$$\mathbf{B} = \frac{\mu_0 I}{2\pi r} \tag{81}$$

where *I* is the current and *r* is the distance from the point of interest to the straight current. Now consider the integration of B along a circular contour on a plane perpendicular to and centered at the current, we have

$$\oint \mathbf{B} \cdot d\mathbf{l} = \mu_0 I \tag{82}$$

Eq(82) is known as the Ampere's law. A little more math can prove that (82) is generally true even for non-circular contours as long as the current is infinitely long.

If the current is not infinitely thin but distributed over certain finite area, the right hand side of Eq(82) has to be replaced by an integral of the current density over the area:

$$\oint \mathbf{B} d\mathbf{l} = \mu_0 \iint \mathbf{j} \cdot d \tag{83}$$

Divide Eq(83) by the surface area enclosed by the contour, and let the size of the contour approach zero, we obtain the curl of B:

$$\nabla \times \mathbf{B} = \mu_0 \mathbf{j} = \frac{4\pi k_1 \mathbf{j}}{c^2} \tag{84}$$

which explains the coefficient of the second term on the right hand side of Eq(80). From our derivation above we see apparently that this coefficient of (4π) is the result of assuming the current to be infinitely long, while the result of Eq(77) is obtained without such assumption. In applications where the assumption of "infinitely-long current" does not apply, say, for a plasma or electromagnetic wave propagating in a dielectric medium, the correct coefficient of (8π/3) should be used instead of (4π). This difference is not noticed in many textbooks. In discussing the electromagnetic waves, the charge and current are usually assumed to be zero in free space, and the difference does not show. If in the boundary conditions where the infinite-current assumption does apply, say, the surface current on the inner surface of a wave guide, the coefficient of (4π) should be used.

c) Induced motive potential

The field f is equal to the force per unit mass, i.e., f = F/*m'*. The testing mass cannot distinguish the dynamic force from the static force. If a mass *m'* is moved by the gravitational force F from point *a* to point *b*, the work done by the force field is

$$W = \int_a^b \mathbf{F} \cdot d\mathbf{s} = -Gmm' \int_a^b \frac{1}{r^2}\left[\hat{r} + \frac{1}{c^2}\mathbf{v}' \times \left(\mathbf{v} \times \hat{r}\right)\right] \cdot d\mathbf{s} \tag{85}$$

The field will move the particle from a point with higher potential energy to a point with lower potential energy. We have:

$$\mathbf{f} = \frac{\mathbf{F}}{m'} = -G\frac{m}{r^2}\left[\hat{r} + \frac{1}{c^2}\mathbf{v}' \times \left(\mathbf{v} \times \hat{r}\right)\right] \tag{86}$$

The potential difference between points *a* and *b* is the negative work done by the gravitational force per unit mass:

$$V_{ab} = -\frac{W}{m'} = -\int_a^b \mathbf{f} \cdot d\mathbf{l} = Gm\left[\int_a^b \frac{\hat{r}}{r^2} \cdot d\mathbf{l} + \int_a^b \frac{1}{r^2 c^2}\mathbf{v}' \times \left(\mathbf{v} \times \hat{r}\right) \cdot d\mathbf{l}\right] \tag{87}$$

The first term of integration is the electrostatic potential difference, which is conservative. The second term is the dynamic potential difference, which is non-conservative. Consider the contour integration

$$\oint \mathbf{f} \cdot d\mathbf{l} = -Gm\left[\oint \frac{\hat{r}}{r^2} \cdot d\mathbf{l} + \oint \frac{1}{r^2 c^2}\mathbf{v}' \times \left(\mathbf{v} \times \hat{r}\right) \cdot d\mathbf{l}\right] \tag{88}$$

The first term of the integration on the right side yields zero because

$$\oint \frac{\hat{r}}{r^2} \cdot d\mathbf{l} = \iint \nabla \times \left(\frac{\hat{r}}{r^2}\right) \cdot d\boldsymbol{\sigma} = 0 \tag{89}$$

The second term of the integration can be easily calculated for a dynamic field h (Eq 46):

$$-Gm\oint \frac{1}{r^2 c^2}\mathbf{v}' \times \left(\mathbf{v} \times \hat{r}\right) \cdot d\mathbf{l} = \oint \frac{1}{c}\left(\mathbf{v}' \times \mathbf{h}\right) \cdot d\mathbf{l} = \frac{1}{c}\oint \mathbf{h} \cdot \left(d\mathbf{l} \times \mathbf{v}'\right) = \frac{1}{c}\oint \mathbf{h} \cdot \left(d\mathbf{l} \times \frac{d\mathbf{r}}{dt}\right)$$

But $d\mathbf{r} \times d\mathbf{l} = d\boldsymbol{\tau}$, where $d\boldsymbol{\tau}$ is the area element according to the right-hand rule (Fig 5). We have

$$\oint \mathbf{f} \cdot d\mathbf{l} = \frac{1}{c}\oint \mathbf{h} \cdot \left(d\mathbf{l} \times \frac{d\mathbf{r}}{dt}\right)\boldsymbol{\tau} = -\frac{d}{dt}\left[\iint_s \frac{\mathbf{h} \cdot d}{c}\right] = -\frac{d\Phi}{dt} \tag{90}$$

where *s* is the area enclosed by the contour, and

$$\Phi \equiv \iint_s \frac{\mathbf{h}}{c} \cdot d\boldsymbol{\tau} \tag{91}$$

Φ is called the *dynamic flux*.

Equation (90) is known as Faraday's law in electrodynamics, which says that the contour integration of the field is equal to the negative rate of change of the dynamic flux. We have presented a proof that Faraday's law can be derived from the Lorentz force. Faraday's law, discovered by Faraday in 1880, is actually generally valid regardless if the change of the flux is caused by the change of contour, or the change of the dynamic field.

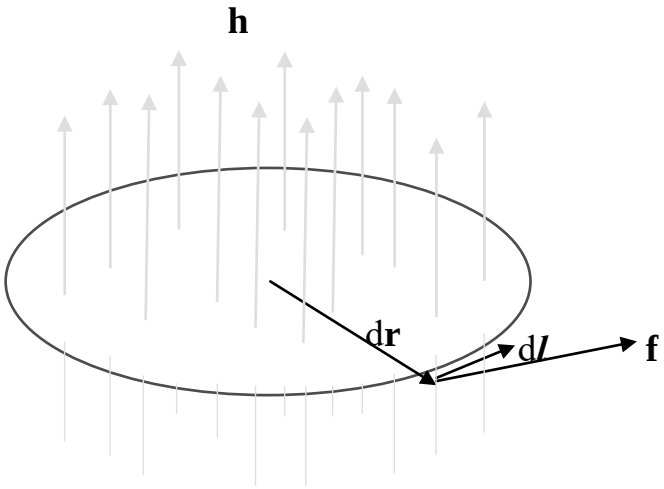

Figure 5: Faraday's law

According to the Stoker's theorem,

$$\oint \mathbf{f} \cdot d\vec{l} = \iint (\nabla \times \mathbf{f}) \cdot d\tau \tag{92}$$

Comparing Eq(90) and (92), we have

$$\nabla \times \mathbf{f} = -\frac{1}{c}\frac{\partial \mathbf{h}}{\partial t} \tag{93}$$

Eq (93) is the differential form of Faraday's law. The partial differentiation instead of total differentiation is used in Eq(93) because the value of h is fixed at the point of interest during the limiting process of letting the size of the contour approaching zero.

IX. Wave Equation

We now have a set of equations that allows us to understand the propagation of gravitational wave. First, we have the divergence of h (Eq 65):

$$\nabla \cdot \mathbf{h} = 0 \tag{65}$$

The divergence of the field f is given by Eq(67):

$$\nabla \cdot \mathbf{f} = -4\pi G\left(\rho + \frac{2}{3c}\boldsymbol{\beta}' \cdot \mathbf{j}\right) \tag{67}$$

The curl of h is given by Eq (77):

$$\nabla \times \mathbf{h} = \frac{1}{c}\frac{\partial \mathbf{f}}{\partial t} + \frac{8\pi G}{3c}\mathbf{j} \tag{77}$$

The curl of f is given by Eq (93):

$$\nabla \times \mathbf{f} = -\frac{1}{c}\frac{\partial \mathbf{h}}{\partial t} \tag{93}$$

The above equations constitute the fundamental equations of the gravitational field. In a free space where $\rho = 0$ and $j = 0$, these equations take more simple and symmetric form:

$$\nabla \cdot \mathbf{f} = 0 \tag{94}$$

$$\nabla \cdot \mathbf{h} = 0 \tag{95}$$

$$\nabla \times \mathbf{h} = \frac{1}{c}\frac{\partial \mathbf{f}}{\partial t} \tag{96}$$

$$\nabla \times \mathbf{f} = -\frac{1}{c}\frac{\partial \mathbf{h}}{\partial t} \tag{97}$$

Eqs (94)-(97) form a complete set of equations that describes the propagation of the gravitational wave in vacuum. To obtain the wave equation, we take the curl of Eq (97):

$$\nabla \times (\nabla \times \mathbf{f}) = -\nabla \times \left(\frac{1}{c}\frac{\partial \mathbf{h}}{\partial t}\right) = -\frac{1}{c}\frac{\partial}{\partial t}(\nabla \times \mathbf{h}) \tag{98}$$

Using Eq(96), we have

$$\nabla \times (\nabla \times \mathbf{f}) = -\frac{1}{c}\frac{\partial}{\partial t}(\nabla \times \mathbf{h}) = -\frac{1}{c^2}\frac{\partial^2 \mathbf{f}}{\partial t^2} \tag{99}$$

But

$$\nabla \times (\nabla \times \mathbf{f}) = \nabla(\nabla \cdot \mathbf{f}) - \nabla^2 \mathbf{f} = -\nabla^2 \mathbf{f} \tag{100}$$

We have used Eq(94) in the last step. We have

$$\nabla^2\mathbf{f} = \frac{1}{c^2}\frac{\partial^2\mathbf{f}}{\partial t^2}$$

Or,

$$\nabla^2\mathbf{f} - \frac{1}{c^2}\frac{\partial^2\mathbf{f}}{\partial t^2} = 0 \qquad (101)$$

This is the wave equation for the field **f**. The solution is

$$\mathbf{f} = \mathrm{f}_0 \sin\left(\omega t - \mathbf{k}\cdot\mathbf{r}\right) \qquad (102)$$

where

$$\omega = 2\pi f = \frac{2\pi}{T} \qquad (103)$$

is the angular frequency. *f* and *T* are the frequency and the period. $\mathbf{k} = k\hat{\mathbf{k}}$ is the wave number:

$$k = \frac{2\pi}{\lambda} \qquad (104)$$

And

$$\lambda = cT \qquad (105)$$

is the wavelength. *c* is the speed of the gravitational wave.

X. Unification of Gravitational and Electromagnetic Forces

The discussions above show that the gravitational force and the electromagnetic force can be described by exactly the same set of equations. The only difference here is that the mass *m* in the gravitational theory is replaced by the electric charge *q* in the electromagnetic theory. The different constants *G* and *k* are merely the indicators of strength of the interacting forces. As a matter of fact, we can combine the gravitational and electromagnetic forces into a unified equation:

$$\mathbf{F} = (k_1 qq' - Gmm')\frac{1}{r^2}\left[\hat{r} + \frac{1}{c^2}\mathbf{v}'\times\left(\mathbf{v}\times\hat{r}\right)\right] \qquad (106)$$

Eq(106) states explicitly that the gravitational and electromagnetic waves travel at the same speed.

It is amazing that the force equation alone is sufficient to derive all the relevant laws governing the electromagnetic and gravitational interactions. It is a testimony of the consistency of our theory and justification of inclusion of a dynamic term in the law of gravitation.

XI. Discussions

a) The speed of gravitational wave

The unification of gravitational and electromagnetic forces is so simple, and the identity of all the equations that govern the propagation of the interactions are so compelling that we believe the two interactions are propagating through the same universal medium ether, by causing static and dynamic stresses. We thus have good reason to predict that the speed of gravitational wave is the same as the speed of electromagnetic wave, or the speed of light. However, this is to be verified experimentally in the future. If the speed of gravitational wave turns out to be different from speed of light, the structure of our unification theory would remain intact and valid in the sense that both gravitational and electromagnetic interactions can be described by the same set of force law, field equations and wave equations, with different speeds of wave.

b) The theoretical derivation of gravitational wave equation

We have rigorously derived the gravitational wave equation first time ever from our unification theory. It is generally believed that Einstein's theory of general relativity predicted the gravitational wave. Such is not true. The gravitational wave equation is not derived from Einstein's general relativity but manufactured with linear approximation of Einstein's field equation and a few *ad hoc* hypotheses. It is proper and fitting here to give a brief account of how general relativity manufactured a gravitational wave equation. Einstein's field equation is

$$G_{\beta\delta} = \frac{8\pi G T_{\beta\delta}}{c^4} + \Lambda g_{\beta\delta} \qquad (107)$$

Or, alternatively [7],

$$R_{\beta\delta} = \frac{8\pi G\left(T_{\beta\delta} - T^{\mu}_{\mu} g_{\beta\delta}/2\right)}{c^4} - \Lambda g_{\beta\delta} \qquad (108)$$

A number of *ad hoc* hypotheses are then inserted:

1. The first hypothesis: The space is supposed to be vacuum so the stress-energy tensor $T_{\beta\delta} = 0$.
2. The second hypothesis: The cosmological constant is zero: $\Lambda = 0$.

With these two hypotheses, the field equation reduces to

$$G_{\beta\delta} = R_{\beta\delta} = 0 \qquad (109)$$

3. The third hypothesis: The field is week and the metric tensor $g_{\alpha\beta}$ can be approximated as nearly Minkowski:

$$g_{\beta\delta} = \eta_{\beta\delta} + h_{\beta\delta} \qquad (110)$$

Under linear approximation, Eq(109) reduces to

$$R_{\beta\delta} = \frac{1}{2} g^{\alpha\nu} \left(h_{\nu\delta,\beta\alpha} - h_{\delta\beta,\nu\alpha} + h_{\alpha\beta,\nu\delta} - h_{\alpha\nu,\beta\delta} \right) = 0 \quad (111)$$

Therefore,

$$h_{\nu\delta,\beta\alpha} - h_{\delta\beta,\nu\alpha} + h_{\alpha\beta,\nu\delta} - h_{\alpha\nu,\beta\delta} = 0 \quad (112)$$

4. The fourth hypothesis: It is assumed that each term in Eq(112) is separately zero:

$$h^{\alpha}_{\beta\delta,\alpha} = 0 \quad (113)$$

$$h^{\alpha}_{\alpha} = 0 \quad (114)$$

$$h^{\alpha}_{\delta,\alpha} = h^{\alpha}_{\alpha\beta,} = 0 \quad (115)$$

$$h_{\alpha 0} = 0 \quad (116)$$

In general the symmetric tensor $h_{\alpha\beta}$ has 10 independent components. Only two of Eqs(113)-(116) are independent. These are interpreted as the two polarizations of the gravitational wave. Eq(113) is the familiar form of wave equation:

$$\frac{\partial^2 h_{\beta\delta}}{\partial x^2} + \frac{\partial^2 h_{\beta\delta}}{\partial y^2} + \frac{\partial^2 h_{\beta\delta}}{\partial z^2} - \frac{\partial^2 h_{\beta\delta}}{c^2 \partial t^2} = 0 \quad (117)$$

Now let us examine the hypotheses needed to yield the wave equation Eq(117). The first hypothesis (vacuum hypothesis) assumes that the universe is a vacuum with zero mass density. The second hypothesis assumes the cosmological term to be zero. These two hypotheses are in direct conflict with the current mainstream cosmology which claims that the cosmological constant is mainly responsible for the dark energy, and the universe is filled with dark energy and dark matter that count 97% of the total mass of the universe. How can one set 97% to zero? The third hypothesis is certainly invalid near the black holes because that is where the metric tensor diverges to infinity, not anything close to Minkowski metric. The fourth hypothesis cannot be justified in any way mathematically. There is no base for assuming each individual terms of an equation to be zero simply because the theory does not work otherwise.

Apparently, the gravitational wave equation is not "derived" from Einstein's field equation. It is manufactured with a number of invalid hypotheses. The true derivation of gravitational wave equation is given first time ever by our unification theory published in 2018.

c) The experimental verification

The experimental detection of the dynamic term is extremely difficult at the current level of technology. The relative strength of the dynamic term over the static term is at least a factor of (vv'/c^2) smaller at the most advantageous orientation of the velocities. The velocities must be measured with respect to the medium ether. We do not really know the velocities of the planets and the sun with respect to the ether. The orbital velocity of the earth is about 30 km/s. The velocity of the sun relative to the center of mass of the sun-earth system is about 10^{-4} km/s. If we assume that the center of mass of the solar system is at rest with ether, it would mean that the dynamic term of the gravitational force is about a factor of $3x10^{-14}$ smaller than the static term. The velocities of the objects on the earth are much smaller than the orbital velocity of the earth. The dynamic term of gravitation should be many orders of magnitude smaller than the above figure. Little wonder the dynamic term of gravitation escaped detection by astronomers, scientists and engineers. It is our hope that in the future the technology would be advanced to allow the detection of the dynamic term.

We do realize the importance of experimental support to the acceptance of a new theory. Historically, Urbain Le Verrier predicted in 1840 the position of the then-undiscovered planet Neptune and its position based on Newton's theory of gravitation after analyzing perturbations in the orbit of Uranus. Subsequent observations of Neptune in the late 19th century led astronomers to speculate that Uranus's orbit was being disturbed by another planet besides Neptune (Pluto). These predictions are celebrated as proof of Newton's theory of gravitation. But the significance of such predictios is overemphasized. Newton's law of gravitation was published in 1687 in his "Principia". Urbain Le Verrier's prediction came almost 200 years later. Newton's theory of gravitation was accepted long before the predictions on Neptune and Pluto. The main reason for the acceptance was the success of Newton's theory in explaining Kepler's three empirical laws and in explaining the phenomena on Earth. It would be nice if some time down the road predictions based on our ether dynamics is supported by experiments. However, the value of our theory is evident even before such triumphant predictions are available. The credit of our theory of unification and ether dynamics rests on the detailed derivation of the dynamic term of gravitation, which is theoretically as significant as the discovery of Newton's static term of gravitation, and completes the theory of gravitation with a rigorous wave equation and removes the spooky action-at-distance. The theoretical derivation of the empirical Biot-Savart law and Lorentz force based on ether dynamics is as significant as Newton's derivation of Kepler's empirical laws of planetary movements.

A significant achievement of our theory is the newly discovered Wang's Law which says that the total momentum transmitted into space is conserved, a discovery not known before to physics community.

Another achievement of our theory is the revelation of the essence of the inverse-square law that governs both the electrodynamic and the gravitational interactions. We have demonstrated that the inverse square law is the result of the conservation of the total static and dynamic fluxes as expressed in Gauss' Law and Wang's Law. The inverse square law is as accurate as the surface area of a sphere is proportional to the square of the radius.

d) The unification of gravitational and electromagnetic interactions

The century long dream of the physics community to unify the gravitational and electromagnetic forceis finally realizedwith our unification theory and ether dynamics in a rigorously classical way.

Ever since Maxwell unified the theory of electricity and magnetism, the unification of the gravitational and electromagnetic fields had become the dream of the physics community. Early attempts were made by Hermann Weyl, Arthur Eddington, Theodor Kaluza and Albert Einstein.

Hermann Weyl's theory of infinitesimal geometry [8] was based on general relativity. He believed that in addition to a metric field there could be additional degrees of freedom along a path between two points in a manifold. He introduced a gauge field as basic method for comparison of local size measures along such a path. It generalized Riemannian geometry in that there was a vector field *Q* in addition to the metric *g*. The vector field and the metric together generated both the electromagnetic and gravitational fields. His theory was mathematically complicated, resulting in high-order field equations. Weyl's theory was found physically unreasonable after extensive communication with Einstein and others.

Kaluza's approach of unification was to embed space-time into a five-dimensional cylindrical world, consisting of four space dimensions and one time dimension [9,10]. The extra dimension allowed the electromagnetic field vector to be incorporated into the geometry. After discussion with Einstein it was discovered that Kaluza's theory did not allow a non-singular, static, spherically symmetric solution, a critical test of the validity of the theory.

Being the most influential early promoter of Einstein's general theory of relativity, Sir Arthur Eddington[11] proposed an extension of the gravitational theory based on the affine connection as the fundamental structure of the gravitational field, instead of the metric tensor as the fundamental structure according to general relativity. Eddington believed that the stress–energy tensor in Einstein's field equations was provisional, and that in a unified theory the source term would automatically come up from the field equations. Eddington's theory were sketchy and difficult to understand. Very few physicists followed up on his work.

In the spirit of his theory of relativity, Einstein considered the electromagnetic field energy being equivalent to mass according to his mass-energy relationship $E=mc^2$, and contributes to the stress tensor and to the curvature of space-time [12]. Namely, certain configurations of curved space-time should incorporate effects of an electromagnetic field. Einstein then treated both the metric tensor and the affine connection as fundamental fields. His unified-field equations were derived from a variational principle expressed in terms of the Riemann curvature tensor for the presumed space-time manifold. However, Riemannian geometry is unable to describe the properties of the electromagnetic field as a purely geometric phenomenon. The abstract nature and the lack of mathematical tools for analyzing nonlinear equations made it hard to connect such a theory with the physical reality. Einstein became isolated from physics community since then, and his attempts to unify gravity with electromagnetic field was not successful.

The unification theories of Einstein and his contemporaries are considered "classical unification theories". These theories were built around Einstein's general relativity with different ways of modification, all met with failure. After the 1930s, few scientists worked on classical unification, partially due to the failure of Einstein and others' theories, partially due to the emergence of quantum field theory. The unification of electromagnetic interaction with the weak nuclear interaction under the framework of the Standard Model [13-17] seems to be very encouraging, and many are hoping that the further development of quantum field theory might eventually lead to the unification to include the strong nuclear interaction and the gravitational interaction in a final Theory-of-Everything (TOE). The picture is not as rosy as the public is led to believe. It is fair to say that the chances for unifying these forces under the framework of Standard Model are extremely slim.

The unification of the strong interaction within the framework of the standard model seems to be the next logical step after the unification of electrodynamic and week forces. The effort in this direction, however, has not been very successful. Sheldon Glashow and Howard George proposed in 1974 a model to include the strong interaction into the electro-week theory, known as the Goerge-Glashow model [18]. It was the first Grand Unified Theory (GUT). The major problem with GUT is that the energy needed to check these theories is way beyond what the current technology could reach, in the order of 10^{16} GeV. It means that the accelerator needs to be bigger than the solar system. It is absolutely impossible. A theory that is not experimentally verifiable and falsifiable cannot be considered as a scientific theory.

Another problem with the GUT is that some of its predictions contradict the experimental findings. For instance, many GUT theories predict that the proton would decay, but the experiments show that the lifetime of the proton is at least 10^{35} years. This is 24 orders of magnitude longer than the lifetime of the universe predicted by the Big Bang cosmology. It is a heavy blow on the effort to unify the strong nuclear force.

The unification of gravitational force with other fundamental forces is even harder than the unification of the strong nuclear force. An unsurmountable obstacle is that the gravitational field is not renormalizable, which means that a unification theory including the gravitational force in the framework of the standard model is a divergent theory. Any divergent theory does not make any sense. It is now generally realized that general relativity is not compatible with quantum field theory.

From the point of view of energy scale, Theory of Everything requires an energy scale of the Plank energy of 10^{19} GeV. That is 1000 times higher than the energy scale of the Grand Unification Theory. It is far beyond the reach of modern accelerators.

The unification of gravitational force with other forces is a failure along the approaches of either general relativity or quantum field theory. However, for over a hundred years, the physics community has been educated to believe that any possible future theory of unifying gravity with other forces would have to be built upon general relativity or the standard model of quantum field theory. Whether or not confirming general relativity and quantum field theory has been used to judge and reject a manuscript for publication. Our unification theory shows that the unification of gravitational and electromagnetic forces could be done within classical framework without resorting to general relativity and quantum field theory. The simplicity, rigorousness and completeness of our unification theory are so compelling that it leaves no doubt on the correctness of the classical approach. It will certainly shake the confidence of physics community in the paradigm and doctrine of theoretical physics of the 20th century. The fundamental problems with General Relativity and the Standard Model of particle physics are analyzed by Wang in two review articles [21, 22].

e) Existence of ether

As we commented earlier on that Einstein never disproved the existence of ether. He just disliked it and believed that field is matter. We have shown that the concept of field as matter is illogical and invalid. The fact that our ether dynamics gives a theoretical derivation of the dynamic term of gravitation and the empirical Biot-Savart law and Lorentz force is a verdict that ether does exist, and it is a highly viscous incompressible fluid capable of local movements. Nowadays, the concept of a universal space medium is a common knowledge of physics community, but the knowledge of such space medium as a highly viscous incompressible fluid, however, is a new discovery.

Our ether dynamics and unification of gravitational and electromagnetic forces would certainly open up a new landscape of physics research into many fundamental questions:

1) Are mass and charge internally related? Can the unification theory lead us to a deeper and more general understanding of the charge-mass relationship? If so, such relationship would reveal a whole new microscopic world. Mathematically, this question can be formulated as: Is it possible to reduce the two terms in the first bracket of Eq(106) into a single term only?
2) Why are the two interactions dramatically different in strength? The question can be asked differently: Are the gravitational constant G and the Coulomb constant k_1 internally related? We know that the Coulomb constant k_1 is related to another constant k_2 in the Biot-Savart law. It turns out that the k_1 is equal to (c^2k_2). This relationship manifests that the electrostatic field and the magnetic field are actually the two aspects of a single electromagnetic field, and these two constants determine the speed of electromagnetic wave. If we find the interrelationship between the gravitational constant G and the Coulomb constant k_1, we could have much deeper understanding of the unification of the two well-known macroscopic forces.
3) Our theory predicts per Eq(106) that the speed of gravitational wave is the same as the speed of light. How to verify this experimentally?

Our theory of unification of gravitational and electromagnetic forces would have enormous impact on physical science in many ways. It will change our way of thinking, foster new assessment and evaluation of the approach that physics has been following in the last century, and raise questions on the entire edifice of the prevailing doctrine of theoretical physics.

XII. Conclusions

We have derived the dynamic term of the gravitational force based on fluid dynamics of ether. It provides a solid theoretical foundation for our unification theory of gravitational and electromagnetic forces based on generalization of Newton's law of gravitation to include a dynamic term similar in form to the Lorentz force of electromagnetic interaction. Such generalization is very logical and reasonable [1,2], but nonetheless speculative in nature. The ether dynamics presented in the present article has removed the speculative nature, completed the law of gravitation started by Newoton and consummated our unification theory.

Our ether dynamics has proved the existence of ether by giving a rigorous derivation of Biot-Savart law

and Lorentz force and the dynamic term of gravitation. These laws aretaken as empirical lawsuntil this date. Many aspects of these laws, such as the inverse square dependence on the distance, the sinusoidal dependence on the angle between the velocity and the displacement vector, the direction of the magnetic field and the Lorentz force determined by the right hand rule, are none less mysterious than Kepler's three laws. Our rigorous derivation of Biot-Savart law and Lorentz force based on ether dynamics is a convincing proofof the existence of ether. There is simply no other way to explain Biot-Savart law and Lorentz force without accepting a highly viscous incompressible fluid ether serving as the medium to propagate these interactions. Our ether dynamics certainly deepens our understanding of the gravitational and electromagnetic interactions and justifies their unification.

References Références Referencias

1. Wang, Ling Jun, "Unification of Gravitational and Electromagnetic Fields", *Physics Essays,* Vol. 31 No. 1, 2018.
2. Wang, Ling Jun, *Unification of Gravitational and Electromagnetic Forces,* Scholar's Press, ISBN 978-3-639-51331-8, 2019.
3. Wang, Ling Jun, "First-order ether drift experiment", *Physics Essays,* Vol. 23 No. 3(2010).
4. Yuan, S.W., *Foundations of Fluid Mechanics,* Civil Engineering and Engineering Mechanics Series, Prentice-Hall International, Inc., London, Sydney, Torento, New Delhi, Tokyo; Lamb, Horace, *Hydrodynamics,* 6th ED., Dover Publications, New York 1945, ISBN0-486-60256-7.
5. Stokes, G. G., "On the Effects of the Internal Friction of Fluids on the Motion of Pendulums", *Cambridge Phil. Trans.* 9, 1851.
6. Lamb, Horace, *Hydrodynamics,* 6th ED., Dover Publications, New York 1945, ISBN0-486-60256-7.
7. I.R. Kenyon, *General Relativity*, Oxford University Press, Oxford, New York, Tokyo, 1990, ISBN 0 19 851996 6.
8. *Weyl, H. (1918). "Gravitation und Elektrizität". Sitz. Preuss. Akad. Wiss.: 465.*
9. Daniela Wuensch. *Kaluza—Klein Theory*. Compendium of Quantum Physics 2009, pp 328–331.
10. *Sitzungsberichte der Preussischen Akademie der Wissenschaften* (1918) (*Proceedings of the Prussian Academy of Sciences* (1918)). archive. org. pp. 966–974.
11. *Eddington, A. S. (1924), The Mathematical Theory of Relativity, 2nd ed. Cambridge Univ. Press.*
12. *Einstein, A. (1956). The Meaning of Relativity. 5th ed. Princeton Univ. Press.*
13. *S.L. Glashow. "Partial-symmetries of weak interactions". Nuclear Physics. 22 (4): 579–588. Bibcode:1961NucPh.22.579G. doi:10.1016/0029-5582(61)90469-2.*
14. *A. Salam (1968). N. Svartholm, ed. Elementary Particle Physics: Relativistic Groups and Analyticity.* Eighth Nobel Symposium. *Stockholm:* Almquvist and Wiksell. *p. 367.*
15. *S. Weinberg (1967). "A Model of Leptons".* Physical Review Letters. *19 (21): 1264–1266.* Bibcode**:** 1967PhRvL.19.1264W. doi*:* 10.1103/PhysRevLett. 19.1264.
16. *P.W. Higgs (1964). "Broken Symmetries and the Masses of Gauge Bosons". Physical Review Letters. 13 (16): 508–509.*
17. *'t Hooft, G.; Veltman, M. (1972). "Regularization and renormalization of gauge fields". Nuclear Physics B. 44: 189.* Bibcode**:** 1972NuPhB.44.189T. doi*:* 10.1016 /0550-3213(72)90279-9.
18. *Georgi, Howard; Glashow, Sheldon (1974). "Unity of All Elementary-Particle Forces",* Physical Review Letters. *32 (8): 438.* Bibcode*:*1974PhRvL.32.438G. doi*:*10.1103/PhysRevLett.32.438.
19. *Witten, Edward (1995). "String theory dynamics in various dimensions". Nuclear Physics B. 443 (1): 85–126.*
20. M. Veltman, *Facts and Mysteries in Elementary Particle Physics,* World Scientific, New jersey, London, Singapore, Hong Kong, (2003), ISBN 981-238-149-X.
21. Ling Jun Wang, *"One Hundred Years of General Relativity – a Critical View"*, *Physics Essays,* Vol. 28 No. 4, 2015.
22. Ling Jun Wang, *"Physics needs nothing less than a Renaissance – On the relation between physics and philosophy",* 2020 *J. Phys.: Conf. Ser.* 1466 012002.

Global Journal of Science Frontier Research: a
Physics and Space Science
Volume 20 Issue 13 Version 1.0 Year 2020
Type : Double Blind Peer Reviewed International Research Journal
Publisher: Global Journals
Online ISSN: 2249-4626 & Print ISSN: 0975-5896

Generation and Recombination Processes in Disordered Semiconductor Structures with Deep Centers

By Sergey V. Bulyarskiy
Institute of Nanotechnology of Microelectronics

Abstract- The article represents the physical processes and mechanisms that accompany the work of the real p-n-junction in disordered semiconductor structures with deep centers. A model for the transfer of electrons and holes in disordered semiconductors has been developed and expressions for the recombination rate have been obtained, which take into account the exchange of charge carriers between neighboring localized regions. The probability of electronic transitions is calculated. It takes into account the electron-phonon interaction and explains the rapid build-up of reverse currents as the applied voltage increases. The new model of recombination in space charge region of p-n-junction has been developed. This model made it possible to develop a new method for processing current-voltage characteristics and determining the parameters of recombination centers in semiconductor devices including electron-phonon interaction parameters.

Keywords: p-n-junction; current-voltage characteristic; generation; recombination; electron transition probability; electron-phonon interaction.

GJSFR-A Classification: FOR Code: 091306

Strictly as per the compliance and regulations of:

Generation and Recombination Processes in Disordered Semiconductor Structures with Deep Centers

Sergey V. Bulyarskiy

Abstract- The article represents the physical processes and mechanisms that accompany the work of the real p-n-junction in disordered semiconductor structures with deep centers. A model for the transfer of electrons and holes in disordered semiconductors has been developed and expressions for the recombination rate have been obtained, which take into account the exchange of charge carriers between neighboring localized regions. The probability of electronic transitions is calculated. It takes into account the electron-phonon interaction and explains the rapid build-up of reverse currents as the applied voltage increases. The new model of recombination in space charge region of p-n-junction has been developed. This model made it possible to develop a new method for processing current-voltage characteristics and determining the parameters of recombination centers in semiconductor devices including electron-phonon interaction parameters. The nature of the reverse and forward currents of p-n-junctions is studied as the basis for the operation of these devices. The mechanisms of formation of the reverse current of the p-n-junction were discussed and it was concluded that the current is determined by the generation with the participation of deep centers and electron-phonon interaction.

Keywords: p-n-junction; current-voltage characteristic; generation; recombination; electron transition probability; electron-phonon interaction.

I. Introduction

Models of generation and recombination in homogeneous semiconductor structures were created in fundamental works for microelectronics [1, 2]. The results of these works perfectly describe the current-voltage characteristics (CVC) of ideal structures with a depletion region and defects in this region, photoelectric processes involving defects, and other important phenomena in semiconductors. These works have numerous applications and an extensive bibliography of citations, for example [3]. Nevertheless, these works require refinement and development when disordering, strong electric fields, and electron-phonon interaction take place. Nanoscale disorder in diamond-like semiconductors can be caused by different factors. Artificial nanoscale disorder is obtained by forming an array of quantum wells, for example, in crystals based on III–V solid solutions and other complex semiconductors, including those based on oxides. This process can be initiated, for example, by irradiation or ion implantation of a semiconductor and silicon too. Natural nanoscale disorder can also be due to different factors: compensation, structural damage, glass formation, high defect concentration[4].Silicon contains a wide variety of defects, including vacancy -impurity complexes. Oxygen is an important impurity located at interstitial sites in the silicon lattice. Vacancies are easily trapped by oxygen atoms, leading to a formation of vacancy-oxygen (VO)complexes. Upon annealing, VO complex can combine with vacancy or interstitial oxygen to form more complicated complexes, such as V2O, VO2, VO3, and so on [4]. Defects in semiconductor devices are studied by various methods, most of which use capacitance measurement. Current-voltage characteristics of p-n junctions with defects contain all information about defects and deep centers that they create. However, the analysis of these characteristics is poorly developed. This article partially fills this research gap.

Disorders in semiconductors accompanied by spatial localization of electronic states. As a result, to recombine, charge carriers must overcome a potential barrier; barriers over come through tunnelling is referred to as the tunneling recombination. Transport models with allowance for disordering were proposed in [5, 6].Generation and recombination are accompanied by electronic transitions between localized states. A good description of the experimental results cannot be made without taking into account the electron-phonon interaction, which increases the probability of the mentioned transitions. The probabilities of such transitions have been investigated by many authors [7-12], however, results that are easy to compare with experiment were obtained in [13] and they successfully explained various experimental results [13 - 17].

This work is a review in which the author strives to show what fundamental processes underlie the transport phenomena in disordered semiconductor nano- and microelectronics structures with structural defects that create deep centers. Much attention is paid to the current-voltage characteristics of p-n-junctions based on such semiconductors and practical methods for determining the parameters of defects in them.

Author: Institute of Nanotechnology of Microelectronics of the Russian Academy of Sciences (INME RAS), Leninskiy prospect, 32A, Moscow, 119991, Russia. e-mail: bulyar2954@mail.ru

II. Generalized Recombination Theory

A schematic diagram of recombination processes in nanoscale-disordered materials is shown in Fig. 1.

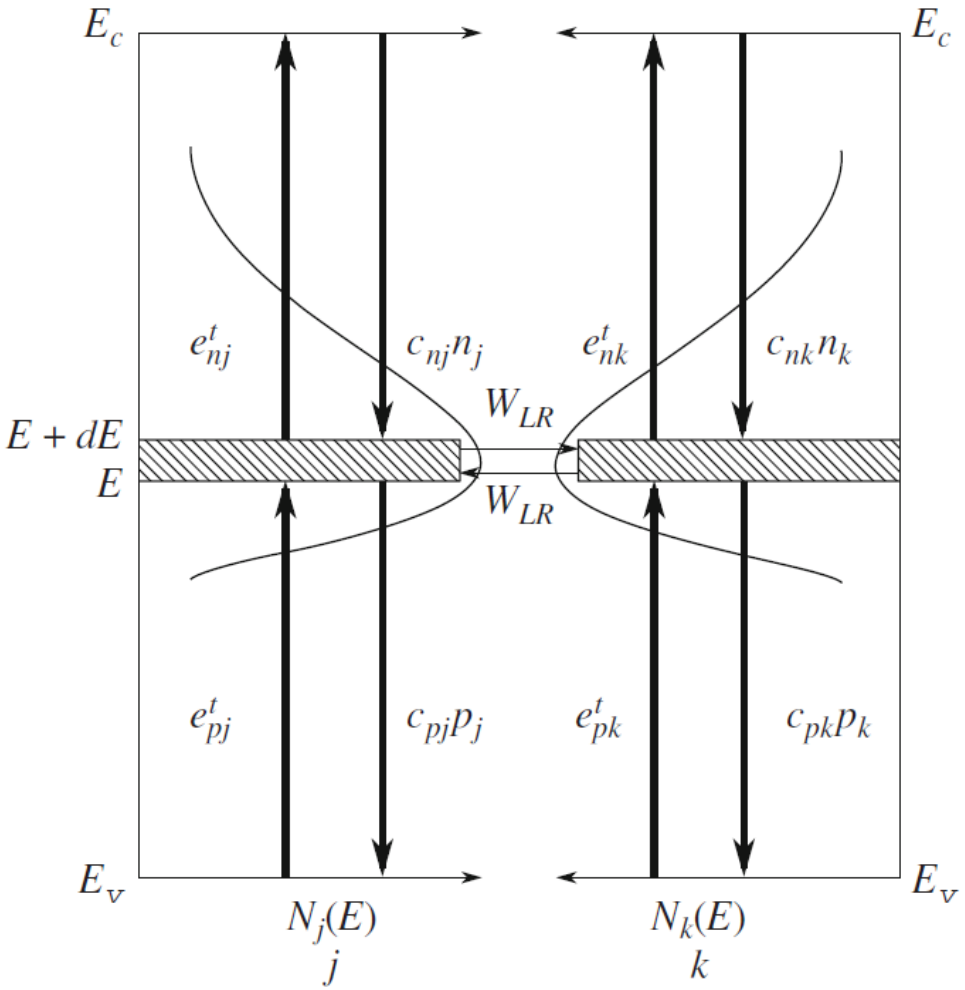

Fig. 1: Diagram of the recombination processes and electron transitions in our model

In accordance with this diagram, there are two regions in a semiconductor, separated by a potential barrier. Due to the nano scale disorder, localized states with different concentrations are formed in them, which can play the role of recombination centers. The barrier is tunnel-transparent between this regions. Recombination centers are present in each region, which are energy-distributed according to some (generally unknown) law. Recombination of charge carriers in each region may occur independently. There is also an additional mechanism of generation of non-equilibrium charge carriers, for example, injection.

Let us consider in more detail the model properties. We analyze a quasi-equilibrium stationary problem. Accordingly, both free and bound charge carriers have steady concentrations at each point of space. For various reasons (primarily, due to the spatially no uniform distribution of electric potential), these concentrations are different in each bound region. However, since quasi-equilibrium is established in the system (tunneling, injection, and generation occur simultaneously), free charge carriers of each type are formed a unified subsystem. The electron and hole concentrations are generally different. A change in these concentrations is the sum of changes in the concentrations in all regions. Energy distribution of traps is determined by the physical features of nano scale disorder. They can be different in neighboring bound regions.

To calculate the total recombination rate, we will write the electron and hole recombination rates taking in to account the following:

1. The total recombination rate is determined by the recombination rates in all bound regions;
2. Localized states in each region are distributed over energies and characterized by both density and kinetic coefficients, which also have some energy distribution;

3. The occupation of localized states by charge carriers is generally described by not the Fermi–Diracfunction, because the system is not in complete equilibrium but in a steady state; therefore, this occupation function must be sought during the solution of the problem. The change in electron (*n*) and hole (*p*) concentrations in time *t* can be written as:

$$\frac{\partial n}{\partial t}=\int_E\left\{\begin{matrix}-c_{nj}(E)n_jN_j(E)\left[1-f_j(E)\right]-c_{nk}(E)n_kN_k(E)\left[1-f_k(E)\right]+\\ c_{nj}(E)n_{1j}(E)N_j(E)f_j(E)+c_{nk}(E)n_{1k}(E)N_k(E)f_k(E)\end{matrix}\right\}dE\,, \tag{2. 1}$$

$$\frac{\partial p}{\partial t}=\int_E\left\{\begin{matrix}-c_{pj}(E)p_jN_j(E)f_j(E)-c_{pk}(E)p_kN_k(E)f_k(E)+\\ c_{pj}(E)p_{1j}(E)N_j(E)\left[1-f_j(E)\right]+c_{pk}(E)p_{1k}(E)N_k(E)\left[1-f_k(E)\right]\end{matrix}\right\}dE\,, \tag{2. 2}$$

Where: $c_{nj.k}(E)$ & $c_{pj,k}(E)$ is the coefficient of electron &hole capture by localized states in the range between *E* and *E* + *dE* in regions *j* and *k*: $n_{j,k}(p_{j,k})$ is the density of the electron concentration at the bottom of the conduction band (at the corresponding percolation level) or the hole concentration (at the top of the valence band or at the corresponding percolation level); $n_{1i,1k}(E)=N_c\exp\left[-(E_c-E)/kT\right]$ is a parameter characterizing the rate of electron emission; $p_{1j,1k}(E)=N_v\exp\left[-(E-E_v)/kT\right]$ is a parameter characterizing the rate of hole emission; E_c is the energy of the bottom of the conduction band (the corresponding percolation level); E_v is the energy of the top of the valence band (the corresponding percolation level); $N_{j,k}(E)$ are the energy density distributions of the localized states in the j_{th} and k_{th} regions; $f_{j,k}(E)$ is the probability of electron occupancy of the localized states.

Eq. (2.1) and (2.2) include only thermal processes; however, it is not difficult to take into account optical processes, both between states inside the mobility gap and outside it.

1) The filling functions of the electronic states of defects differ from the Fermi-Dirac function and include the injection processes. We can show this if we equate Eq. (2.1) and Eq.(2.2), how it should be done in equilibrium. For the region *J* we have for example:

$$f_j(E)=\frac{\left\{\begin{matrix}\left[c_{pj}(E)p_{1j}(E)+c_{nj}(E)n_j\right]N_j(E)+\left[c_{pk}(E)p_{1k}(E)\right]N_k(E)-\\ -\left[t_{nk}(E)+t_{pk}(E)\right]N_k(E)f_k(E)\end{matrix}\right\}}{\left[t_{nj}(E)+t_{pj}(E)\right]N_j(E)}\,, \tag{2.3}$$

Where: $t_{nj,k}(E)=c_{nj,k}(E)\left[n_{j,k}+n_{1j,1k}(E)\right]$; $t_{pj,k}(E)=c_{pj,k}(E)\left[p_{j,k}+p_{1j,1k}(E)\right]$.

2) The probability of filling the traps is determined not only by vertical thermal and optical transitions, but also by horizontal ones between neighboring localized states. It is this fact that leads to a generalization of the theory of generation and recombination processes. We take into account the probability of transitions between localized states and thus include ballistic transfer, hopping conduction, and tunneling in the theory. This is important for disordered semiconductors, when charge carriers are localized in a certain region, they cannot move freely along the semiconductor, the transition to an adjacent state occurs with a certain probability, which must be calculated separately. The conclusion of this statement was made in [5,6]. Here we give the result for the rate of change in the filling of localized states:

$$\begin{aligned}\frac{\partial n_{tj}}{\partial t}=&\int_E c_{nj}(E)n_jN_j(E)+c_{pj}(E)p_{1j}(E)N_j(E)-\left[t_{nj}(E)+t_{pj}(E)\right]N_j(E)f_j(E)dE-\\ &-\int_E\int_{E'}w_{LR}(E,E')N_j(E)f_j(E)N_k(E')\left[1-f_k(E')\right]dEdE'+\\ &+\int_E\int_{E'}w_{RL}(E,E')N_J(E)\left[1-f_j(E)\right]N_k(E')f_k(E')dEdE'\end{aligned} \tag{2.4}$$

Where: $w_{LR}(E)$ and $w_{RL}(E)$ are the probabilities of transition between neighboring regions. These probabilities include not only purely electronic transitions, but can take into account the interaction of charge carriers with the crystal lattice, which is expressed in the formation of polarons and is called the electron-phonon interaction. These expressions will be given below in the text.

The final expression for the recombination rate taking into account the transition between localized states [5,6] is:

$$R = R_j + R_k + R_{jk}, \qquad (2.5)$$

Where: The rate of recombination in the region J:

$$R_j = \int_E \frac{c_{nj}(E)c_{pj}(E)\left(n_i^2 - p_j n_j\right)\left(T_{pnk} + w(E)N_j + AUN_j\right)N_j(E)}{T_{pnk}T_{pnj} + w(E)N_k T_{pnk} + w(E)N_j T_{pnj} + AUN_j T_{pnj}}dE,$$

The rate of recombination in the region K:

$$R_k = \int_E \frac{c_{nk}(E)c_{pk}(E)\left(n_i^2 - p_k n_k\right)\left(T_{pnj} + w(E)N_K\right)N_K(E)}{T_{pnk}T_{pnj} + w(E)N_k T_{pnk} + w(E)N_j T_{pnj} + AUN_K T_{pnK}}dE,$$

The rate of transition from the localized state of the region J to the region K and back:

$$R_{jk} = \int_E \frac{w(E)\left\{N_j N_k(E)D_{jk} + N_k N_j(E)D_{kj}\right\} + AU\left\{N_j N_k D_{jk}\right\}}{T_{pnk}T_{pnj} + w(E)N_k T_{pnk} + w(E)N_j T_{pnj} + AUN_j T_{pnj}}dE,$$

The designations used are:

$$D_{jk} = t_{nj}(E)c_{pk}(E)p_{1k}(E) - t_{pj}(E)c_{nk}(E)n_k,$$

$$D_{kj} = t_{nk}(E)c_{pj}(E)p_{1j}(E) - t_{pk}(E)c_{nj}(E)n_j.$$

This expression seems cumbersome and incomprehensible, but it can be easily converted into simple and understandable formulas:

a) Shockley recombination rate through deep traps

We assume that the recombination occurs in one region J, the transition probabilities $w_{LR}(E)$ and $w_{RL}(E)$ are equal to zero. Recombination is done through discrete levels ($N_{tj} = N_{tj}(E)\delta(E - E_{tj,k})$). We will take these remarks into account and obtain from Eq.(2.5) the well-known formula:

$$R = \frac{c_{nj}c_{pj}\left(p_j n_j - n_i^2\right)N_{tj}}{c_{nj}\left(n_{1j} + n_j\right) + c_{pj}\left(p_{1j} + p_j\right)} \qquad (2.6)$$

b) Tunneling and tunneling recombination transport of charge carriers [5,6].

In most disordered semiconductors, electrons and holes are localized and spatially separated. Recombination can take place only if one of the stages of the process is tunneling and one of the charge carriers makes a jump into a new localized state. The charge carriers come to quasi-equilibrium after that. Hence the name of the model - tunneling recombination.

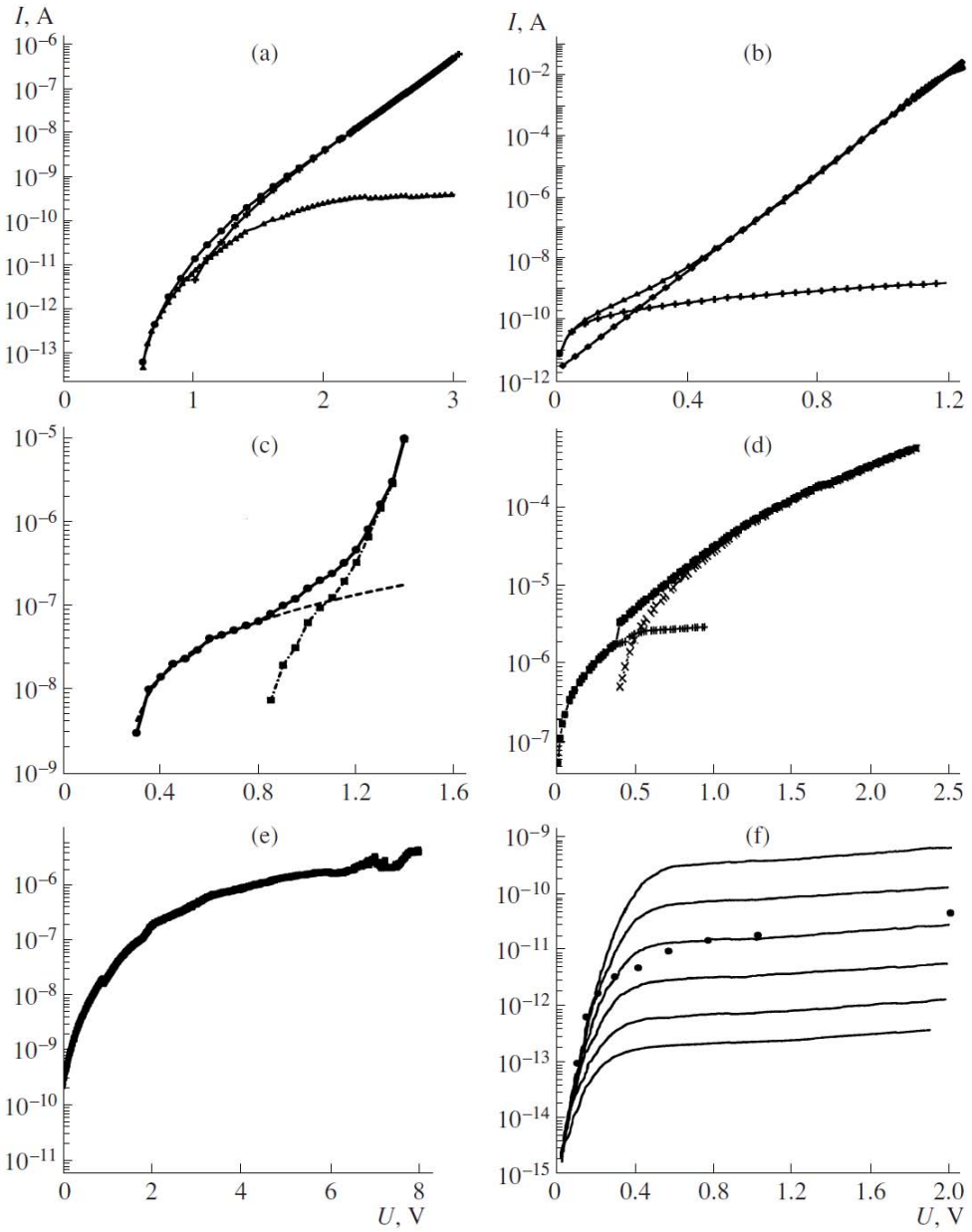

Fig. 2: Current–voltage characteristics of nanoscale disordered structures: (symbols) experiment and (lines) calculation from formula (2.7). (a) LEDs with a set of In GaN quantum wells, (b) GaAs LEDs with a high concentration of *EL2* traps, (c) *p–n* junctions in Be-implanted GaP, (d) In/CdMnTeSchottky barriers, (e) Cu/TlGaSe$_2$ Schottky barriers, and (f) In/glassy As2S3 contacts.

The above-described exchange model also follows from formula (2.5). We will assume that in one region the traps exchange only with the electronic percolation level, and in the other, with the hole percolation level. Assuming that $c_{pj} = 0$ and $c_{nk} = 0$, from Eq. (2.5) we obtain:

$$R = \int_E \frac{w(E)N_jN_k(E)c_{nj}(E)n_{1j}(E)c_{pk}(E)p_{1k}(E) - w(E)N_kN_j(E)c_{nj}(E)n_jc_{pk}(E)p_k + AUN_kN_j(E)t_nc_{pk}p_{1k}}{t_{pk}(E)t_{nj}(E) + w(E)N_k(E)t_{pk}(E) + w(E)N_jt_{nj}(E) + AUN_jt_{nj}} dE \qquad (2.7)$$

Formula (2.7) can be used to describe various disordered semiconductors, as well as for ballistic transfer of charge carriers in carbon nano tubes. Examples of application of Eq. (2.7) are in work [5], the results of which are shown in Fig. 2.

Formula (2.5) is general and can be used for almost all cases of carrier transfer between localized electronic states. This article is discussing the use of formula (2.5) for the analysis of generation and recombination processes in p-n-junctions with deep centers.

III. The Probability of Electronic Transitions between Localized States taking into Account the Electron-Phonon Interaction

The transition of a charged particle (electron or hole) between localized states causes a change in the electric field, which leads to the appearance of a polar on state and a change in lattice vibrations. This is the essence of the electron-phonon interaction, which changes the probability of an electronic transition. Accurate calculations should take into account changes in the potential energy of the electron-crystal lattice system, the displacement of the atoms of the crystal lattice, which in turn leads to a change in the density of phonon states, etc. They are complex and cannot be used in practice. There is a simple one-coordinate model, which is similar to Einstein's model for thermal conductivity, it can be accurately calculated and fairly accurately describes the result of electron-phonon interaction. Ridley's book allows you to get acquainted with it in detail and understand the basic principles of the one-coordinate model [11].This model is well represented by the configuration-coordinate diagram, which reveals the features of the electronic transition with electron-phonon interaction (Fig.3).

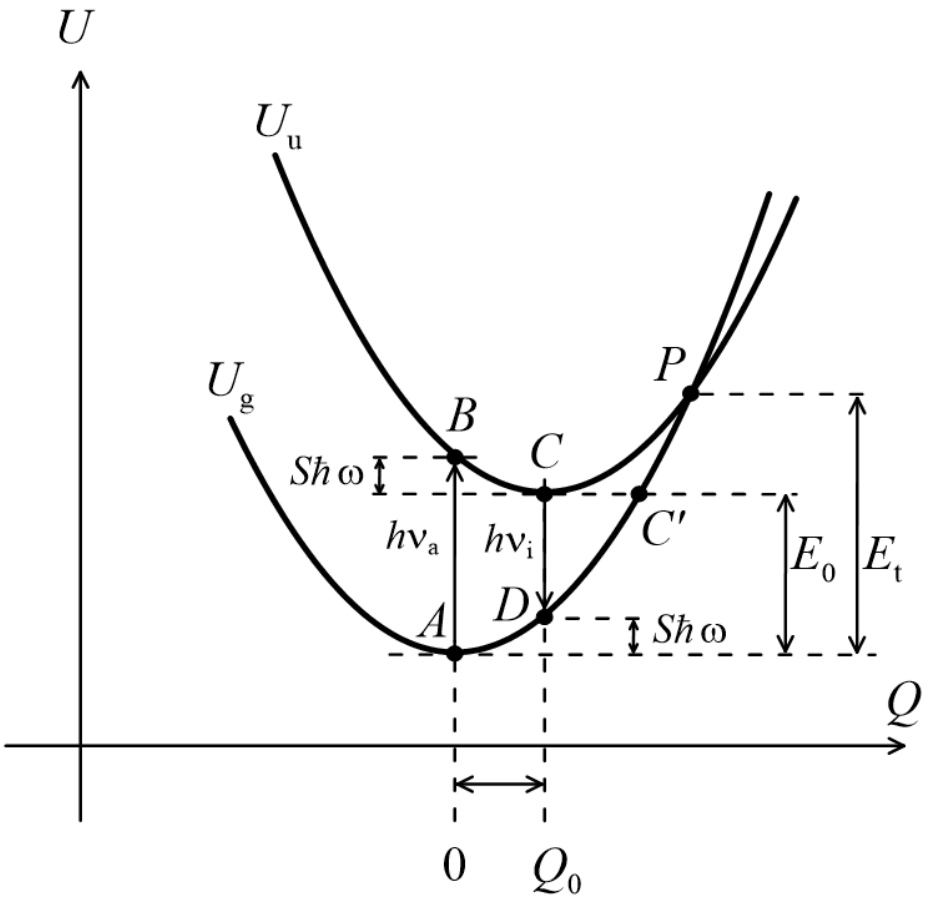

Fig. 3: Configuration-coordinate diagram

We will talk about an electron that passes between localized states, but all our reasoning is valid for a hole. The construction of such a diagram is based on a simplified approximation of the one-coordinate model, according to which the ground and excited states of the centers are described by adiabatic potentials, the energy of which is proportional to the square of a certain generalized coordinate *Q*. When the system passes from the ground state to the excited one, the polaron effect takes place, as a result of which the adiabatic potential of the excited state is shifted relative to the main potential by the amount Q_0(polaron shift) and they intersect at point *P* (Fig 3.)

$$U_g = \frac{\hbar\omega Q^2}{2}; \qquad U_u = \frac{\hbar\omega\left(Q-Q_0\right)^2}{2} + E_0 \qquad (3.1)$$

Where: Q is generalized coordinate; $Q_0 = \sqrt{2S}$, $S\hbar\omega$ is a value equal to half of the heat release that accompanies the electron-phonon interaction; E_0 is the energy of a purely electronic transition, S is the Huang and Rees factor, $\hbar\omega$ is the energy of the characteristic phonon in the one-coordinate model; U_g is the adiabatic potential of the ground state of a center, U_u is the adiabatic potential of the excited state of a center, hv_a is the energy of the absorption maximum during the transition from the ground state to the excited state, hv_i is the energy of the maximum radiation during the transition from the excited state to the ground state, E_t is the energy of thermal activation.

$$E_t = \frac{(E_0 + S\hbar\omega)^2}{4S\hbar\omega}; \quad \begin{matrix} h\nu^{abc} = E_0 + S\hbar\omega, \\ h\nu^{em} = E_0 - S\hbar\omega, \end{matrix} \qquad (3.2)$$

This model is used to describe the possibility of multi phonon non-radiative transitions of charge carriers and avoids the difficulties of explaining the simultaneous interaction of many particles. With a non-radiative transition from the ground state (point A in Fig. 3) to an excited one (point C, Fig. 3), the system absorbs one phonon after another, while increasing the amplitude of the generalized coordinate. The transition itself occurs at the saddle point (point P, Fig. 3), when the energy of the ground state takes on the value E_t, and then the system relaxes to point C, also emitting phonons one after another to reduce the energy.

The probability W of transition between unperturbed states 1 and 2 is determined by the square of the absolute value of the matrix element $\hat{H}'$ of the perturbation operator causing the transition:

$$W = \frac{2\pi}{\hbar}\left|\left\langle 1\left|\hat{H}'\right|2\right\rangle\right|^2 \qquad (3.3)$$

The exact calculation of this probability was made in [12, 13], its result is that for the probability of a quantum-mechanical transition, taking into account the electron-phonon interaction, in general form, it can be written as:

$$W = \sum_{i,j}\int_{-\infty}^{\infty} W_{0i,j}\left(E_{ti,j} - \varepsilon\right) f_{i,j}(\varepsilon)d\varepsilon \ , \qquad (3.4)$$

Where: $W_{0i,j}\left(E_{ti,j} - \varepsilon\right)$ is the probability of a purely electronic transition from i- the sublevel of the multiplet of the initial state of the center to j- the sublevel of the final state of the multiplet, $f_{i,j}(\varepsilon)$ is the expression for the shape function of the optical transition from - the sublevel of the multiplet of the initial state of the center to i - the sublevel of the final state j of the multiplet, $\sum_{i,j}$ is summation over all sublevels of the multiplets 1 and 2.

Eq.(3.4) is common for transitions between different localized states. It can be used for multiphonon thermal, tunneling, and optical transitions. Probability of a purely electronic transition $W_{0i,j}\left(E_{ti,j} - \varepsilon\right)$ is presented in numerous monographs, including [11].The shape function that reflects the electron-phonon interaction can be calculated from experiments on radiation or energy absorption during transitions with the participation of deep centers[12, 13]. This is often difficult. Therefore, this function can be approximated by the Gauss normal distribution:

$$f_{i,j}(\varepsilon) = \frac{1}{\sigma\sqrt{2\pi}}\exp\left[-\frac{(\varepsilon - E_0)^2}{2\sigma^2}\right]; \ \sigma = \sqrt{2S\hbar\omega kT} \quad (3.5)$$

The parameters of the function forms can be found by analyzing the current-voltage characteristics. This important and interesting method will be discussed below.

IV. Recombination in the Depletion Region of the P-N Junction at Forward Bias Voltage. Recombination Spectroscopy

The recombination in the space charge region (SCR) determines the current-voltage characteristics (CVC) of almost all semiconductor devices with a low injection level, which occurs at low forward bias voltages at the *p-n*-junction. This section begins near zero voltage and lasts up to a voltage of the order of the diffusion potential, which, as is well known, characterizes a potential barrier in the contact area at zero displacement. The main results of this chapter were partially obtained earlier [18-22]. In an ideal diode, it is assumed that there are no generation-recombination processes in the space charge region (SCR) and the current through the p-n-junction is determined by carrier injection through the barrier. The equation of the Current-Voltage characteristic (CVC) has the form:

$$j = j_S\left[\exp\left(\frac{qU}{mkT}\right) - 1\right] \qquad (4.1)$$

Where: j_S is revers saturation current density; U is a voltage on the p-n-junction; k is the Boltzmann constant; q is electron charge; m is the ideality factor.

Ideality factor (m) has the meaning 1 in the Shockley's diffusion theory [1] and 2 in the model generation and recombination in p-n-junctions [2]. The revers saturation current density is associated with the parameter lifetime (τ) in last model and it is a display in

the form: $j_S = j_{S0}/\tau$. Classical reverse current does not depend on voltage. The dependence of the current on the voltage takes place in the so-called short-base diodes, when the base thickness is of the order of the diffusion length.

Scientific articles do not consider the problem that the ideality factor and the lifetime can depended on the voltage applied to the p-n-junction. Such an understanding of these values is not true, since the voltage value changes the flow of injected charge carriers. Ideality factor and the lifetime should change with a change in bias voltage too, because they depend on the injection. Numerous training courses and lectures do not pay enough attention to this problem.

The CVC during recombination in the SCR was obtained in [25] and can be represented as:

$$I = \frac{qAw(U)n_i}{2\tau}\left(\exp\left(\frac{qU}{2kT}\right)-1\right) \qquad (4.2)$$

where $w(U)$ is the width of the SCR of the p-n junction; n is a concentration of intrinsic charge carriers; A is the area of the p-n junction,τ is the lifetime of non-equilibrium charge carriers. The differential slope in this case is 2. Such an expression for recombination in the SCR was obtained under the simplifying assumption that the capture coefficients at the recombination center are equal for electrons and holes.

The recombination rate from Shockley's theory Eq.(2.6) allows one to obtain a more accurate expression for the current-voltage characteristic, from which it follows that the differential slope and the lifetime depend on the number of charge carriers injected into the SCR, and, consequently, on the forward bias voltage. The concentration of free carriers in the SCR can be obtained by multiplying the concentration of free carriers in the corresponding region by the Boltzmann factor, taking into account the influence of the electric field of the p-n-junction. These concentrations are calculated by the formulas in a one-dimensional model:

$$n(x) = n_n \exp\left(-\frac{\varphi(x)}{kT}\right), \qquad p(x) = p_p \exp\left(-\frac{q(V_d - U) - \varphi(x)}{kT}\right). \qquad (4.3)$$

Where: $\phi(x)$ is potential of semiconductor structure at point x. Eq.(4.3) must be substituted into Eq. (2.6), then we obtain an important formula for CVC, the derivation and application of which is described in detail in [18 - 22]:

$$I_r = qA\int_{-x_p}^{x_n} R(x)dx \approx \frac{qAR_{\max}w}{2}, \qquad (4.4)$$

$$R_{\max} = \frac{c_n c_p n_i^2 N_t\left[\exp\left(\frac{eU}{kT}\right)-1\right]}{2n_i\sqrt{c_n c_p}\exp\left(\frac{eU}{2kT}\right)+c_n n_1 + c_p p_1} \qquad (4.5)$$

$$I_r(U) = qAw(U)\cdot\frac{c_n c_p n_i^2 N_t\left(e^{qU/kT}-1\right)}{2n_i\sqrt{c_n c_p}e^{qU/2kT}+c_n n_1 + c_p p_1}\cdot\frac{2kT}{e(V_d - U)} \qquad (4.6)$$

Where:V_d is the diffusion potential of the p-n junction.

$$m = \frac{e}{kT}\left(\frac{d\ln I_r}{dU}\right)^{-1} = \frac{eI_r}{kT}\left(\frac{dI_r}{dU}\right)^{-1} \qquad (4.7)$$

The current-voltage characteristic, the rate of recombination in the space-charge region, and the differential slope depend on the parameters of the recombination centers with deep levels in the band gap of the semiconductor and the voltage at the p-n-junction [15]. Therefore, the parameters of deep levels can be calculated from the CVC. We will do this using the example of deep centers in silicon p-i-n structures [16]. The calculation results of β for the diodes that were studied are shown in Fig. 6.

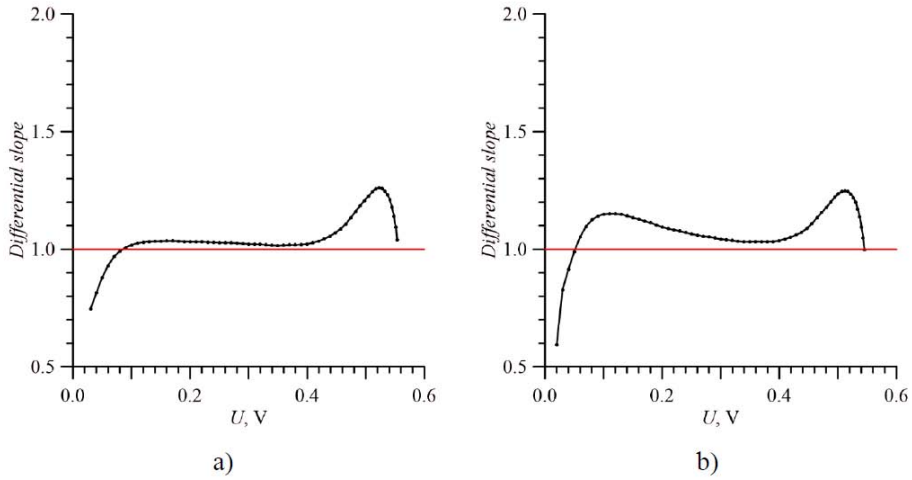

Fig. 4: Differential slope of the forward CVC of the diodes at room temperature
a) before irradiation; b) after irradiation [16].

The experimental results of Fig. 4 show that the values of the differential slope are in the range $1 < \beta < 2$. The value of β exceeds 1 after irradiation more significantly. According to the results of [20, 21], the presence of maxima in the dependence of the differential slope on the forward bias voltage indicates the existence of recombination centers. The differential slope shows two maximum(see Fig. 4), the first of which is blurred, which may be due to the influence of several recombination centers. These facts indicate that the direct CVC is determined by recombination in the SCR.

The experimental CVC underwent a transformation, which made it possible to better reveal their features. The dependence of a certain quantity on the forward bias voltage was calculated, which was called the reduced recombination rate ($R(U)np$). This value is the inverse of the lifetime and has features that are associated with the parameters of recombination centers. The reduced recombination rate is defined as [22]:

$$R_{pr} = \frac{I_r(U)}{eSw(U)n_i\left[\exp\left(\frac{eU}{2kT}\right)-1\right]}\frac{e(V_d-U)}{2kT} = \frac{c_n c_p n_i N_t\left[\exp\left(\frac{eU}{2kT}\right)+1\right]}{2n_i\sqrt{c_n c_p}\exp\left(\frac{eU}{2kT}\right)+n_1 c_n + p_1 c_p} \quad (4.8)$$

The dependence of the reduced recombination rate on the bias voltage is shown in Fig. 5. This curve consists of two sections. Eq. (4.8) is described by the following dependency, then

$$2n_i\sqrt{c_n c_p}\exp\left(\frac{eU}{2kT}\right) < n_1 c_n + p_1 c_p :$$

$$R_{pr} = c_p\left(\frac{m_p^*}{m_n^*}\right)^{3/4} N_t \exp\left(-\frac{E_g - E_{tn}}{kT}\right)\exp(eU/2kT). \quad (4.9)$$

Eq. (4.8) is described by the following dependency, then: $2n_i\sqrt{c_n c_p}\exp\left(\frac{eU}{2kT}\right) > n_1 c_n + p_1 c_p$:

$$R_{pr} = R_{pr}^{\max} = \sqrt{c_n c_p}N_t/2. \quad (4.10)$$

We will define the value of U_0 as the voltage at which the condition ($R_{pr} = R_{pr}^{\max}/2$) is satisfied, then $c_n n_1 + c_p p_1 = 2n_i\sqrt{c_n c_p}\exp\left(\frac{eU_0}{2kT}\right)$. We will assume that the energy of the recombination center lies above the middle of the forbidden band, i.e., $c_p p_1 << c_n n_1$ and we find:

$$E_{tn} = \frac{E_g - eU_0}{2} + \delta, \text{ where: } \delta = \frac{kT}{2}\ln\left(\frac{1}{4}\frac{c_n N_c}{c_p N_v}\right). \quad (4.11)$$

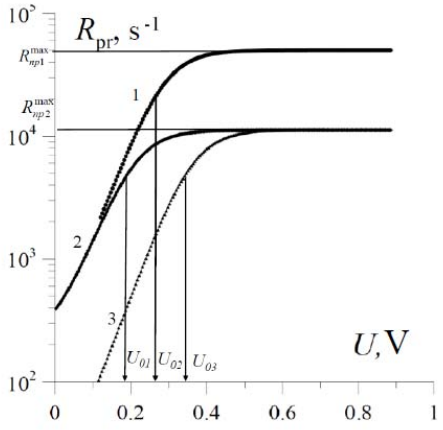

Fig. 5: Modeling the reduced recombination rate for a recombination center with an activation energy of 0.4 eV and three ratios of capture coefficients

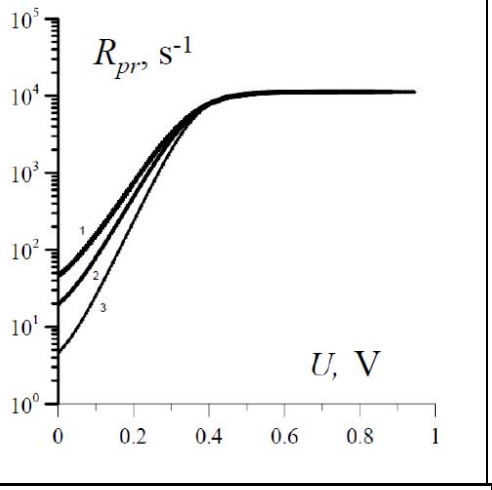

Fig. 6: Modeling the reduced recombination rate of a deep center with activation energy of 0.4 eV at different temperatures [15]*T*, K:
1 - 350; 2- 295; 3 - 220.

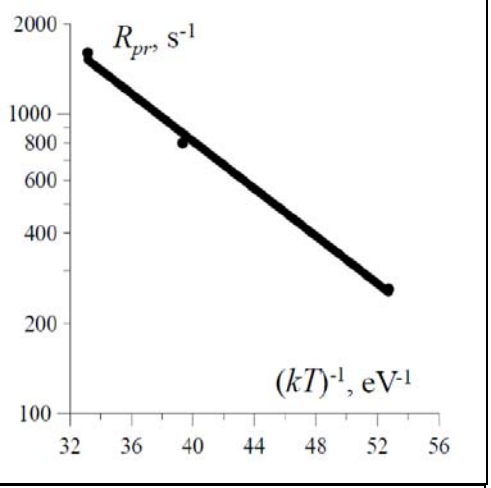

Fig. 7: Temperature dependence of the of reduced recombination rate at U = 0.1 V [15].

The activation energy of this straight line is equal to($E_A = 0.5E_g - E_{tn} - eU_1$)and allows you to calculate the activation energy of the recombination center.

$$E_{tn} = 0.5E_g - E_A - eU_1 \qquad (4.12)$$

The activation energy, which was obtained as a result of the calculation, is equal to the energy of 0.4 eV, at which the simulation was performed.

Thus, the study of temperature dependences allows us to accurately estimate the activation energy, and then the ratio of the capture rate constants using Eq. (4.12).Calculate the ratio of the capture rate constant coefficients by the formula, if you know the voltage at which the reduced recombination rate is halved (U_0), and the level of thermal activation energy:

c_n / c_p : 1 – 1; 2 - 10; 3 –0.1.

Fig. 5 is showing the results of the simulation of the reduced recombination rate for various ratios of the values of the capture coefficients. We took into account that the correction is equal to 0.01 eV for the ratio of the ratio of the effective masses of silicon and can be neglected. The ratio of the capture rate constant coefficients can introduce a certain systematic error. For calculations Fig. 6 this value is 0.06 eV. The reduced recombination rate must be measured at several temperatures to avoid this error. The results are shown in Fig. 6. to simulate the reduced recombination rate at different temperatures. The temperature dependence ($R_{np} = f(1/T)$) at a fixed bias voltage (U_1) is shown in Fig. 7 [15].

$$\frac{c_n}{c_p} = 4\left(\frac{m_p^*}{m_n^*}\right)^{3/2} \exp\left[\left(eU_0 + 2E_{tn} - E_g\right)/kT\right]. \qquad (4.13)$$

If the ratio of the capture rate constant coefficients (c_n/c_p) is known (from other experiments or calculations), then it is possible to calculate the lifetimes in the heavily doped n-type material for the p-type:

$$\tau_{po} = \left(c_p N_t\right)^{-1} = \frac{1}{2}\sqrt{\frac{c_n}{c_p}}\left(R_{pr}^{\max}\right)^{-1},$$

$$\tau_{n0} = \left(c_n N_t\right)^{-1}\frac{1}{2}\sqrt{\frac{c_p}{c_n}}\left(R_{pr}^{\max}\right)^{-1}. \qquad (4.14)$$

Eq. (4.14) allows us to conclude that the temperature dependences of the reduced

recombination rate are determined by the lifetime of charge carriers. We can construct a diagram that shows the relationship between the lifetime with the temperature of the experiment and the level of injection if we use Eq.(4.12) and Eq.(4.14) and the results of the experiment at different and sufficiently close to each other temperatures. This was done in article [23]. We can represent expressions Eq.(4.8) - (4.11) as a function of the lifetimes of electrons and holes when captured by the recombination center Ex.(4.14):

$$R_{pr} = \frac{\frac{\tau_{n0}^{-1}\tau_{p0}^{-1}}{N_t} n_i \left[\exp\left(\frac{qU}{2kT}\right)+1\right]}{\frac{2n_i\sqrt{\tau_{n0}^{-1}\tau_{p0}^{-1}}}{N_t}\exp\left(\frac{qU}{2kT}\right)+c_n n_1};$$

$$R_{prS} \approx \tau_{n0}^{-1}\tau_{p0}^{-1}/2\,;\; R_{pr} \approx \frac{1}{\tau_{p0}}\frac{n_i^2}{n_1}\left[\exp\left(\frac{qU}{2kT}+1\right)\right]. \quad (4.15)$$

Eq. (4.15) are the basis for calculating the parameters of the recombination center. The calculation algorithm is as follows: by Eq. (4.11) we determine the activation energy of the recombination center; we select a certain point with coordinates on the dependence of the reduced recombination rate, then solving the system of Eq. (4.15) together, we obtain the following relations for the characteristic lifetimes:

$$\tau_{n0}^{-1} = \frac{4R_{prS}^2 n_i}{n_1 R_1}\exp\left(\frac{U_1}{2kT}\right);$$

$$\tau_{p0}^{-1} = \frac{n_1 R_1}{n_i}\exp\left(-\frac{U_1}{2kT}\right);\; \frac{c_p}{c_n} = \frac{n_1^2 R_1^2}{4R_{prS}^2 n_i^2}\exp\left(\frac{eU_1}{kT}\right) \quad (4.16)$$

The calculation results are shown in Fig. 7 [23]

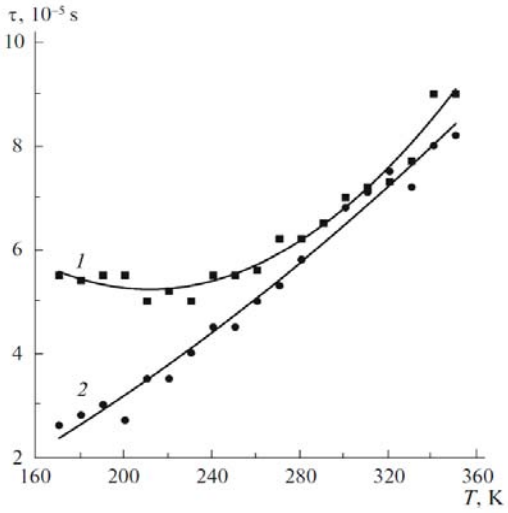

Fig. 8: Temperature dependence of the lifetime through levels with activation energy, eV: 0.45 (1); 0.39 (2).[23].

In order to select areas (in space of the forward bias voltage - the temperature) in which the recombination fluxes pass through these or those centers, we will proceed as follows:

– Plot the temperature dependences of the forward current at various forward bias voltages in the coordinates of Arenius;
– Select straight sections on them and calculate the activation energies;
– Calculate the activation energies of deep centers by Eq.(4.12).

Thus, by finding the activation energy at different bias voltages and temperatures, one can roughly single out the regions where recombination through one or another center predominates. Such a diagram is plotted in Fig. 9.[23].

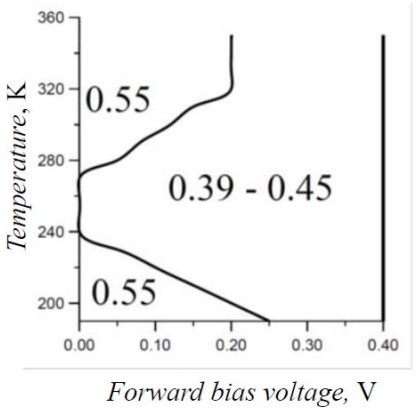

Figure 9: Regions in space of temperatures and forward bias voltages in which recombination through one center or another prevails. The energies of the recombination centers are shown in the figure in eV [23].

Recombination through levels with an activation energy of 0.55 eV prevails in two regions at low temperatures and low biases and at high temperatures and high biases. In the remaining region, recombination dominates through levels with activation energies of 0.39 and 0.45 eV. This behavior of recombination flows is not random. For the 0.55 eV level, in the indicated regions, the lifetime decreases rapidly and it intercepts recombination fluxes. According to Fig. 9. The lifetime for recombination through the levels of 0.39 and 0.45 eV in the region of small displacements increases rapidly. This is due to the fact that in this voltage region the injection level is still small, and the processes of emission from these centers prevail over the processes of capture.

Several recombination centers can exist simultaneously in a semiconductor and the recombination processes with their participation proceed in parallel and independently from each other [16-23]. Recombination currents are added to the total current additively. At the same time, the real dependence is the sum of these processes. The

recombination process proceeds with the participation of three recombination levels belonging to independent recombination centers. This dependence can be expressed by the formula:

$$R_{pr}(U)=\sum_k \frac{c_{nk}c_{pk}n_i N_{tk}\left[\exp\left(\frac{eU}{2kT}\right)+1\right]}{2n_i\sqrt{c_{nk}c_{pk}}\exp\left(\frac{eU}{2kT}\right)+c_{nk}n_{1k}+c_{pk}p_{1k}}. \quad (4.17)$$

The algorithm for dividing an experimental curve into components is based on analytical approximations Eq. (4.15) as well as on the following provisions:

1. The Current-Voltage characteristic of a directly biased *p-n*-junction is measured at voltages less than the diffusion potential (V_d). Note that the measurement points should be quite a lot. The reduced recombination rate (R_{pr}) is calculated for each voltage using Eq. (4.8). The width of the space charge region (w (U)) and the diffusion potential (V_d) are calculated from capacitive measurements.
2. We build a dependency $\ln(R_{pr}(U))$ graph and graphically decompose this dependency into its components.. Each component of the reduced recombination rate has a saturation, the value of which is determined by Eq. (4.8). In the initial area $R_{pri}(U)$ there is a change according to the law $\exp(eU/2kT)$ Eq.(4.83).
3. We find U_{0i} for each curve that characterizes recombination through a single level. Then we estimate the activation energy of the corresponding deep center by the Eq. (4.11), neglecting the value δ. The systematic error, which is associated with neglect δ, is determined by the ratio of the capture rate constant coefficients (c_n / c_p) and, as a rule, has amounts about 0.05 eV at T = 300 K.

Thus, the formulas and calculation algorithm for simple recombination processes can be applied after the separation of complex processes into components.

Thus, one can approximately find the parameters of deep centers from current-voltage and voltage-farad measurements at each fixed temperature. These measurements can be made even on a semiconductor wafer and carry out the screening of diodes on the basis of the presence of deep centers even before dividing the wafer into separate semiconductor devices.

V. Determination of the Parameters of the Electron-Phonon Interaction by Analyzing the Temperature Dependences of Direct Currents.

The analysis of current-voltage characteristics does not allow calculating the concentration of recombination centers, but this can be done by the thermostimulated capacitance (TSC) or DLTS methods. The lifetime of electrons and holes during capture at the recombination center is related to the concentration of deep centers and the coefficients of capture of electrons and holes at the center using the relations:

$$\tau_{po}=(c_p N_t)^{-1}=\frac{1}{2}\sqrt{\frac{c_n}{c_p}}\left(R_{np}^{\max}\right)^{-1}, \quad \tau_{n0}=(c_n N_t)^{-1}=\frac{1}{2}\sqrt{\frac{c_p}{c_n}}\left(R_{np}^{\max}\right)^{-1}. \quad (5.1)$$

The current-voltage characteristics were measured in the range of 290–343 K [15].

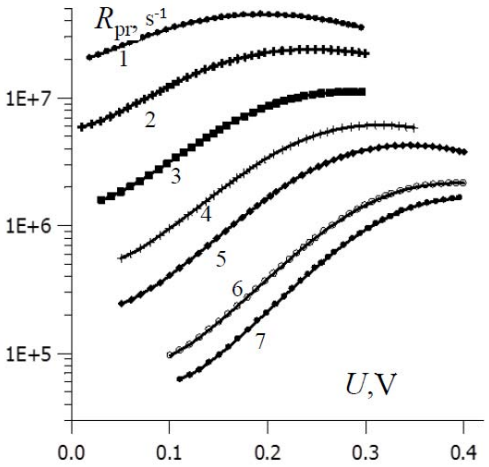

Fig. 10: Temperature dependence of the superficial recombination rate, T, K: 1 – 343; 2 – 333; 3 – 323; 4 – 313; 5 – 303; 6 – 294; 7 – 290 [15]

The temperature dependences of the reduced recombination rate are shown in Fig. 10. The strong temperature dependence of the saturation region of a given value takes place. The separation of the reduced recombination rate into components was done for each temperature independently and the capture rate constant coefficients of holes and electrons for them were calculated. The results of the calculations are shown in Fig. 11 at the normal scale, and in fig. 12 - semi-logarithmic. In addition, analytical approximations are defined for all capture rate constant coefficients in the form:

$$c_i = c_{0i} \exp\left(-\frac{E_{bi}}{kT}\right)$$

$$E_t = 0.53эВ\begin{cases} c_n = 8.6\exp\left(-\dfrac{0.30}{kT}\right) \\ c_p = 1.9*10^8 \exp\left(-\dfrac{0.85}{kT}\right) \end{cases} \qquad E_t = 0.45эВ\begin{cases} c_n = 0.022\exp\left(-\dfrac{0.16}{kT}\right) \\ c_p = 10^3 \exp\left(-\dfrac{0.57}{kT}\right) \end{cases} \tag{6.1}$$

Where: E_{bi} is energy of nonradiative transition from excited to ground states.

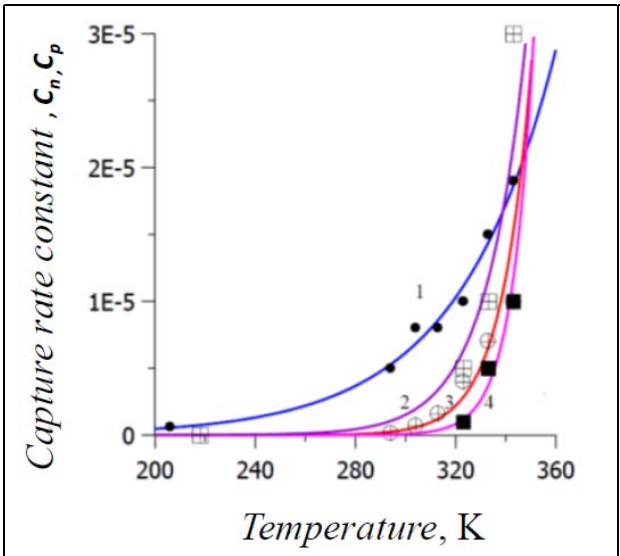

Fig. 11: Temperature dependences of the capture rate constant coefficients of deep centers with activation energies [15]:

2, 4 - 0.53eV; 1,3 - 0.45 eV.

1,2–C_n; 3,4 –C_p.

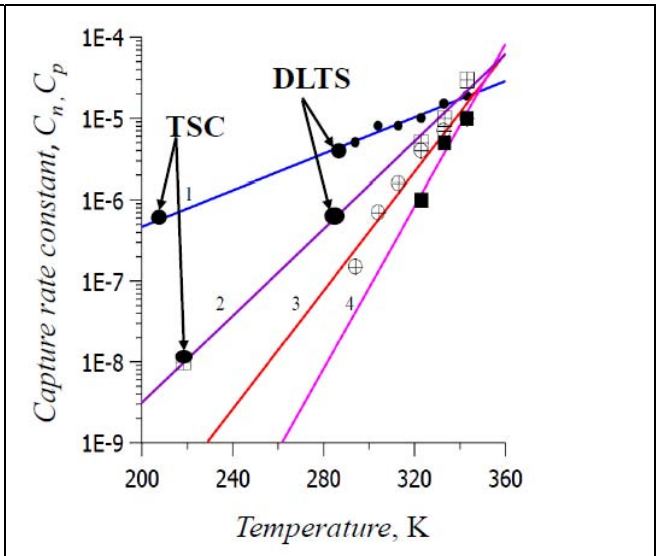

Fig. 12: Temperature dependences of the capture rate constant coefficients of deep centers with activation energies [15]:

2, 4 - 0.53eV; 1.3 - 0.45 eV.

1,2 –C_n; 3,4 –C_p :

The results of measuring the capture rate constant coefficients by various methods are consistent with each other. The capture rate constant coefficients, which were calculated from the TSC and DLTS experiments, are less than the results of calculations from the current-voltage characteristics. This fact is due to the strong temperature dependence of these coefficients and the fact that they were measured at different temperatures. The temperature at which these coefficients were calculated from TSC experiments is the lowest, so their value is the smallest. The agreement of the results is there shows the correctness of the used models, experiments and calculations.

To determine the parameters of the electron-phonon interaction, we use the characteristic energies of non-radiative transitions[15]. This energy corresponds to the energy in the configuration diagram. It is associated with the parameters of the electron-phonon interaction as follows:

$$E_{Bi} = \frac{(E_0 - s\hbar\omega)^2}{4\ s\hbar\omega}. \tag{6.2}$$

Where: S is Huang and Rhys factor, which is equal to the number of phonons involved in the electron-vibrational transition; $s\hbar\omega$ is heat release in the theory

of electron-phonon interaction. This value is equal to the energy that is transmitted to the lattice during the non-radiative capture of an electron or hole to a deep center.

We will take the energy that must be expended for the non-radiative ejection of an electron from a deep center as the second quantity to be calculated. These energies were determined experimentally from current-voltage characteristics and are 0.45 and 0.55 eV. In the configuration diagram, they correspond to the energy E_{tj}. In our notation, this value, and it is associated with the parameters of the electron-phonon interaction as follows:

$$E_{tj} = E_0 + E_B = \frac{(E_0 + s\hbar\omega)^2}{4\, s\hbar\omega}. \qquad (6.3)$$

We get the desired parameters when we decide together Eq.(6.2) and Eq.(6.3):

$$s\hbar\omega = \left(\sqrt{E_{tj}} - \sqrt{E_B}\right)^2$$

$$E_0 = \left(\sqrt{E_{tj}} - \sqrt{E_B}\right)\left(\sqrt{E_{tj}} + \sqrt{E_B}\right) \qquad (6.4)$$

$$\sigma = \sqrt{2kT\, s\hbar\omega}\,. \qquad (6.5)$$

Thus, the strength of the electron-phonon interaction is mainly determined by heat generation and leads to an increase in the emission rate in an electric field.

The results of calculations and experiments performed on two recombination centers are summarized in Table. 1

Table 1: Parameters of deep centers taking into account the electron-phonon interaction

№	E_{nt}, eV	E_{pt}, eV	E_{n0}, eV	E_{p0}, eV	E_{Bn}, eV	E_{Bp}, eV
1	0.45	2.8	0.29	0.83	0.16	0.57
2	0.53	6.2	0.23	0.89	0.30	0.85
	$s\hbar\omega$, eV		N_t, cm^{-3}	C_{n0}, cm^3s^{-1}	C_{p0}, cm^3s^{-1}	σ, eV
1	0.073		$3*10^{11}$	0.022	1000	0.061
2	0.082		$4*10^{11}$	8.6	$1.9*10^8$	0.065

Table1 represents a complete set of parameters for two deep centers that allow one to calculate all the thermal, optical, and field dependences of deep centers.

VI. Analysis of Current-Voltage Characteristics by the Example of the Silicon Photodetectors before and after Irradiation

Forward and reverse CVC before and after irradiation of the silicon photo detectors are shown in Figure 13 [16]. In the initial section of the CVC with forward bias, an increase in current was observed after irradiation. Since the current in this region is due to recombination in the SCR, we can conclude that the concentration of recombination centers increases. Reverse current also increased. The current through the diode at the reverse bias is due to generation in the SCR and is proportional to the concentration of recombination centers. The generation current after irradiation increased 10 times. It can be assumed that the concentration of recombination centers increased 10 times after irradiation.

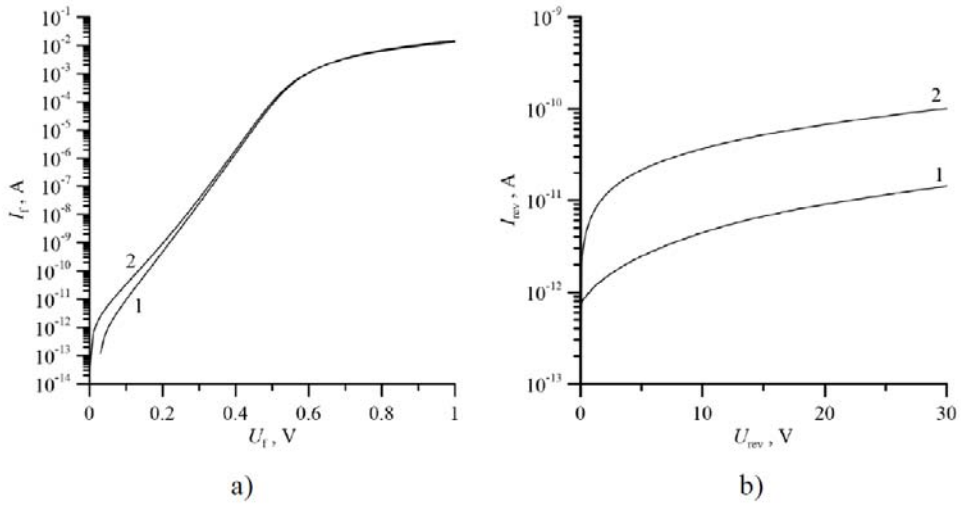

Figure 13: Forward (a) and reverse (b) current-voltage characteristics at room temperature before (1) and after (2) irradiation [16]

Reverse CVC plotted in coordinates $\ln(I) = f\left(F^{1/2}\right)$(where *F* is the electric field strength in the SCR of the diode) are linear (see Fig. 14). These facts indicate that the current through the diode at the reverse bias is caused by generation and the Pool-Frenkel effect takes place, which lowers the height of the generation barrier in proportion to the root of the electric field strength [15].

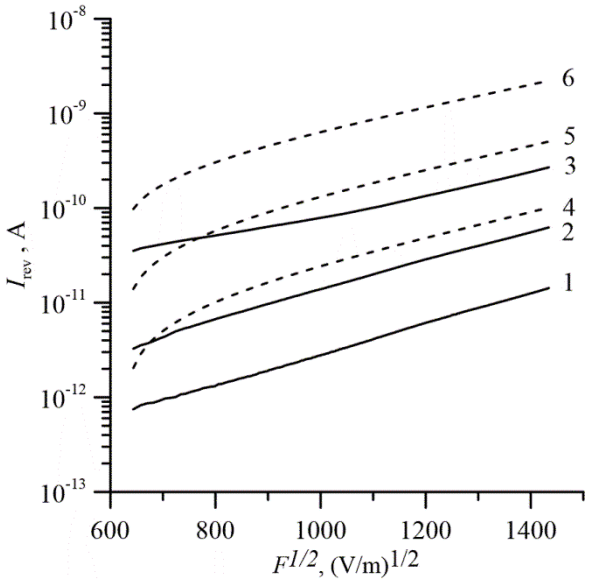

Figure 14: CVC plotted in Poole-Frenkel coordinates before irradiation (1,2,3) and after irradiation (4,5,6) measured at temperatures [16],°C: 1,4 - 0; 2.5 to 20; 3.6 -4.0

The temperature dependences of the reverse current plotted in the Arrhenius coordinates for various reverse bias voltages on the diode (see Fig. 15) allow us to determine the generation energies of charge carriers at various electric field strengths in the SCR of the p-n junction. We must pay attention to the fact that the energies that are calculated from the Arrhenius dependences correspond to 0 K. These energies, which were calculated from the slope of the experimental CVC(see Fig. 15), depend on the electric field (see Fig. 16), which is also a manifestation of the Poole-Frenkel effect.

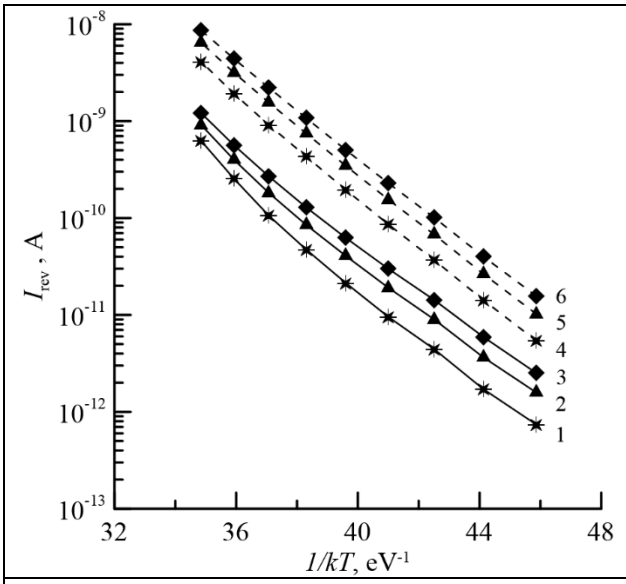

Fig. 15: Temperature dependences of the reverse current before irradiation (1-3), and after (4-5) atvoltages, V: 1.4 -10; 2.5 -20; 3.6-30.

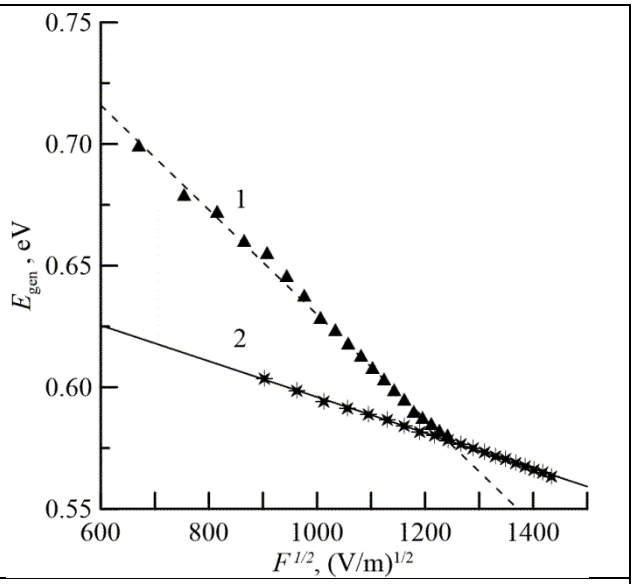

Fig. 16: Change in the activation energy of the generation process depending on the electric field: 1 - before irradiation; 2 – after irradiation.

The experimental data presented show that the generation and recombination processes involving recombination centers determine the magnitude of the forward and reverse currents of the diodes. We will determine the parameters of these centers from the CVC.

At reverse voltage, the SCR of the p-n junction is depleted in free charge carriers; the equilibrium between recombination and generation is shifted toward generation. The reverse current is determined by the expression:

$$I_{rev} = qA\int_0^w Rdx \qquad (7.1)$$

Where: R is the generation rate. In the case of generation with the participation of the recombination center (RC), which has one deep level in the band gap of these miconductor, its rate can be found from the system of kinetic equations:

$$R_n = \frac{dn}{dt} = -c_n n(N_t - n_t) + e_n^t n_t$$

$$R_p = \frac{dp}{dt} = -c_p p n_t + e_p^t (N_t - n_t), \qquad (7.2)$$

Where: n_t is the concentration of electrons on RC. When calculating the generation rate, it is taken into account that in thee quilibrium position, we get:

$$I_{rev} = qA\int_0^w \frac{e_n^t(x)e_p^t(x)N_t(x)}{e_n^t(x)+e_p^t(x)}dx, \qquad (7.3)$$

Where: $e_n^t = \gamma_n c_n N_c \exp\left(-(E_C - E_t)/k_B T\right)$, $e_p^t = \gamma_p c_p N_v \exp\left(-(E_t - E_V)/k_B T\right)$; γ_n, γ_p are the degeneration factors of the deep center level for electrons and holes. These factors vary from 0.5 to 2.

It should be noted that the rate of thermal emission depends on the temperature exponentially, therefore, if the RC level differs from the middle of the band gap by (3 −5)kT, then, as a rule, the rate of emission of electrons or holes is much higher than the rate of another transition. We make the following approximations: the recombination level is located closer to the conduction band; RCs are evenly spaced across the SCR; thermal emission rates are independent of the electric field. It turns out a simple expression for the reverse current of the diode:

$$I_{rev} = qAw(U)N_t e_p^t \qquad (7.4)$$

Eq. (7.4) includes the emission rate of holes, not electrons, since the magnitude of the current at reverse bias is determined by the slowest process, namely, the emission rate with higher activation energy. Therefore, in the case of thermal generation through the RC, the energy experimentally obtained is more than half the band gap. Accordingly, the energy of the recombination center at zeroelectric field strength ($E_t(0)$) is related to the activation energy of the generation process (E_{gen}) by the expression:

$$E_t(0) = E_g(0) - E_{gen}(0). \qquad (7.5)$$

Eq. (7.4) shows that the generation current at reverse bias is directly proportional to the concentration of recombination centers and has voltage dependence, however weak. Therefore, it grows after irradiation. Eq.

(7.5), as a first approximation, correctly describes the temperature dependence of the current (see Fig. 14), however, this formula gives a dependence of the current on the reverse bias voltage by square or cubic root, which is due to a change in the width of the depletion region, and it does not follow that the activation energy of hole emission depends on the voltage. The experimentally measured current (see Fig. 14) varies exponentially from the reverse bias voltage, which is due to a change in the probability of emission depending on the electric field strength in the SCR of the p-n junction. Lowering the height of the potential barrier due to the Pool-Frenkel effect[15] has the form:

$$\Delta E_t = \frac{q^{3/2}}{\sqrt{\pi\varepsilon\varepsilon_0}}\sqrt{F} = \beta_F\sqrt{F}\ . \qquad (7.6)$$

The factor in front of the root of the electric field, which is called the Frenkel constant ($\beta_F = q^{3/2}/\sqrt{\pi\varepsilon\varepsilon_0}$), does not depend on the technological parameters of the device, but is determined only by constants. Its value is in practical units0.00023 eV·cm$^{1/2}$/V$^{1/2}$.With the help of formula (7.6), the expression for the CVC of the p-n junction at reverse bias is calculated:

$$I_{rev} = qAe^t_{p0}\int_0^w N_t(x)\exp\left(\frac{\Delta E_t(x)}{kT}\right)dx = qAe^t_{p0}\int_0^w N_t(x)\exp\left(\frac{\beta_F\sqrt{F(x)}}{kT}\right)dx\ , \qquad (7.7)$$

Where: e^t_{p0} is the hole emission rate without taking into account the influence of the electric field.

Eq. (6.7) takes into account the effect of both temperature and electric field strength. The energy of the generation process taking into account the Poole-Frenkel effect is:

$$E_{gen}(F) = E_{gen}(0) - \beta_F\sqrt{F}\ , \qquad (7.8)$$

Where: $E_{gen}(0)$ is the energy of the generation process in the absence of an electric field.

This dependence in coordinates $E_{gen}(F) = f\left(F^{1/2}\right)$ looks like a straight line. The approximation of the experimental results in Fig. 16 has the same form, which makes it possible to determine the energy of the generation process in the absence of an electric field ($E_{gen}(0)$) and the experimental value of the Frenkel constant (β_{Fex}). These parameters are shown in Table 2. The electron-phonon interaction leads to the fact that the defect must be characterized by several parameters, and not by one activation energy.

Table 2: Parameters of generation centers, which determine the reverse current before and after irradiation

Experimentaland calculated parameters	β_{Fex}, eVcm$^{1/2}$/V$^{1/2}$	$E_{gen}(0)$, eV	$E_t(0)$, eV	$S\hbar\omega$, eV	E_0, eV	ΔE, eV
Beforeirradiation	21.5·10^{-4}	0.85	0.32	0.003	0.063	0.46
Afterirradiation	7.4·10^{-4}	0.67	0.50	0.045	0.254	0.17

Note: The energy $E_t(0)$ was calculated using formula (19). For silicon $E_g(0) \approx 1.17\ eV$ .The values of the parameters $S\hbar\omega$ and E_0 were calculated from the joint solution of equations(6.3) and (7.9). The values β_{Fex}, $E_{gen}(0)$, ΔE were found from the experiment.

In our case, the experimental values β_{Fex} are several times higher than the theoretical ones, which is associated with the electron-phonon interaction. In the work by S.F. Timashev, it is shown [24] that:

$$\beta_{Fex} = \beta_F\left(1 + \frac{E_0 - S\hbar\omega}{2S\hbar\omega}\right) \qquad (7.9)$$

Eq. (7.8) and (7.9) allow calculating the parameters of the electron-phonon interaction $S\hbar\omega$ and E_0. These parameters are given in Table 2. The value of the experimental Frenkel constant and the thermal activation energy of the generation process in the absence of an electric field *Et(0)* are calculated from the experimental data shown in Fig. 16. The results of calculations are presented in Table 2. These parameters, as well as the energy of thermal activation *Et(0)*, after irradiation take on different values (Table 2).The data given in Table 2 allow us to construct the configuration-coordinate diagrams of the centers, which determine the magnitude of the reverse currents of the p-n junction before and after irradiation. They are shown in Fig. 17.

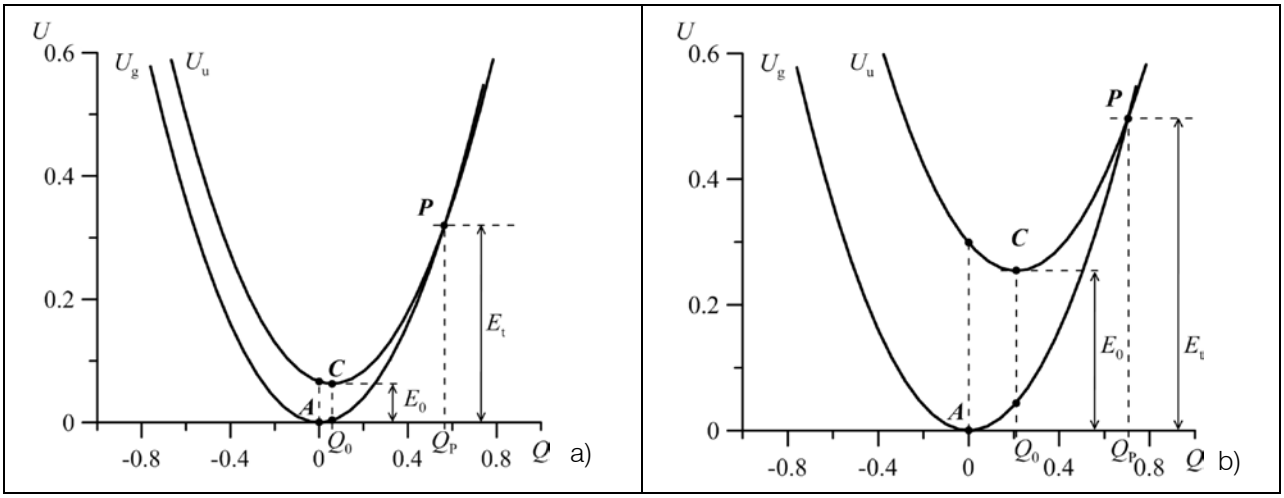

Figure 17: Configuration-coordinate diagrams of recombination centers:
a) before irradiation; b) after irradiation [16]

These diagrams differ in the energies of purely electronic transitions and in the polar on shift, which also indicates a change in the nature of the recombination center after irradiation. The activation energies ΔE for the capture of charge carriers by the recombination center in the classical one-coordinate model and at high temperatures are related to the thermal activation energy $E_t(0)$ and the purely electronic transition energy E_0:$\Delta E=E_t(0)-E_0$ At lower temperatures, the energy E decreases because capture occurs by a tunneling method, rather than activation through a barrier with a maximum at point P. In our case, ΔE agrees with the difference between the thermal activation energy of the RC and the energy of a purely electronic transition.

The polar on shift ($Q0$) and the activation energies of capture to there combination center differ before and after irradiation. The polar on shift before irradiation is smaller, the capture energy is higher than after irradiation, which indicates that the electron-phonon interaction is less pronounced before irradiation. The electron-phonon interaction, as a rule, manifests itself more strongly in molecular objects; therefore, it can be assumed that the nature of the recombination centers found in this work is associated with molecular complexes of a silicon vacancy with an impurity and is consistent with the conclusions of Section 2, according to which, after irradiation, the V2O center appears. It is known that at high irradiation doses in silicon diodes, there are processes associated with the meta stability of such centers and with the Jahn-Teller effect, which are inherent in them [25,26], which is also a manifestation of the electron-phonon interaction.

The experimental results of measuring the reverse currents agree with the analysis of the recombination currents, which show that irradiation results in the formation of centers of two silicon vacancies with oxygen, which also determine the magnitude of the reverse currents of diodes. In this case, the generation of charge carriers is influenced by the electron-phonon interaction. We have developed a technique for determining the parameters of this interaction from the reverse CVC.

VII. Calculation of the Magnitude of the Reverse Currents of P-N-Junctions Taking into Account the Influence of Electron-Phonon Interaction on the Generation of Electrons and Holes in Strong Electric Fields

a) Poole-Frenkel effect

The electric field leads to a decrease in the height of the potential barrier for the generation of an electron or a hole from a deep center to one of the allowed bands. This phenomenon is called the Poole-Frenkel effect and leads to an increase in reverse current as the voltage across the diode rises. The change in the current is is described by the formula (7.7), the lowering of the potential barrier is shows (7.8). The Frenkel constant taking into account the electron-phonon interaction can be calculated by the formula (7.9). The calculation results using these formulas are shown in Figure 18 a. The data in Table 1 were used for the calculation.

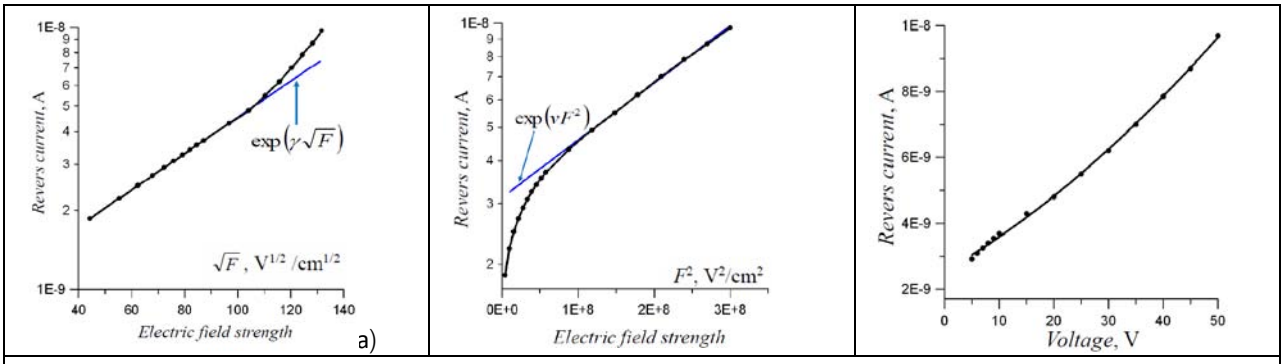

Fig. 18: Reverse current-voltage characteristics of the diodes. Point are experiment. *F* is the electric field strength in the space charge region of the device

The line is approximation by Eq.(7.7)	The line is approximation by Eq.(8.1)	The line is approximation by Eq.(8.5)

The calculation result describes the change in the reverse current in the region of low and medium electric field strengths. At high field strengths, the current increases faster than predicted by dependence (7.7), even taking into account the electron-phonon interaction. We can conclude that the mechanism for the generation of electrons and holes is more complex and that not only the Poole-Frenkel effect but also other phenomena are involved in its formation.

b) Refinement of the Poole-Frenkel theory

Tima she v came to the conclusion that localized states appear in a strong electric field near the allowed bands [24]. Thermal generation is complemented by the tunneling of electrons and holes to these states, and then the charge carriers pass into the allowed conduction and valence bands. Tunneling increases the likelihood of thermal generation. Franz and Keldysh predicted this earlier for optical transitions [11]. Timashev obtained the following expressions for the rate of thermal emission taking into account the strong electric field and electron-phonon interaction, which were experimentally confirmed in [7]

$$e_n^t = e_{n0}^t(0)\exp(\gamma F^{1/2} + \lambda F^2) \qquad (8.1)$$

Where: $\gamma = \beta_F\left[1+\frac{(E_{p0}-s\hbar\omega)kT}{\sigma^2}\right]$; $\lambda = \frac{1}{24}\left[1+\frac{(E_0-s\hbar\omega)kT}{\sigma^2}\right]\frac{q\hbar^2}{m_n^*(kT)^3}$

The first term in the exponent describes the Poole-Frenkel's effect, and the second additional increase in the rate of thermal emission in a strong electric field. Current-voltage characteristic should be linear in the coordinates $\ln(I_{rev}) = f(F^2)$, which is observed experimentally (Fig. 18b).This result confirms the influence of the electron-phonon interaction, which accelerates the processes of emission in an electric field (Eq.(8.1)).Eq. (8.1) there is a good description of the change in the reverse current in a strong electric field, but this approximation is worse at low field strengths.

c) Quantum-mechanical calculation of the probability of an electronic-vibration transition from localized states of deep centers

The calculation of the probability of electronic transitions with the participation of deep centers must be performed taking into account the interaction of an electron or hole with lattice vibrations. Transitions between energy states are called electronic-vibration in this case.

There are two difficulties that are associated with the calculation of such transitions. The first is related to the calculation of the wave functions of the electrons localized at the center. This is a difficult task. It is solved by applying model representations for the wave functions of the deep center. The second difficulty is associated with a lack of information about the nature of the electron-phonon interaction, which has a significant impact on the speed of electronic transitions.

These problems were overcome in works[12, 13]. The expression for the probability of a quantum-mechanical transition, taking into account the electron-phonon interaction, can be written in the form in accordance with this Eq. (3.4)

Eq. (3.4) is written for a situation where the energy spectrum consists of two groups of close levels $(1_i; 2_j)$separated by a large energy gap. Let the electron transition be between singlet states, then:

$$W_{n,p}(F,T) = \int_{-\infty}^{\infty} W_{0n,p}\left(E_{t\,n,p} - \varepsilon\right) f_{n,p}(\varepsilon)\, d\varepsilon \qquad (8.2)$$

Eq. (8.2) is a generalized expression for the probability of an electronic transition, which allows us to calculate the dependences of the probabilities of electronic-vibration transitions on the electric field strength and temperature and not use the single-coordinate model. Such an approach makes it possible to avoid simplifying the complex interaction of electrons with a lattice. This expression can be used for multiphon on thermal, tunnel, and optical transitions. Eq. (8.2) can be used when the formula of a purely electronic

transition is the formula that expresses this mechanism. In the first approximation, we consider that a purely electronic transition is a tunnel one, and the Gauss function is the form-function of the electronic-vibration transition. The probability of a tunnel junction for tunneling through a potential triangular barrier has the form [13]:

$$W_{0n}(E_{ti}-\varepsilon)=\frac{eF}{2\sqrt{2m^*(E_{tn}-\varepsilon)}}\exp\left(\frac{4(E_{tn}-\varepsilon)^{3/2}\sqrt{m^*}}{3\hbar eF}\right) \quad (8.3)$$

Where: $E_{tn,p}$ there is the energy of a purely electronic transition from the deep level to the conduction band or the valence band; *F* is the electric field strength; $f_{n,p}(\varepsilon)$ is a form-function of an electronic-vibration transition. The form-function is:

$$f_{n,p}(\varepsilon)=\frac{1}{\sigma\sqrt{2\pi}}\exp\left(-\frac{(\varepsilon-E_{tn,p})^2}{2\sigma^2}\right) \quad (8.4)$$

The transition probability Eq. (8.9) is equal to the thermal emission rate in Eq. (8.3), then the expression for the reverse current of the diode is:

$$I_{rev}=eSwN_tW_{n,p}(F,T) \quad (8.5)$$

The magnitude of the reverse current of the diode was calculated from Eq. (8.5), taking into account Eq. (8.2) - Eq. (8.4), as well as the data presented in Table. 1. Moreover, we take into account the parameters of transition of holes from the valence band to the level of a recombination center with an energy of 0.53 eV, since this center is located near the middle of the silicon band gap. The calculation results are compared with the experiment in Fig. 18c. The results of the calculation and experiment are in agreement between themselves, which proves the calculations are correct.

The parameters of the electron-phonon interaction can be calculated from experiments on luminescence and light absorption [12, 13]. The EL2 trap plays an important role in gallium arsenide devices. In this regard, relying on the results of [27-29], we will estimate the parameters of the electron-phonon interaction of this trap.

For the calculations, the spectra of the photoionization and absorption cross sections, which are given in [16, 19], and the following algorithm for obtaining the parameters of the electron-phonon interaction were used. The photoionization cross sections for electrons of the recombination center are described by the expression:

$$q_n(h\nu)=G_0\int_{h\nu-\Delta}^{h\nu}\sqrt{h\nu-\varepsilon}\,f_{abs}(\varepsilon)d\varepsilon\,. \quad (8.6)$$

To find the form-function of optical absorption $f_{abs}(h\nu)$, it is necessary to solve equation (8.6), which is the Fredholm integral equation of the first kind. This equation is solved with respect to quant energy $h\nu$ using the integral Riemann-Liouville transformation [12.13]:

$$f(h\nu)=\frac{4}{G_0}\frac{d}{dh\nu}\left\{\int_{-\infty}^{h\nu}\frac{q_n'(\xi)d\xi}{\sqrt{h\nu-\xi}}\right\}=\frac{4}{G_0}D^{1/2}\{q_n'(h\nu)\}\,, \quad (8.7)$$

Where: $D^{1/2}$ is the fractional derivative of degree 1/2. The sought-for form-function was calculated using the Tikhonov's 0th order regularization method, according to which the problem was reduced to solving a system of linear equations:

$$\alpha f_{abs}(h\nu)+\int_a^b k(h\nu,s)f_{abs}(s)ds=w(h\nu),\quad a\le h\nu\le b\,, \quad (8.8)$$

Where: $k(h\nu,s)=\int_c^d K(t,h\nu)K(t,s)dt$, $w(h\nu)=\int_c^d K(t,h\nu)W_{abs}(t)dt$, $K(x,y)=\begin{cases}\sqrt{x-y}, & npu\ x>y\\ 0, & npu\ x<y\end{cases}$,

a,c and b,d here are the lower and upper energy boundaries of the range of measured photoionization rate spectra. The calculation results are shown in table 4.

Table 4: Parameters of the electron-phonon interaction of the EL2 trap

	S	$\hbar\omega_u$, эВ	$\hbar\omega_g$, эВ	E_0, эВ
EL2→E_c	7	0.020	0.019	0.73
E_v→EL2	7	0.021	0.018	0.74

These parameters were used to calculate the reverse current of Ga As-based diodes. The calculation results are shown in Figure 19.

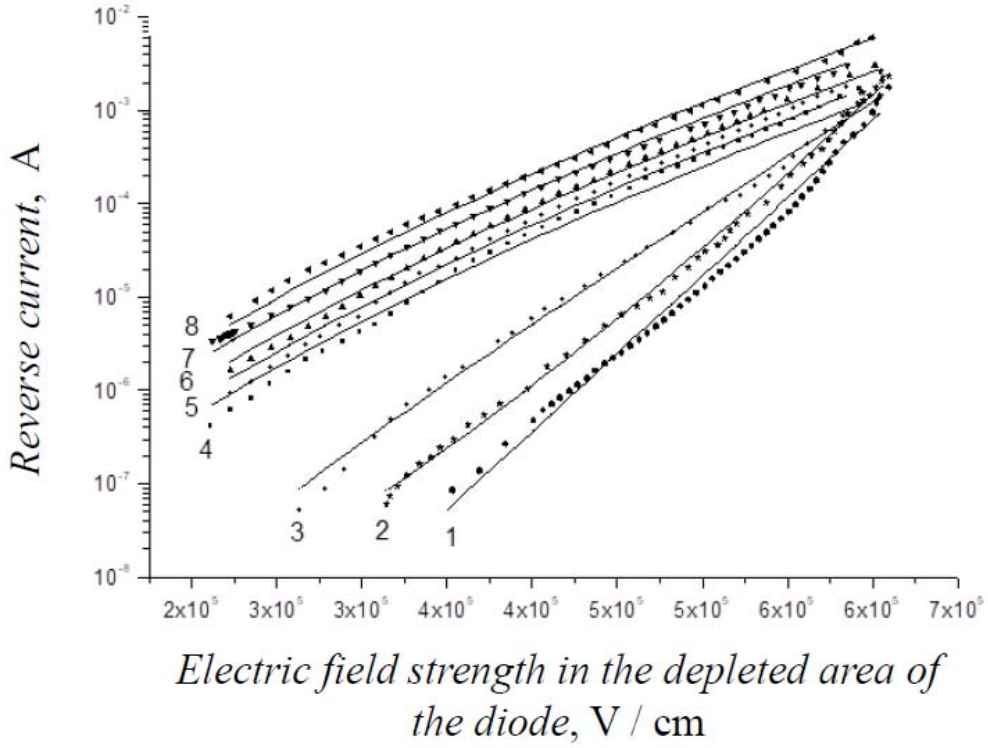

Figure 19: Experimental backward I - V characteristics of p - n junctions based on GaAs (points) and calculation using formula (8.5) (solid lines) at temperatures, K:1 - 88; 2 - 170; 3 - 230; 4 - 295; 5 -303; 6 - 313; 7 - 323; 8 - 333.

The calculation results are in good agreement with the experiment. This proves the adequacy of the theory that is developed in this article, and shows that to calculate the form function, you can use various experiments, and then calculate the magnitude of the reverse currents of semiconductor devices.

VIII. Conclusion

We have developed new approaches to generation-recombination processes in semiconductor materials and devices. Two important factors were taken into account when developing a new recombination model: localization and electron-phonon interaction. The model of exchange between localized states combines generation-recombination processes and charge carrier transport. Therefore, it can be applied to semiconductors with nanostructured ordering and combines the Shockley recombination model with the Mott hopping conductivity model and tunneling. It implies the model of tunnel recombination, which is used in a sufficiently large number of semiconductor structures. We demonstrate the success of this model on the any examples. Thus, we have obtained formula) for the exchange rate between neighboring localized areas. This formula allows you to study the complex transfer mechanisms. It combines such important mechanisms as the Shockley recombination model and the Mott hopping conductivity.

We have developed a model of electron-vibrational transitions of electrons and holes from deep levels to allowed zones, and an expression is obtained for the probability of such a transition from first principles. The results is shown the leading role of the electron-phonon interaction in the ionization of deep centers.

The theory of recombination in the space charge region of semiconductor devices was further developed in this work. The method for determining the parameters of the recombination centers is developed. It is called recombination spectroscopy. This method allows you to determine the activation energy and lifetimes at a constant temperature, including at room temperature. It is simple from the point of view of measurements. It uses standard equipment and allows automation of the determination of the parameters of deep centers. Moreover, it allows measurement directly on a semiconductor wafer, before sorting out semiconductor structures and cutting the wafer into individual crystals.

The calculations and experiments that were performed in this article show the drawbacks of simple classical formulas for describing recombination and generation processes in semiconductor p-n-junctions.

The ideality factor is not constant and depends on the recombination fluxes of electrons and holes, which change as a result of injection. Algorithms for converting current-voltage characteristics are taking place. These algorithms allow one to estimate the parameters of the recombination centers when the temperature of the experiment does not change. Processing current-voltage characteristics together with measurements of the capacitance of p-n-junctions allow us to calculate a large set of parameters of the recombination centers, including the parameters of the electron-phonon interaction. The electron-phonon interaction leads to the fact that the reverse current of p-n-junctions increases with increasing voltage faster, which is predicted by the Poole-Frenkel's theory. This is proved by the calculations and experiments that are carried out in this article. General considerations of a physical nature suggest that the electron-phonon interaction should be stronger when the recombination centers are molecules of the type of complexes of a vacancy with an impurity. Such centers may be weakly associated with the main lattice, and in this case the vibrations of the main lattice less suppress the molecular vibrations inside such centers.

Acknowledgements

This work was supported by the Ministry of Science and Higher Education of the Russian Federation, project No. 0004-2019-0001.

References Références Referencias

1. Shokley W. The theory of p-n-Junction in semiconductor and p-n-Junction transistors.// Bell Syst Tech 1949; 28:435.
2. Sah CT, Noyce RN, Shockley W. Carrier generation and recombination in p-n junctions and p-n junction characteristics. //Proc IRE 1957; 45(9):1228–43.
3. Sah CM, Forbes A. Thermal and optical emission and cross section of electrons and holes at imperfection centers in semiconductors from photo dark junction current capacitance experiment. // Sol State Electron 1970: 13.758-769.
4. Pichler P. "Intrinsic point defects, impurities, and they diffusion in silicon", Springer-Verlag, 2004. 554 p.
5. S. V. Bulyarskiy, N. S. Grushko Generalized Model of Recombination in Inhomogeneous Semiconductor Structures.//Journal of Experimental and Theoretical Physics, 2000; 91, No. 5, 1059–1065.
6. S. V. Bulyarskiy, Yu. V. Rud', L. N. Vostretsova, A. S. Kagarmanov. O. A. Trifonov. Tunneling Recombination in Semiconductor Structures with Nanoscale Disorder. Semiconductors, 2009, Vol. 43, No. 4, pp. 440–446.
7. Bulyarskiy SV, Grushko NS, Gudkin AA. Field dependences of thermal ionization of deep centers in the space charge layer of Au – n-InP: Fe barriers. Semiconductors1975;9:287–91.
8. Makram-Ebeid S. Effect of electric field on deep-level transients in Ga As and GaP. Appl PhysLett 1980;37(5):464–70.
9. Makram-Ebeid S, Lannoo M. Quantum model for phonon assisted tunnel ionization of deep levels in semiconductors. Phys Rev 1982; 25(10):1082–90.
10. Perel Karpus VI. Multiphonon ionization of deep centers in semiconductors in anelectric field. J Exp Theoretical Phys 1986;64:1376–91.
11. Ridley B. Quantum Processes in Semiconductors. 2nd ed. Oxford: Clarendon Press; 1988.
12. Bulyarskiy SV, Grushko NS, Zhukov AV. Calculation of the field dependence of therates of emission of carriers from deep centers based on an experimental form function for the optical transition. J. Exp. Theor. Phys 1999;89(3):547–51.
13. Bulyarskiy SV, Grushko NS, Zhukov AV. Calculation of the probability of nonradiativeelectronic transitions from deep centers in GaAs in the one-coordinate approximation.// Opt Spektrosk 2001;90(3):440–5.
14. S. V. Bulyarskiey, A. V. Zhukov, O. S. Svetukhina, O. A. Trifonov. Effect of Stationary Ionization of Traps Near the Midgapon the Spectrum of Thermally Stimulated Capacitance of Semiconductor Devices// Semiconductors, 2006, Vol. 40, No. 9, pp. 1105–1108
15. S. V. Bulyarskiy The effect of electron-phonon interaction on the formation of reverse currents of p-n-junctions of silicon-based power semiconductor devices.//Solid State Electronics 160 (2019) 107624. doi.org/10.1016/j.sse.2019.107624.
16. S. V. Bulyarskiy, A. V. Lakalin, M. A. Saurov, G. G. Gusarov. The effect of vacancy-impurity complexes in silicon on the current–voltage characteristics of p–n junctions// J. Appl. Phys. 2020. DOI: 10.1063/5.0023411/
17. S. V. Bulyarskiy˘, N. S. Grushko, A. I. Somov, A. V. Lakalin. Recombination in the space charge region and its effect on the transmittance of bipolar transistors.// 1997 American Institute of Physics.@S1063-7826~97!02509-X#. Semiconductors 31 (9), September 1997.
18. S. V. Bulyarskiy , N. S. Grushko, A. V. Lakalin. Differential methods for determination of deep-level parameters from recombination currents of p –n junctions.// 1998 American Institute of Physics, 1063-7826/98/32, Semiconductors 32 (10), October 1998.
19. S. V. Bulyarskiy , M. O. Vorob'ev, N. S. Grushko, A. V. Lakalin Deep-level recombination spectroscopy in GaP light-emitting diodes//1999 American Institute of Physics, 1063-7826/99/33(6)/4/, Semiconductors 33 (6), June 1999.

20. S. V. Bulyarskiy, Determination of the parameters of deep levels from the relaxational delay of breakdown of a p–n junction//1999 American Institute of Physics, 1063-7826/99/33(4)/4. Semiconductors 33 (4), April 1999.
21. S. V. Bulyarskiy , M. O. Vorob'ev, N. S. Grushko, and A. V. Lakalin Determination of the parameters of deep levels using the differential coefficients of the current–voltage characteristics//1999 American Institute of Physics, 1063-7850/99/25(3)/3/. Tech. Phys. Lett. 25 (3), March 1999.
22. S. V. Bulyarskiya, A. V. Lakalin, I. E. Abanin, V. V. Amelichev, and V. V. Svetuhin. Optimization of the Parameters of Power Sources Excited by β-Radiation// Semiconductors, 2017, Vol. 51, No. 1, pp. 66–72.
23. Timashev SF. On the Frenkel effect during thermofield ionization of deep centers in the space charge layer in semiconductors. Phys Solid State 1974;16:804–811.
24. L. I. Murin, V. P. Markevich, I. F. Medvedeva, L. Dobaczewski. Bistability and Electrical Activity of the Vacancy–Dioxygen Complex in Silicon. Semiconductors, 2006, Vol. 40, No. 11, pp. 1282–1286.
25. S. B. Lastovskii, V. P. Markevich, H. S. Yakushevich, L. I. Murin, V. P. Krylov. Radiation-Induced Bistable Centers with Deep Levels in Silicon n+–p Structures// Semiconductors, 2016, Vol. 50, No. 6, pp. 751–755.
26. Silverberg P., Omling P. Samuelson L. Optical cross sections of the two energy levels of EL2 in GaAs // Paper present. At 5th Conf. On Semi-insulating III-V materials. Malmo. Sweden. 1988. P. 369.
27. Reddy C.V., Fung S. and Beling C.D. Nature of the bulk defects in GaAs through high-temperature quenching studies //Phys. Rev.B. V.54, 11290.
28. Bagraev N. T. The EL2 center in GaAs: symmetry and metastabifity//J.Phys. I France 1 (1991) P. 1511-1527.

Global Journal of Science Frontier Research (A) Volume XX Issue XIII Version I Year 2020
40

This page is intentionally left blank

Global Journal of Science Frontier Research: a
Physics and Space Science
Volume 20 Issue 13 Version 1.0 Year 2020
Type : Double Blind Peer Reviewed International Research Journal
Publisher: Global Journals
Online ISSN: 2249-4626 & Print ISSN: 0975-5896

A New Descriptive Paradigm in the Physics of Hadrons, And their Interactions

By G. Guido

Abstract- Here, we report a summary of some works already published. We highlight the existence of a new paradigm in physics of hadrons, based on the idea that quarks, and hadrons are geometric structures of coupled quantum oscillators. The geometric form is "Aurea" (golden), and, so, the representative model is called Aurum Geometric Model (AGM). To realize these structures, the quantum oscillators must be to structure at sub-oscillators, and half-quanta (IQO). To a structure-particle, we associate a structure equation, and, by, an appropriate mathematic procedure, we find the values of hadronic masses, like quarks, mesons, and nucleons.

Keywords: *golden number, IQuO, hadron, quark, proton, neutron, meson.*

GJSFR-A Classification: *FOR Code: 020399*

Strictly as per the compliance and regulations of:

A New Descriptive Paradigm in the Physics of Hadrons, and their Interactions

G. Guido

Abstract- Here, we report a summary of some works already published. We highlight the existence of a new paradigm in physics of hadrons, based on the idea that quarks, and hadrons are geometric structures of coupled quantum oscillators. The geometric form is "Aurea" (golden), and, so, the representative model is called Aurum Geometric Model (AGM). To realize these structures, the quantum oscillators must be to structure at sub-oscillators, and half-quanta (IQO). To a structure-particle, we associate a structure equation, and, by, an appropriate mathematic procedure, we find the values of hadronic masses, like quarks, mesons, and nucleons.

Keywords: golden number, IQuO, hadron, quark, proton, neutron, meson.

I. The Geometric Hypothesis

The start point of a new path in physics is an apparent coincidence [1]: the numerical ratio between the Compton's wavelength ($\lambda\!\!\!^{-}_{pl}$) , and ($\lambda\!\!\!^{-}_{p}$) is:

$$\left(\frac{\lambda\!\!\!^{-}_{p}}{\lambda\!\!\!^{-}_{pl}}\right) = (1{,}301)(10)^{19} \approx (\phi^2/2)(10)^{19} \tag{1}$$

Where (ϕ) is the golden number ($\phi \approx 1{,}618$). The scale factor $(10)^{19}$ can be due to the expansion of the universe, which maintains invariant the relation between physical quantities. Recall the golden segments (Fig. 1):

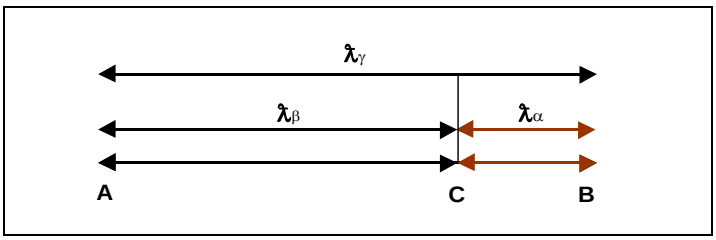

Fig. 1: "Aureus" segments

A property of the is:

$$\begin{cases} \lambda\!\!\!^{-}_{\beta} = \left(\dfrac{\lambda\!\!\!^{-}_{\gamma}}{\phi}\right) \\ \lambda\!\!\!^{-}_{\gamma} = \phi^2 \lambda\!\!\!^{-}_{\alpha} \end{cases} \tag{2}$$

These relations are in a pentagon, between the side, and apothem. As is well known, the protons are composed of three quarks: three centers of elastic diffusion positioned in a triangular form in diffusion experiments with "bullet" electrons. These centers can indicate three vertices in a pentagon, Fig. 2:

Author: e-mail: gioguido54@gmail.com

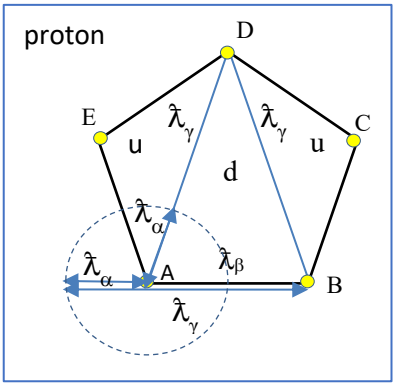

Fig. 2: The internal *geometric* structure of the proton

We could conjecture a proton having a geometric structure, where the component quarks are coincident with three constituent triangles (u,d,u). Specifically [2][3], quarks having a well-defined "***Aurea* G*eometric Structure.*"** We will refer to this as the ***Aurum Geometric Model*** of quarks (AGM), where these particles cannot be punctual objects in Space-Time (see the Quantum Relativistic Theory of fields), but "golden" geometric forms of a not separable set of coupled quantum oscillators. The new paradigm consists, so, of affirm that all massive particles are geometric structures of coupled quantum oscillators (geometric hypothesis**)**. Thanks to AGM, it is possible to explain fundamental issues: the origin of the mass of hadrons, and quarks, the hadron spin, isospin, decay, and other aspect fundamentals. To the geometric form of a particle, we associate a ***structure equation,*** by which we can calculate the masses of quarks, mesons, , and nucleons [4]. So, the proton is a golden particle, , and the three quarks (*u,u,d*) are golden triangles, where [1] the diagonals (AD) or (BD) are proportional to Compton wavelength assigned to the proton ($\lambda\!\!\!^{-}_p = \hbar/m_p c$), thus [$\lambda\!\!\!^{-}_p = k_p \lambda\!\!\!^{-}_u$]. The ($\lambda\!\!\!^{-}_u$) is the Compton wavelength of "free" quark, while (k_p) is a coefficient of "***elastic adaptation***" when *(u,d)* quarks reciprocally bind for origin the proton. Just k_p can be in relation with binding gluons of the *(u,d)* quarks; we point out [$V(r)_{QCD} \Leftrightarrow k_p$], where V(r) is gluonic potential in QCD theory [5][6]; so in this theory, the elastic tension k replaces the potential V(r). The ratio between the masses (both bare, and bounded) of the two quarks is: [$(\lambda\!\!\!^{-}_u / \lambda\!\!\!^{-}_d) = (m_d/m_u) = \phi \approx 1{,}618$] with ($m_d > m_u$)

We can depict the geometric form of a quark [1] by three *spheres* (Vertex) being placed at the vertices of a golden triangle and connected by springs (Joining). We notice that this structure can be realizable only through "particular" quantum oscillators, point out by the acronym (**IQuO**) [7][8]. We emphasize the necessity that the vertex – oscillators, and junction oscillators must have a structure with two "hooks" at the far end. This last aspect induces us to talk about a "sub-structure" into the quantum oscillator, highlighted only in a quantum oscillator coupled to other oscillators (you see forward). Because the three quantum oscillators constitute a unique physical object, *i.e.* a unique quark, they cannot be detected separately, as shown in Fig. 3:

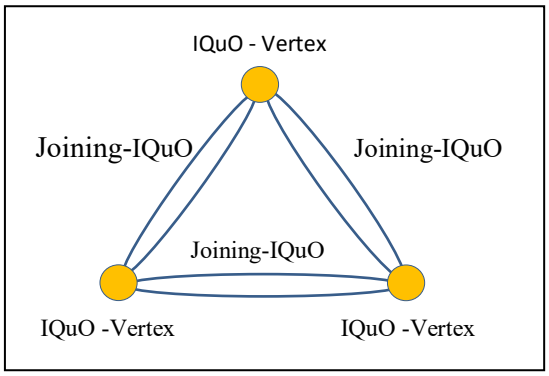

Fig. 3: Quark sub-structure

We have mathematically confirmed the golden hypothesis of two quark (u,d) in two articles [9][10]: we have coupled three quantum oscillators (vertices) placed at energy level (n = 2) with quantum oscillators of junction (sides) at energy level (n = 2) of sides , and base junction (n = 1). In ref. [11], we have also shown the golden geometric structure of quark (s,c,b,t) , and demonstrated that the number of quarks structures is six.

II. The Geometric Structure of the Pion

Recalling the light mesons composed of quark-antiquark pairs, in pion [1], the structure equation is: $[(\pi^{+}) = (u \oplus \underline{d}), (\pi^{-}) = (\underline{u} \oplus d)]$. The elements (u,d) are matrices built by the representative operator of IQuO [1][2]. The sign ($\oplus$) point out the dynamics coupling between quarks; it could involve both gluon coupling, and electromagnetic: $[\oplus = \oplus_g + \oplus_{em}]$. Then, the representation is, see Fig. 4:

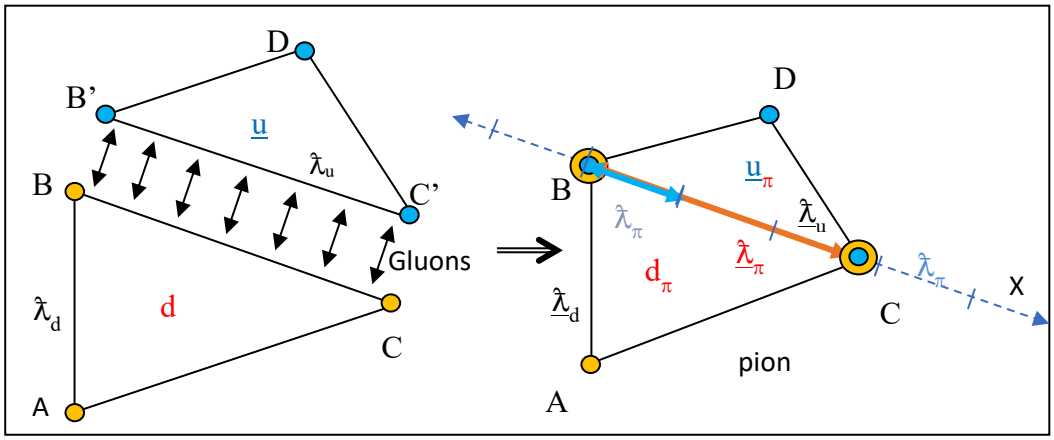

Fig. 4: The geometric form of pion

So, a quadrangular structure (ABDC) expresses a pion propagating along the X-axis. The bonds (gluons) between two ***free*** quarks ($u \Leftrightarrow d$) increases the elastic tension between the IQuO components of quarks $[(k_u , k_d)_{free} \rightarrow (\underline{k}_u , \underline{k}_d)_{bounded}]$: so, increasing the "free" frequencies $[(\omega_u , \omega_d) \rightarrow (\underline{\omega}_u , \underline{\omega}_d)]$ or masses $[(m_u , m_d) \rightarrow (\underline{m}_u , \underline{m}_d)]$. The π-structure is a similar system to two coupled oscillators ($u \Leftrightarrow d$), which oscillates with frequency (ω_π), period (τ_π), and ($\lambda\!\!\!^{-}_\pi$,m_π). Each quark (u,d) contributes to total mass (m_π) with its mass value ($\underline{m}_u$, $\underline{m}_d$), maintaining the golden ratio $[(\underline{m}_d / \underline{m}_u) = \phi]$. We can

admit that in the ($\underline{k}_i$) are contained the mass defects (recall that k replaces the potential V(r)), so that we have [$m_\pi = \underline{m}_u + \underline{m}_d$]. To the frequency ω_π we associate k_π elastic coefficient, which is related to the ***gluon potential*** V(r) of the QCD [5] , and thus, in turn, is related to coupling ($\oplus$).

III. The Quarks' Masses (u,d)

Then, combining the two massive relations in pion, we have [1]:

$$\begin{cases} \underline{m}(u_\pi) + \underline{m}(d_\pi) = m_\pi^{\pm} \\ \underline{m}(d_\pi) / \underline{m}(u_\pi) = \phi \end{cases} \tag{3}$$

with solutions

$$\begin{cases} \underline{m}(u_\pi) = (53{,}31)MeV \\ m(u_\pi)\phi = (86{,}26)MeV \end{cases} \tag{4}$$

Where $m(\pi^{\pm}) \approx (139{,}57)$ MeV.

The two quarks (u_π, d_π) with their gluons are called ***dressed quarks***. We have also calculated the free masses of quarks from mass defect between charged pion, and that neutral π^0. A system of two equations can give the ***bare masses*** of quarks (u,d) if we admit their masses in golden relation:

$$\begin{cases} (1/2)\left[m(u_f) + m(d_f)\right] = \Delta m_\pi^0 \\ m(d_f) / m(u_f) = \phi \end{cases} \Rightarrow \begin{cases} m(u_f) = (3{,}51)MeV \\ m(d_f) = (5{,}67)MeV \end{cases} \tag{5}$$

IV. The Hadron Spin

The possibility of more relative orientations between two quarks implies a reciprocal *rotation* of two quarks *(u*, and *d)* around the X-axis (as orbital motions) [1][2][3]. Thus, these configurations, or orientations, can induce us to think about ***spin*** [4]. If the quarks are fermions, then the oscillation propagating along sides is described by a spinor, with an *intrinsic spin* ($\boldsymbol{s}_q$). Besides, we associate an *orbital spin* ($\boldsymbol{s}_l$) to rotations of (u,d)-quarks around the X-axis. Note the rotations of quarks around X-axis involve the gluons; therefore, there is a *gluonic orbital motion* ($\boldsymbol{s}_g$). This model is so consistent with experimental observations [12][13], where the spin is: [$\boldsymbol{s}_h = \boldsymbol{s}_q + \boldsymbol{s}_l + \boldsymbol{s}_g$]

V. The $\underline{\otimes}$- Operation of Hadronic Mass Calculation

Thanks to the structure equation, it is possible to calculate, by a mathematical procedure, the masses of the light mesons composed of quarks (u, d), and two nucleons. We used a similar procedure to one of QCD but without using its potentials: to incorporate the binding energy of the quarks, consisting of binding gluons, into the global mass of the quarks [1][2][4]:

$$[m_{\text{global hadron}} = m_{\text{quarks}} + m_{\text{binding}}]$$

This way, the bonded quarks inside the hadron would have enough mass to reach the mass value of the hadron. The pion mass can be placed as a base mass to determine the mass of the most massive mesons. We proved (see the calculations in [2][3]) that all light mesons, following the pion, are elaborated structures of pion compositions , and {d,d}-lattice of d-quarks, see the structure equations. However, for obtaining the mesons masses, and nucleons, we need to introduce a new operation of mass calculation ($\underline{\otimes}$-operation). This operation considers both interactions, and ***interpenetration*** between quarks; this last is an aspect purely quantum-undulatory, see the superposition of particles-waves. The latter may exist if we admit that two different structures (states) of coupled quantum oscillators (or quarks) can overlap without exchanging energy. In the global mass of a hadron must be in account all the possible configurations of quark components, both the ones with interpenetration, and the ones with interactions. The $\underline{\otimes}$ operation is a combination of two operations ($\oplus$,$\otimes$): the ($\oplus$) represents dynamics interaction, while the ($\otimes$) is the operation of interpenetration.

The interpenetration must be considered as a mere "representation" of a quantum state associated with different configurations; see Fig. 2, and 4: recall spin connected with possibilities of spatial orientations. Thus, between the interpenetration and spin there is a reciprocal correlation in a quantum way**.** The interpenetration leads us to review the concept of mass of a composite particle. We need to consider all possible configurations of its structure components inside the calculation of its mass. The $\otimes$-operation of interpenetration follows, in algebraic calculations, the properties of the multiplication. Instead, $\oplus$-operation follows, in algebraic calculations, the properties of the sum. For the calculation of meson masses, and mass defects, we have used two functions [(F_m), ($F_{\Delta m}$)]. The (F_m) is an application on the components of the structure equation, which gives us the mass values (m_i) of the component particles.

To obtain the mass defects ($\Delta m > 0$, $\Delta m < 0$), we have used [3] a Function ($F_{\Delta m}$), represented by a matrix A_{ij}, applied to structure equation [3][4], of the mass defects (Δm_i), see table 1:

Table 1: Table of the coupling with the interaction of quarks

$\Delta m(X)$	q_1	q_2	…	q_n
q_1	$\Delta m(q_1, q_1)^{R}{}_{\oplus}$	$\Delta m\ (q_1\ q_2)^{G}{}_{\oplus}$	…	$\Delta m\ (q_1\ q_n)^{B}{}_{\oplus}$
q_2	$\Delta m\ (q_2, q_1)^{G}{}_{\oplus}$	$\Delta m\ (q_2, q_2)^{R}{}_{\oplus}$	…	$\Delta m\ (q_2\ q_n)^{G}{}_{\oplus}$
…	…	…	…	…
q_n	$\Delta m\ (q_n, q_1)^{B}{}_{\oplus}$	$\Delta m\ (q_n, q_2)^{G}{}_{\oplus}$	…	$\Delta m\ (q_n\ q_n)^{R}{}_{\oplus}$

Where q_i are the particles (in mesons are pions) which compose the particle X. Besides, it is $\Delta m(q_i, q_j)^{R,B,G}{}_{\oplus} = \Delta m(q_i \oplus q_j)^{R,B,G}$

Here, we report the values of mesons masses obtained by calculations, see table 2:

Table 2: Mass values of mesons

Meson	Level	Structure Equation	Theory Mass (MeV)	Exper. Mass (MeV)
π^0	1	$[\pi^+ \otimes \pi^-] \oplus [(u \oplus \underline{u}) \otimes (d \oplus \underline{d})]$	(134,97)	(134,97)
η^0	2	$(\pi^0)_r \otimes (\pi^0)_r = (\pi^+ \oplus \pi^-) \otimes (\pi^+ \oplus \pi^-)$	(547,95)	(547,86)
η'	3	$\{(\pi^0)_r \otimes (\eta)\} = (\pi^0)_r \otimes (\pi^0)_r \otimes (\pi^0)_r$	(957,44)	(957,78)
ρ	3	$[(d,\underline{d})_\pi] \otimes \{[(2\pi^+ \oplus \pi^0_r) \otimes (2\pi^- \oplus \pi^0_r)]\}$	(775,49) (774,91)	(775,26)
$\rho^\pm$	3	$[(d,\underline{d})_\pi] \otimes \{[(2\pi^+ \oplus \pi^0_r) \otimes (2\pi^- \oplus \pi^\pm_r)]\}$	(776,44) (777,52)	(775,26)
ω	4	$[(d,\underline{d})_\pi] \otimes \{[(2\pi^+ \oplus 2\pi^0) \otimes (2\pi^- \oplus 2\pi^0)]\}$.	(782,33)	(782,65)
ϕ^0	4	$\phi^0 = \{[(d,\underline{d}) \otimes (2\pi^0 \oplus \eta)] \oplus (\eta)\}$	(1019,87)	(1019,41)

By this model, it is possible to calculate the masses of all other mesons more massive. Not only, but we can also calculate the mass values of the nucleons [4].

VI. The Calculation of Proton Mass

In a preprint [4], we have calculated, by theoretical physics aspects, and suitable mathematical procedure, the masses of the nucleons, while in a next study of light baryons without strangeness (Δ°, Δ^-, Δ^{++}). In light mesons, we highlighted a mass spectrum built employing lattices of base pions $\{\pi\}$, and quarks $\{d,\underline{d}\}$[3]. In proton, the coupling of quarks with interpenetration is expressed [4] by $\underline{\otimes}$-operator: $(q_1 \underline{\otimes} q_2 \underline{\otimes} q_3)$. The product $[u \underline{\otimes} d \otimes \underline{u}]$ implies the combination of all possible configurations between quarks (u, d, u). The structure equation of the proton is:

$$[u_1 \underline{\otimes} d \underline{\otimes} u_2] = \left\{ [(u_1) \otimes (d \oplus u_2)]_{A_1} \oplus [(d) \otimes (u_2 \oplus u_1)]_{A_2} \oplus [(u_2) \otimes (u_1 \oplus d)]_{A_3} \right\}_{A_3} \quad (6)$$

By this equation, and using the F_m-function, the partial proton mass is: m(p) = (964,45) MeV. The mass defect, by the matrix $A_{ij,}$ is, see table 3:

Table 3: Table of the coupling with the interaction of quarks in the proton

$\Delta m^*(p)$	u_1	d_1	u_2
u_1	$\Delta m(u_1, u_1)^R_\oplus$	$\Delta m\ (u_1\ d_1)^G_\oplus$	$\Delta m\ (u_1\ u_2)^B_\oplus$
d_1	$\Delta m\ (d_1, u_1)^G_\oplus$	$\Delta m\ (d_1, d_1)^R_\oplus$	$\Delta m\ (d_1\ u_2)^G_\oplus$
u_2	$\Delta m\ (u_2, u_1)^B_\oplus$	$\Delta m\ (u_2, d_1)^G_\oplus$	$\Delta m\ (u_2, u_2)^R_\oplus$

We obtain the total mass defect of (25,48) MeV. In ref. [3][4] to each element in the red color of the A_{ij} matrix, relative to all mesons, we gave the values of (1,15) MeV. In the proton, we assume the same value. Then, the total mass of the proton is:

$$m_{tot}(p) = m(p) - \Delta m_{\gamma}(p) = [(964{,}45) - (25{,}48)]MeV = (938{,}97)MeV \tag{7}$$

Value very next to that experimental.

VII. New Quantum Aspects

Giving a numerical value of mass defect to the terms $(q_{we} \otimes q_i)_R$ would imply the interpenetration with the interaction of a quark with itself [3][4]. A quark in rotation around an axis is equivalent to a quark with different configurations of itself to the time flow. Recall the QM admit a not space locality: the superposition of states in the experiments with two fissures. A superposition of states in time is possible only in proper space spin, and not in space translations. The new quantum aspects of the proper rotation, and of not time locality of quarks leads us to conjecture that the elements in red color (in diagonal) of the mass defect matrix can represent the kinetic energy of rotation of quarks around to the side AB; see fig. 2. Therefore, we can have $\Delta m\,(q_{we} \otimes q_i)_{\oplus} \neq 0$. To this orbital kinetic energy, we associate in calculations a mass defect negative $\Delta m_{Kin} < 0$.

VIII. The Calculation of Neutron Mass

In works [2][3] for calculating the mass values of mesons, we needed to admit the presence of a background lattice of pairs {d,$\underline{d}$}, which comes included in the structure equation of mesons. The same it also occurs in the light neutral nucleon, in a submission [4], where a couple (d,$\underline{d}$), belonging to background lattice, is being in "loan" for being incorporated in the structure: then, it needs to add, into calculations of mass a quarks' pair (d,$\underline{d}$). Therefore, the structure equation could be:

$$(n) = 3\kappa_n\left(\left\{(d \otimes \underline{d})_A \underline{\otimes} [d_1 \underline{\otimes} u \underline{\otimes} d_2]_B\right\}\right) \tag{8}$$

With configuration, fig. 5:

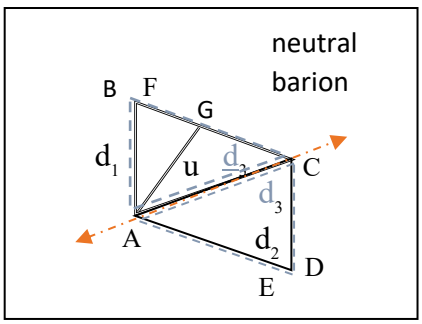

Fig. 5: The neutron configuration

The matrix A_{ij} is, see table 4:

Table 4: Table of the coupling with the interaction of quarks in a neutron

Δm*(n)	d_1	u_1	d_2	d_3	$\underline{d}_4$
d_1	$(d_1\ d_1)^R$	$(d_1\ u_1)^{G1}$	$(d_1\ d_2)^{B1}$	$(d_1\ d_3)^{B1}$	$(d_1\ \underline{d}_4)^{G2}$
u_1	$(u_1\ d_1)^{G1}$	$(u_1\ u_1)^R$	$(u_1\ d_2)^{G1}$	$(u_1\ d_3)^{G1}$	$(u_1\ \underline{d}_4)^{B2}$
d_2	$(d_2\ d_1)^{B1}$	$(d_2\ u_1)^{G1}$	$(d_2\ d_2)^R$	$(d_2\ d_3)^{B1}$	$(d_2\ \underline{d}_4)^{G2}$
d_3	$(d_3\ d_1)^{B1}$	$(d_3\ u_1)^{G1}$	$(d_3\ d_2)^{B1}$	$(d_3\ d_3)^R$	$(d_3\ \underline{d}_4)^{G2}$
$\underline{d}_4$	$(\underline{d}_4\ d_1)^{G2}$	$(\underline{d}_4\ u_1)^{B2}$	$(\underline{d}_4\ d_2)^{G2}$	$(\underline{d}_4\ d_3)^{G2}$	$(\underline{d}_4\ \underline{d}_4)^R$

With mass defect of (19,58) MeV; then, it is:

$$m_{tot}(n) = m(n) - \Delta m_\gamma(n) = \{(959{,}23) - (19{,}58)\} MeV = [(939{,}65)] MeV/c^2 \tag{9}$$

Next to that experimental m(n) = **(939,57) MeV**

IX. The Intrinsic Quantum Oscillators (IQuO)

In sec. one, we have said that, see fig. 3, the oscillators realizing these structures need be "particular" quantum oscillators: the vertex – oscillators , and junction oscillators must have a structure with "hooks"[1][3]: this induces us to talk about a "sub-structure" into quantum oscillator [7][8]. Indication of a "composite structure" in quantum oscillator derives from its wave function, see fig. 6. The probability peaks of detecting the energy quanta in the oscillation can describe some sub-units of oscillation or "sub-oscillators".

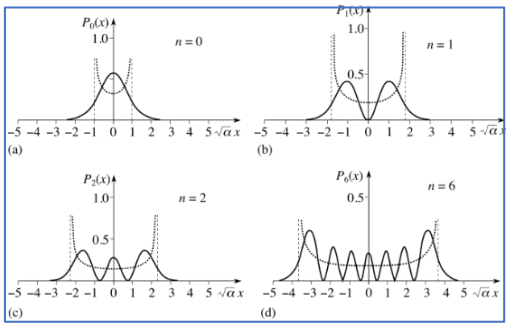

Fig. 6: The probability function of a quantum oscillator

The presence of more components in an oscillator causes the splitting of its quanta of energy into two, and more sub-oscillators: this introduces the idea of half-quanta ("semi-quanta") or individually half-quantum ("semi-quantum"). A quantum oscillator with a sub-structure constituted by sub-oscillators, and "semi-quanta" is an oscillator of type "IQuO" [7][8][10]. The operators (a,a^+), projected in the space of semi-quanta operators, give us the mathematic representation of an IQuO:

$$[\Psi(t)] \equiv \begin{pmatrix} \hat{a}^+_{r'}(t) \\ \hat{a}_{r'}(t) \end{pmatrix} = \begin{cases} \hat{a}^+_{r'}(t) = (\hat{\bullet}^+)_{el}[\exp(ir'\omega t)] + (\hat{o}^+)_{in}[\exp(i(r'\omega t - \pi/2))] \\ \hat{a}_{r'}(t) = (\hat{o})_{el}[\exp(-ir'\omega t)] + (\hat{\bullet})_{in}[\exp(-i(r'\omega t - \pi/2))] \end{cases}$$
$$\text{with } \vec{\Psi}(t) \equiv [\vec{a}^+(t) + \vec{a}(t)] = [(a^+{}_{el}(t) + a^+{}_{in}(t)) + (a_{el}(t) + a_{in}(t))] \tag{10}$$

Where the parameter (r'= ± 1) is connected to the direction of phase rotation, and subscripts [el = elastic component; in = inertial component]. Besides, the operators [(•),(**o**)] are the components of [a,a^+] , and, thus, operators of full semi-quantum (•), with energy [(½) $\hbar\omega$)] , and empty semi-quantum (**o**),with energy [(¼)$\hbar\omega$)]. This representation relieves the presence of an internal degree of freedom into IQuO, which allows of highlight the direction of phase rotation of an oscillator: this direction expresses the electric charge sign. By IQuO oscillators, we can know the meaning of fundamental physical properties [1], such as the mass of the particles, the sign of electric charge [7][8], the Y hypercharge , and the isospin in the quark [9][10][11]. Looking at fig. 6, we can associate to quarks an IQuO at level (n =3), and 3-sub-oscillators. In these IQuO, it is possible to find another internal degree of freedom: the **color charge** [10]. So, in the IQuO model, the sub-oscillators can define the "**gluons**" [10] , and color charge. Here, in the phase plane, we report the representations of the oscillations of the elastic components , and inertial (el, in) associated with the gluon (RB), see fig. 7:

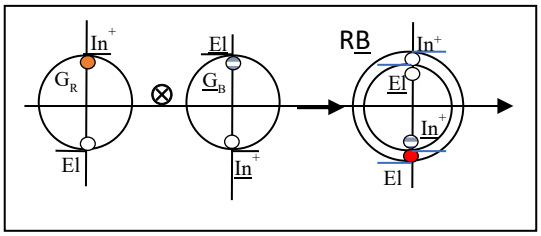

Fig. 7: The RB-gluon

X. Conclusions

Thanks to this paradigm, innovative solutions to experimental problems about particles can be exposed. The IQuO idea (and the AGM) allows us of:

- calculate the masses of quarks, and hadrons using the structure equations by of calculation operations.
- know the origin of the electric charge, and color
- know the gluon structure
- find the structures of leptons, and bosons W, Z
- show decay, and interactions of particles

So, the IQuO idea (, and the AGM) constitutes a new paradigm in physics that allows us of describes with depth the physical phenomenon of particles, and to open new descriptive scenarios of interactions between particles of the Standard Model.

References Références Referencias

1. G. Guido "The Bare , and Dressed Masses of Quarks in Pions via the of Quarks' Geometric Model" JHEPGC Vol.5 No.4, October 11, 2019, DOI: 10.4236/jhepgc.2019.54065
2. G. Guido "The Theoretical value of Mass of the Light η-Meson via the of Quarks' Geometric Model". (JHEPGC), Vol.6 No.3, July 10, 2020, DOI: 10.4236/jhepgc.2020.63030
3. G. Guido "The Theoretical value of Mass of the Light Mesons via the of Quarks' Geometric Model". Journal of High Energy Physics, Gravitation, and Cosmology, (JHEPGC), Vol. 6 No.3, July 15, 2020, DOI: 10.4236/jhepgc.2020.63031

4. G. Guido “Theoretical Spectrum of Mass of the Nucleons: New Aspects of QM”, preprint in JHEPGC
5. Bazavov et al., “Full non perturbative QCD simulations with 2+1 flavors of improved staggered quarks," A. Rev. Mod. Phys. 82, 1349{1417 (2010), [arXiv:0903.3598 [hep-lat]]
6. T. Ishikawa et al., “Light quark masses from unquenched lattice QCD” CP-PACS , and JLQCD Collaborations, Phys. Rev. D78, 011502 (2008) doi: 10.1103/PhysRevD.78.011502
7. G. Guido “The substructure of a Quantum Oscillator field”, arxiv.org/pdf/1208.0948.
8. G. Guido “The substructure of a quantum oscillator field”. Hadronic Journal, vol.37 Issue (1) (2014) page 83. http://dx.doi.org/10.29083/HJ.37.01.2014
9. G. Guido “Regarding the structure of quarks, and hadrons”. *Hadronic Journal,* 40, Issue (2), 187- 219 (2017) http://dx.doi.org/10.29083/HJ.40.02.2017
10. G. Guido “The origin of the colorcharge into quarks”. Journal of High Energy Physics, Gravitation, and Cosmology, (JHEPGC), Vol.5 No.1 November 16, 2018. http://dx.doi:10.4236/JHEPGC.2019.51001
11. G. Guido, “About structure of Quarks”, *Hadronic Journal,* 40, Issue (3), 221-253, (2017) http://dx.doi.org/10.29083/HJ.40.03.2017
12. S. E. Kuhn, J. P. Chen, and E. Leader “Spin structure of the nucleon-status , and recent results," Prog. Part. Nucl. Phys. [arXiv:0812.3535] [hep-ph]]
13. F. Bradamante “COMPASS, and HERMES contributions to our underst, anding of the Nucleon spin," Prog. Part. Nucl. Phys. 61, 229-237 (2008) [doi: 10.1016/j.ppnp.2007.12.046]

Global Journal of Science Frontier Research: a
Physics and Space Science
Volume 20 Issue 13 Version 1.0 Year 2020
Type : Double Blind Peer Reviewed International Research Journal
Publisher: Global Journals
Online ISSN: 2249-4626 & Print ISSN: 0975-5896

Optical Activity in Weakly Coupled Nonorods

By M. A. Kuntman & E. Kuntman

Abstract- We introduce a matrix method and we derive a formula for phase retardation effects in plasmonic systems. We analyze the circular dichroic response (CD) of two orthogonal Au nanorods in detail and we show that, although, theoretically, circular dichroism for forward scattering is directly proportional to the dipole-dipole interaction between the particles, CD response of the system can be much greater in weak coupling due to the trade off between two different types of phases.

GJSFR-A Classification: *FOR Code: 020599*

Strictly as per the compliance and regulations of:

Optical Activity in Weakly Coupled Nonorods

M. A. Kuntman [α] & E. Kuntman [σ]

Abstract- We introduce a matrix method and we derive a formula for phase retardation effects in plasmonic systems. We analyze the circular dichroic response (CD) of two orthogonal Au nanorods in detail and we show that, although, theoretically, circular dichroism for forward scattering is directly proportional to the dipole-dipole interaction between the particles, CD response of the system can be much greater in weak coupling due to the trade off between two different types of phases.

I. Introduction

Achiral and chiral configurations of coupled plasmonic nanorods manifest circular polarization effects due to the phase difference between the light scattered from different parts of the system. In the Born-Kuhn coupled oscillator model and in its plasmonic versions [1–4] optical activity emerges as a result of the coupling (dipole-dipole interaction) between the particles.

For simple nanosystems, it is usually sufficient to investigate the system's behavior under a single polarization excitation. However, for coupled nanoparticles in three-dimensional space, it is often necessary to study different excitation polarizations and matrix methods comprising all possible modes become important [5–7]. In this note, we examine the optical response of coupled metallic nanorods at the far field by means of the scattering matrix (Jones matrix) of the system. In particular, we study the case of two coupled orthogonal metallic nanorods and derive a formula for the far field circular dichroic response (CD) of the system that depends on two different phase factors besides the electromagnetic coupling coefficient. We observe that the phase due to the chiral geometry is doubled and we show that the CD response of the system can be much greater for weakly coupled particles.

II. The Scattering Matrix

Nanorods are the basic elements of a class of more complex systems. Their optical response can be modeled as oriented dipoles with polarization characteristics similar to that of linear polarizers in a certain interval of photon energy. We assume that the polarizability of each rod is fully anisotropic, i.e., it can polarize only along a particular direction. Hence, scattering properties of a nanorod can be represented by a linear polarizer Jones matrix:

$$\mathbf{J} = \alpha \begin{pmatrix} \cos^2\theta & \cos\theta\sin\theta \\ \cos\theta\sin\theta & \sin^2\theta \end{pmatrix} \tag{1}$$

where α is the Lorentzian polarizability associated with the particle and θ is the orientation angle in the x-y plane.

Author α σ: Baran Sitesi F-6, 52200 Ordu, Turkey. e-mail: makuntman@gmail.com

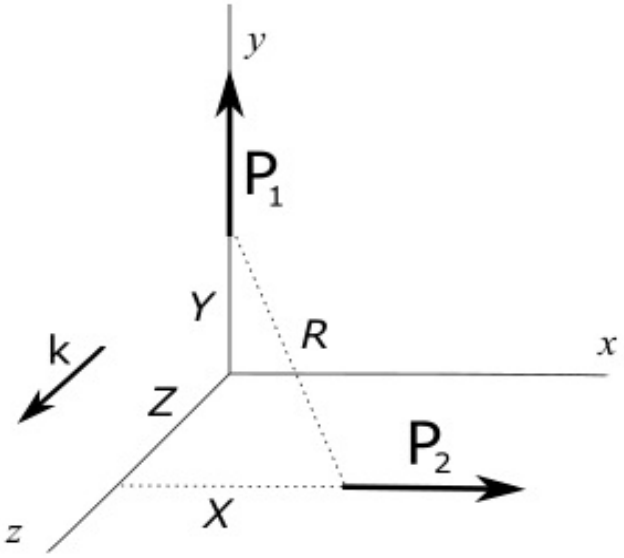

Figure 1: Coupled dipoles (nanorods). CD response is maximum for weak coupling.

We study a chiral configuration of coupled oriented dipoles (nanorods) depicted in Fig.1. Particles are excited by a plane wave that propagates along the z-axis. We calculate the components of the far field electric vector by taking into account the mutual interactions as described in the Appendix.

$$E_x = \frac{F(e_2\varepsilon\alpha E_x + e_1\varepsilon\alpha^2\delta E_y)}{1 - e_1^2\alpha^2\delta^2} \tag{2}$$

$$E_y = \frac{e_2F(e_1e_2\varepsilon\alpha^2\delta E_x + \varepsilon\alpha E_y)}{1 - e_1^2\alpha^2\delta^2} \tag{3}$$

where ε is the permittivity of the medium, E_{0x} and E_{0y} are electric field components at $z = 0$, F is the far field factor, $e_1 = e^{2\pi iR/\lambda}$, $e_2 = e^{2\pi iZ/\lambda}$, δ is the coupling coefficient defined as $\delta = -XYk^2B/R^2$ (B is given in the Appendix). There is an extra e_2 in E_y because the vertical rod is behind the horizontal rod at a distance Z.

From the far field components we extract the Jones matrix of the system:

$$\mathbf{J} = \frac{\varepsilon\alpha F}{1 - e_1^2\alpha^2\delta^2}\begin{pmatrix} e_2 & e_1\alpha\delta \\ e_1e_2^2\alpha\delta & e_2 \end{pmatrix} \tag{4}$$

This is an asymmetric Jones matrix with a non-zero γ parameter which is associated with the circular anisotropy of the system [9]:

$$\gamma = \frac{i(J_{12} - J_{21})}{2} \tag{5}$$

where J_{ij} are the elements of the Jones matrix. According to Eq.(4):

$$\gamma = \frac{\varepsilon\alpha F(1 - e_2^2)e_1\alpha\delta}{2(1 - e_1^2\alpha^2\delta^2)} \tag{6}$$

We also calculate the circular dichroic (CD) response of the system directly from Eq.(4).

$$\Delta I(R,Z,\lambda) = 2i(-J_{11}J_{12}^{*} + J_{12}J_{11}^{*} - J_{21}J_{22}^{*} + J_{22}J_{21}^{*}) \tag{7}$$

where I_{RCP}, I_{LCP} are the scattering intensities corresponding to right- and left-handed circular polarization, and $\Delta I(R,Z,\lambda) = I_{RCP} - I_{LCP}$ is the differential scattering intensity which quantifies the circular dichroic response. By using the property $J_{11} = J_{22}$, Eq.(7) simplifies to

$$\Delta I(R,Z,\lambda) = -4\mathbf{Im}(J_{11}^{*}(J_{12} - J_{21})) \tag{8}$$

In terms of the elements of the Jones matrix given in Eq.(4)

$$\Delta I(R,Z,\lambda) = 8gg^{*}\sin\left(\frac{2\pi Z}{\lambda}\right)\mathbf{Re}\left(\alpha\delta e^{i2\pi R/\lambda}\right) \tag{9}$$

where $g = \varepsilon\alpha F/(1 - e_1^2\alpha^2\delta^2)$.

III. Weak Coupling

In plasmonic models optical activity emerges due to the coupling. As shown in the previous section, the optical activity is directly proportional to the coupling coefficient. When the nanorods are well separated from each other γ and ΔI vanishes, and one may expect that chiroptical effects would increase with decreasing distance. However, according to Eq.(9), for $Z = 0$, the Jones matrix of the system reduces to a symmetric matrix, hence, there is no chiroptical effect for scattering in the z-direction [1]. In short, when $Z = 0$; $\gamma = 0$, $\Delta I = 0$ and, in general, ΔI may not be maximum for too closely packed nanorods. It is worth noting that, there are two phase factors in Eq.(9). $e_2 = e^{i2\pi Z/\lambda}$ is the phase due to the 3D chiral geometry and $e_1 = e^{i2\pi R/\lambda}$ is the phase that involved in the dipole-dipole interaction. Only the imaginary part of e_2 appears in the equation. Maximum of the CD response is determined by the trade off between these two phase factors.

We continue our work with the simulations of the far field scattering intensities I_{RCP} and I_{LCP} corresponding to RCP and LCP excitation polarization states. We observe that it is possible to maximize ΔI by playing with the spatial parameters associated with e_1 and e_2. Especially, for nanorods with length L >200 nm, R can be made very large compared to the size of the rods (weak coupling). As an example, for nanorods with length 400 nm and radius 50 nm, by setting $X = Y = 430$ nm and $Z = 240$ nm ($R = 654$ nm) ΔI is 1/3 of the total intensity at λ_{PR} (plasmon resonance wavelength), i.e., $(I_{RCP} - I_{LCP})/(I_{RCP} + I_{LCP}) \approx 1/3$. BEM simulations for this configuration is given in Fig.2. Dashed line is for ΔI. In the MATLAB implementation of the BEM method [11] we use optical constants of Au by Johnson and Christy [12] (Supplemental Material).

[1] For $Z = 0$, $\Delta I \neq 0$ in other scattering directions [4]

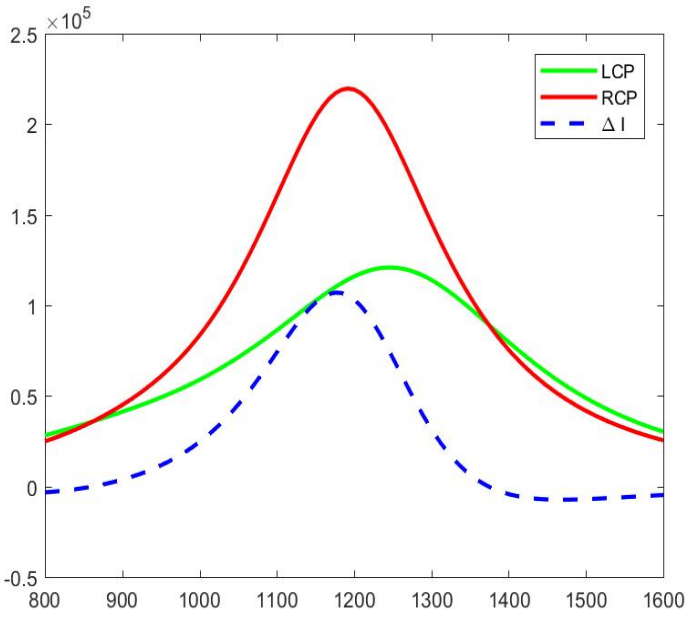

Figure 2: Scattering intensities I_{RCP}, I_{LCP} and ΔI for nanorods of length 400 nm and radius 50 nm with $X = Y = 430$ nm, $Z = 240$ nm.

IV. Conclusion

In the case of coupled nanoparticles in three-dimensional space, it is often necessary to study different excitation polarizations in different scattering directions and matrix methods using all possible modes of excitation become important. In this work, we examine the optical response of coupled metallic nanorods at the far field by means of the Jones matrix of the system. We study the case of two coupled orthogonal metallic nanorods in detail and derive a formula for the far field circular dichroic response of the system that depends on two different phase factors besides the electromagnetic coupling coefficient. We observe that the phase due to the chiral geometry is doubled and the CD response of the system can be much greater for weakly coupled particles.

V. Appendix

When a nanorod is excited by a plane wave the induced electric dipole moment vector, $\mathbf{P}$, is proportional to the incident electric field, $\mathbf{E}_0(\mathbf{r})$:

$$\mathbf{P} = \varepsilon \mathbf{J} \mathbf{E}_0(\mathbf{r}), \tag{10}$$

where ε is the permittivity of the medium at the dipole (nanorod) position and $\mathbf{J}$ is the 2×2 Jones matrix of the nanorod.

When we put two nanorods close to each other we have to consider mutual interaction contributions. Each one of the dipoles experiences the field of the other dipole which should be taken into account to find the actual dipole fields [8]:

$$\mathbf{P}_1 = \mathbf{J}_1[\varepsilon \mathbf{E_o}(\mathbf{r}_1) + k^2 \bar{\bar{\mathbf{G}}}(\mathbf{r}_1 - \mathbf{r}_2) \cdot \mathbf{P}_2], \tag{11a}$$

$$\mathbf{P}_2 = \mathbf{J}_2[\varepsilon \mathbf{E_o}(\mathbf{r}_2) + k^2 \bar{\bar{\mathbf{G}}}(\mathbf{r}_2 - \mathbf{r}_1) \cdot \mathbf{P}_1], \tag{11b}$$

where k is the wavenumber, $\mathbf{J}_1$, $\mathbf{J}_2$ are the Jones matrices of individual nanorods and $\bar{\bar{\mathbf{G}}}$ is the free-space electric dyadic Green's function with the following effect on a dipole vector:

$$\bar{\bar{\mathbf{G}}} \cdot \mathbf{P} = \frac{1}{4\pi R}\left[\left(1 + \frac{i}{kR} - \frac{1}{k^2R^2}\right)\mathbf{P} + \left(-1 - \frac{3i}{kR} + \frac{3}{k^2R^2}\right)(\hat{\mathbf{u}} \cdot \mathbf{P})\hat{\mathbf{u}}\right], \tag{12}$$

where R is the distance and $\hat{\mathbf{u}}$ is the unit vector between the center of masses of particles. The notation can be simplified if we let,

$$A = \frac{1}{4\pi R}\left(1 + \frac{i}{kR} - \frac{1}{k^2R^2}\right), \tag{13a}$$

$$B = \frac{1}{4\pi R}\left(-1 - \frac{3i}{kR} + \frac{3}{k^2R^2}\right), \tag{13b}$$

thus,

$$\bar{\bar{\mathbf{G}}} \cdot \mathbf{P} = A\mathbf{P} + B(\hat{\mathbf{u}} \cdot \mathbf{P})\hat{\mathbf{u}}. \tag{14}$$

We study the circular polarization effects for the geometry given in Fig.3 where $\mathbf{r}$ ($|\mathbf{r}| = R$) is the relative position vector between the dipoles. The plane wave excites $\mathbf{P_1}$ first and excites $\mathbf{P_2}$ after a delay. According to Fig.3 $e_1 = e^{i2\pi R/\lambda}$ is the phase difference between the dipoles along the distance R and $e_2 = e^{i2\pi Z/\lambda}$ is the phase difference in the z-direction. Jones matrix of the first dipole is fixed along the y axis:

$$\mathbf{J}_1 = \alpha_1 \begin{pmatrix} 0 & 0 \\ 0 & 1 \end{pmatrix} \tag{15}$$

The second dipole is tilted at an angle of θ:

$$\mathbf{J}_2 = \alpha_2 \begin{pmatrix} a & b \\ b & c \end{pmatrix} \tag{16}$$

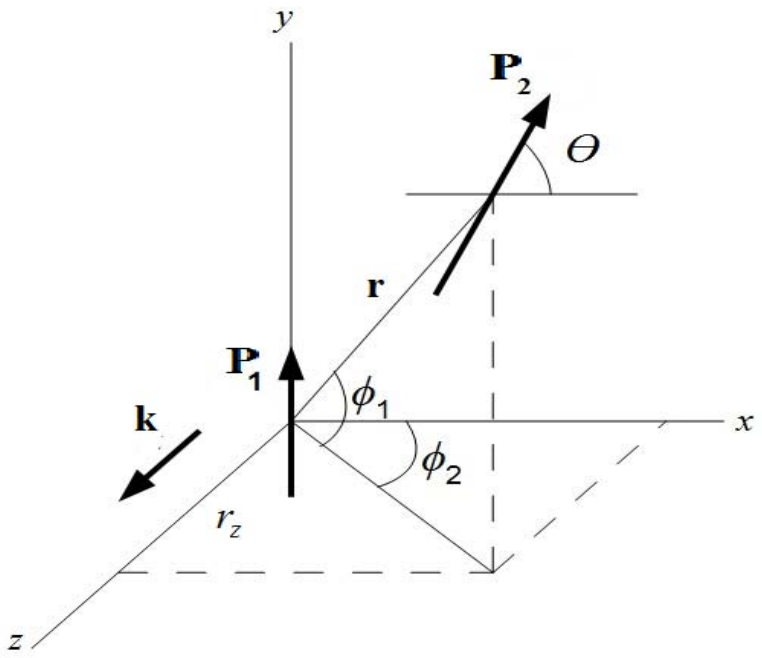

Figure 3: Two oriented dipoles (nanorods)

where α_1 and α_2 are the Lorentzian polarizabilities of the dipoles and $a = \cos^2\theta$, $b = \cos\theta\sin\theta$, $c = \sin^2\theta$. Let $C_1 = \cos\phi_1, S_1 = \sin\phi_1, C_2 = \cos\phi_2, S_2 = \sin\phi_2$ then the unit vector along $\mathbf{r}$ can be written as

$$\hat{\mathbf{u}}(\mathbf{r_2} - \mathbf{r_1}) = (C_1C_2, S_1, C_1S_2) \tag{17}$$

We calculate $\mathbf{P_1}$ and $\mathbf{P_2}$ with the Green function contributions:

$$\mathbf{P}_1 = \varepsilon\mathbf{J}_1\begin{pmatrix}E_{0x}\\E_{0y}\end{pmatrix} + k^2\mathbf{J}_1\begin{pmatrix}e_1AP_{2x} + (C_1C_2P_{2x} + S_1P_{2y})C_1C_2e_1B\\ e_1AP_{2y} + (C_1C_2P_{2x} + S_1P_{2y})S_1e_1B\end{pmatrix} \tag{18}$$

$$\mathbf{P}_2 = \varepsilon\mathbf{J}_2\begin{pmatrix}e_2E_{0x}\\e_2E_{0y}\end{pmatrix} + k^2\mathbf{J}_2\begin{pmatrix}C_1C_2S_1e_1BP_{1y}\\ e_1AP_{1y} + S_1^2e_1BP_{1y}\end{pmatrix} \tag{19}$$

E_{0x}, E_{0y} are the components of the planewave excitation at $z = 0$. We solve the components of the dipoles at the far field for scattering in the z-direction and we find the scattering matrix (Jones matrix) of the interacting system:

$$\mathbf{J} = \frac{\varepsilon F}{N}\left[e_2\alpha_1\begin{pmatrix}0&0\\0&1\end{pmatrix} + e_2\alpha_2\begin{pmatrix}a&b\\b&c\end{pmatrix} + e_1\alpha_1\alpha_2\begin{pmatrix}0&\Delta_1\\e_2^2\Delta_1&(1+e_2^2)\Delta_2\end{pmatrix}\right] \tag{20}$$

where $N = 1 - e_1^2\alpha_1\alpha_2(2b\delta_1\delta_2 + c\delta_1^2 + a\delta_2^2)$, F is the far field factor, $\delta_1 = k^2(A + S_1^2B)$, $\delta_2 = k^2(C_1C_2S_1B)$, $\Delta_1 = b\delta_1 + a\delta_2$ and $\Delta_2 = c\delta_1 + b\delta_2$ are the coupling coefficients that result from the dipole-dipole interaction. Here we write the Jones matrix of the system as a linear combination of three Jones matrices, first two of them corresponding to symmetric

linear polarizer Jones matrices of individual (non-interacting) dipoles and the third one is an asymmetric Jones matrix due to the coupling coefficient and phase (e_2). All elements of the interaction Jones matrix are scaled by coupling coefficients which are functions of the distance between the dipoles so that for distant particles this coupling term consistently vanishes.

As a special case we study a simpler geometry given in Fig.1 where we let $a = 1, b = 0, c = 0$, $\alpha_1 = \alpha_2 = \alpha$, with $\Delta_1 = \delta_2 = \delta$ and $\Delta_2 = 0$. Eq. (20) reduces to the following Jones matrix:

$$\mathbf{J} = g\left[e_2\begin{pmatrix}1 & 0\\ 0 & 0\end{pmatrix} + e_2\begin{pmatrix}0 & 0\\ 0 & 1\end{pmatrix} + e_1\begin{pmatrix}0 & \alpha\delta\\ e_2^2\alpha\delta & 0\end{pmatrix}\right] = g\begin{pmatrix}e_2 & e_1\alpha\delta\\ e_1e_2^2\alpha\delta & e_2\end{pmatrix} \tag{21}$$

where

$$g = \frac{\varepsilon\alpha F}{1 - e_1^2\alpha^2\delta^2} \tag{22}$$

Extremum points of the denominator of the overall factor g determines the intensity peaks corresponding to the hybridized modes which occur at the energies that make $\mathbf{Re}(e_1\alpha\delta) = \pm 1$ [5]. Separation between the higher and lower energy modes decreases and eventually they overlap for large R, but two modes can still be monitored by means of the parameter $e_1\alpha\delta$ which can be found from the Jones matrix.

References Références Referencias

1. W. Kuhn, Zeitschr. Physikal. Chem. 4B, 14 (1929).
2. M. Sch□aferling, Chiral nanophotonics: chiral optical properties of plasmonic systems (Springer, New York, 2017).
3. X. Yin, M. Sch□aferling, B. Metzger, and H. Giessen, Nano Lett. 13, 6238 (2013).
4. A. F. Najafabadi, T. Pakizeh, Analytical chiroptics of 2D and 3D nanoantennas. ACS Photonics 4, 1447{1452 (2017).
5. M. A. Kuntman, E. Kuntman, J. Sancho-Parramon, and O. Arteaga, \Light scattering by coupled oriented dipoles: decomposition of the scattering matrix," Phys. Rev. B 98, 045410 (2018).
6. E. Kuntman, "Mathematical work on the foundations of Jones-Mueller formalism and its application to nano optics," Thesis, University of Barcelona, (2020).
7. M. A. Kuntman, E. Kuntman, O. Arteaga, "Asymmetric Scattering and Reciprocity in a Plasmonic Dimer," Symmetry 12, 1790 (2020).
8. P. Albella, M. A. Poyli, M. K. Schmidt, S. A. Maier, F. Moreno, J. J. Sáenz, and J. Aizpurua, J. Phys. Chem. C 117, 13573 (2013).
9. E. Kuntman, M. A. Kuntman, and O. Arteaga, "Vector and matrix states for Mueller matrices of nondepolarizing optical media," J. Opt. Soc. Am. A 34, 80 (2017).
10. E. Kuntman, M. A. Kuntman, J. Sancho-Parramon, and O. Arteaga, "Formalism of optical coherence and polarization based on material media states," Phys. Rev. A 95, 063819 (2017).
11. U. Hohenester, A. Tr□ugler, "MNPBEM|A Matlab toolbox for the simulation of plasmonic nanoparticles." Comput. Phys. Commun. 2011.
12. P. B. Johnson, R. W. Christy, "Optical constants of the noble metals." Phys. Rev. B 1972, 6, 4370.

This page is intentionally left blank

Global Journal of Science Frontier Research: a
Physics and Space Science
Volume 20 Issue 13 Version 1.0 Year 2020
Type : Double Blind Peer Reviewed International Research Journal
Publisher: Global Journals
Online ISSN: 2249-4626 & Print ISSN: 0975-5896

Research on Conducted EMI Noise Diagnosis Method based on Infomax-WT Algorithm

By Baitong Song, Wu Zhang, Zhou Chen, Hao Ma & Yakang Pei

Nanjing Normal University

Abstract- In this paper, a diagnostic method of conducted EMI noise based on the Infomax-WT algorithm is proposed. Using collected conductive EMI noise samples, several independent noise signals are separated by Infomax. Each noise signal is subjected to wavelet transform to obtain the time-frequency diagram of each noise signal. The noise source is determined according to the frequency characteristic obtained by the time-frequency chart. Finally.

Keywords: electromagnetic compatibility, infomax algorithm, wavelet transform, conducted interference, noise diagnosis.

GJSFR-A Classification: FOR Code: 091301p

Strictly as per the compliance and regulations of:

Research on Conducted EMI Noise Diagnosis Method based on Infomax-WT Algorithm

Baitong Song [α], Wu Zhang [σ], Zhou Chen [ρ], Hao Ma [ω] & Yakang Pei [¥]

Abstract- In this paper, a diagnostic method of conducted EMI noise based on the Infomax-WT algorithm is proposed. Using collected conductive EMI noise samples, several independent noise signals are separated by Infomax. Each noise signal is subjected to wavelet transform to obtain the time-frequency diagram of each noise signal. The noise source is determined according to the frequency characteristic obtained by the time-frequency chart. Finally.

Keywords: electromagnetic compatibility, infomax algorithm, wavelet transform, conducted interference, noise diagnosis.

I. Introduction

At present, the research on conducted electromagnetic interference of electronic equipment mostly focuses on the analysis of the propagation path of conducted electromagnetic interference and the design of EMI filters and other suppression measures. In contrast the research on the diagnosis of interference sources inside electronic equipment is less. In [1], a method of conducted noise diagnosis based on blind source separation was proposed. Literature [2-3] applies the Infomax algorithm to the denoising of EEG signals and proposes an online Infomax algorithm based on the traditional Infomax algorithm, which can effectively eliminate the noise in EEG signals. Literature [4-5] proposed a wavelet transform local feature extraction method to extract the feature of rolling bearing faults, which can effectively diagnose the cause of bearing faults. In this paper, combined with the wavelet transform time-frequency analysis theory, the Infomax-WT algorithm is proposed. The Infomax-WT algorithm is applied to the diagnosis of conducted electromagnetic interference noise, and its feasibility is verified by simulation experiments.

II. Diagnosis Method of Conducted EMI Noise based on Infomax-WT Algorithm

a) Wavelet transform

Compared with the Fourier transform, the wavelet transform is a local transform of space (time) and frequency, to effectively extract information from the signal [6].

Author α σ ρ ω ¥: Nanjing Normal University, Nanjing, Jiangsu China. e-mail: 2499938114@qq.com

Supposing $\psi(t) \in L^2(R)$, $L^2(R)$ represents the square-integrable real number space. That is, the signal space with limited energy, and its Fourier transform is $\hat{\psi}(\omega)$. When the following allowable conditions are met:

$$\hat{\psi}(0) = \int_R \psi(t)dt = 0 \tag{1}$$

$$C_\psi = \int_R \frac{|\psi(\omega)|^2}{|\omega|} d\omega < \infty \tag{2}$$

Where $\psi(t)$ is the mother wavelet or the basic wavelet. After the mother function $\psi(t)$ is stretched and translated, a wavelet sequence is obtained.

For the continuous case, the wavelet sequence is expressed as:

$$\psi_{a,b}(t) = \frac{1}{\sqrt{|a|}}\psi(\frac{t-b}{a}), a, b \in R; a \neq 0 \tag{3}$$

Where: *a* is the expansion factor, *b* is the translation factor, and $\psi_{a,b}(t)$ is the wavelet basis function of the parameters *a* and *b*.

Assuming that the window width of the wavelet mother function $\psi(t)$ is Δt, and the window center is t0, the corresponding window center and window width of the continuous wavelet basis function $\psi_{a,b}(t)$ can be obtained as:

$$t_{a,b} = a_0 + bt, \Delta t_{a,\tau} = a\Delta t \tag{4}$$

Supposing $\hat{\psi}(\overline{w})$ is the Fourier transform of $\psi(t)$, the frequency-domain window width is Δw, and the center of the window is w0, and then:

$$\overline{\psi}_{a,b}(\overline{w}) = \sqrt{|a|}e^{-jwb}\varphi(aw) \tag{5}$$

So this time, the frequency-domain window center and window width are respectively expressed as:

$$w_{a,b} = \frac{1}{a}w_0, \Delta w_{a,b} = \frac{1}{a}\Delta w \tag{6}$$

It can be seen that the time domain and frequency domain window center, and window width of

the continuous wavelet are all functions of the parameter *a*.

$$\Delta t_{a,b} \cdot \Delta w_{a,b} = \Delta t \cdot \Delta w \quad (7)$$

That is, the window area of the continuous wavelet basis function is fixed.

For any function f(t), the continuous wavelet transform on L2(R) can be expressed as:

$$W_f(a,b) =< f, \psi_{a,b} >= |a|^{-1/2} \int_R f(t)\overline{\psi(\frac{t-b}{a})}dt \quad (8)$$

Convert it inversely to:

$$f(t) = \frac{1}{C_\psi}\int_{R^+}\int_R \frac{1}{a^2} W_f(a,b)\psi(\frac{t-b}{a})dadb \quad (9)$$

Where $C_\psi = \int_R \frac{|\overline{\psi}(\overline{w})|^2}{|w|}dw < \infty$ is the admissibility condition of $\psi(t)$.

Moreover, in the process of the wavelet transform, the energy should be kept in proportion, namely:

$$\int_R \frac{da}{a^2}\int_R |W_f(a,b)|^2 db = C_\psi \int_R |f(x)|^2 dx \quad (10)$$

According to the definition of the continuous wavelet transform, wavelet transform is an integral transform and has multi-resolution characteristics. It is realized by the expansion factor *a* and the translation factor *b*. According to the changes of parameters *a* and *b*, the local characteristics of the signal can be obtained. If f(t) is a two-dimensional function, then its continuous wavelet transform is expressed as:

$$W_f(a,b_x,b_y) = \frac{1}{a}\int_{-\infty}^{+\infty}\int_{-\infty}^{+\infty} f(t_1,t_2)\overline{\psi(\frac{x-b_x}{a},\frac{x-b_y}{a})}dxdy \quad (11)$$

Where *bx* and *by* are translations in two dimensions, and the continuous wavelet inverse transform is expressed as:

$$f(x,y) = \frac{1}{C_\psi}\int_0^{+\infty}\frac{da}{a^3}\int_{-\infty}^{+\infty}\int_{-\infty}^{+\infty} W_f(a,b_x,b_y)\psi(\frac{x-b_x}{a},\frac{y-b_y}{a})db_x db_y \quad (12)$$

The characteristic functions of the time-frequency diagram are as follows:

$$M_{SP}(\theta,\tau) = \iint |S_t(\omega)|^2 e^{j\theta(\tau-t)\omega}dtd\omega = A_s(\theta,\tau)A_h(-\theta,\tau) \quad (13)$$

$$A_s(\theta,\tau) = \int s^*\left(t-\frac{1}{2}\tau\right)s\left(t+\frac{1}{2\tau}\right)e^{j\theta t}dt \quad (14)$$

Equation (14) is the ambiguity function of the signal, and the above method can also be used to define the ambiguity function of the window[8] Simultaneous equations (13) and (14):

$$E_{SP} = \iint P_{SP}(t,\omega)dtdw = M_{SP}(0,0) = A_s(0,0)A_h(0,0) = \int |s(t)|^2 dt \times \int |h(t)|^2 dt \quad (15)$$

Therefore, if the energy of the window is set to 1, then the energy of the time-frequency diagram is the energy of the signal, so the energy of the noise signal can be judged by the time-frequency diagram obtained by the wavelet transform time-frequency analysis of the conducted EMI noise signal [9].

b) Simulation Research of conducted EMI noise diagnosis method based on Infomax-WT algorithm

Matlab is used to simulate the basic performance of Infomax-WT algorithm. Three sinusoidal signals are created to form a mixed-signal x(t), which is used to simulate conducted EMI noise signal, namely:

$$x(t) = \sin(2\pi \bullet 100t) + \sin(2\pi \bullet 200t) + \sin(2\pi \bullet 400t) \quad (16)$$

As shown in Fig. 1, the mixed signal is separated into three noise components by the in fomax algorithm, and the waveform of each noise component is shown in Fig. 2. It can be seen that the three noise components are the three noise source signals constructed. Wavelet transform is applied to the three noise components to obtain the time-frequency diagram of each noise component. As shown in Fig. 3, the frequency of each noise component is 100Hz, 200Hz, and 400Hz respectively, corresponding to the three source signals.

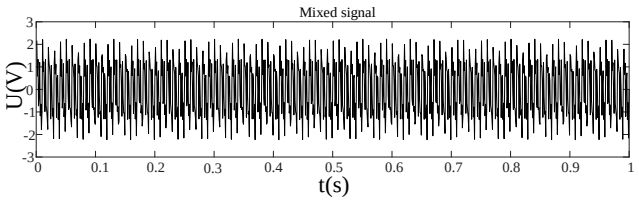

Fig. 1: Time-domain wave of the conducted noise signal

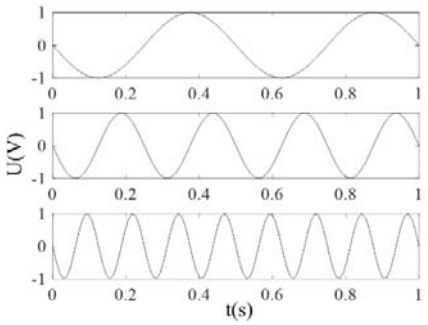

Fig. 2: Waveform of noise components

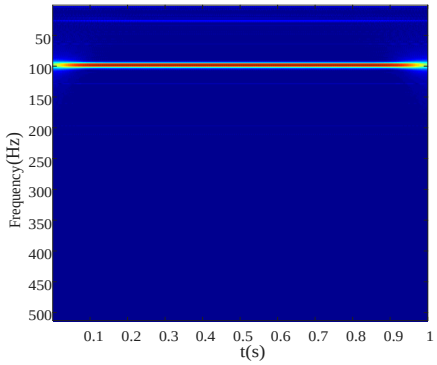

(a) Noise component 1

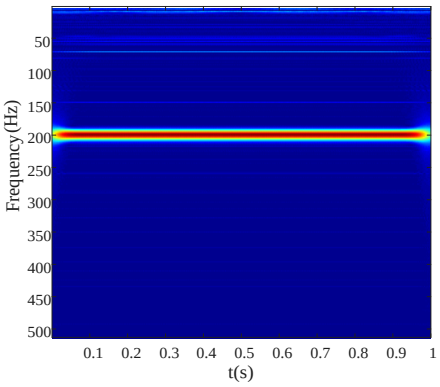

(b) Noise component 2

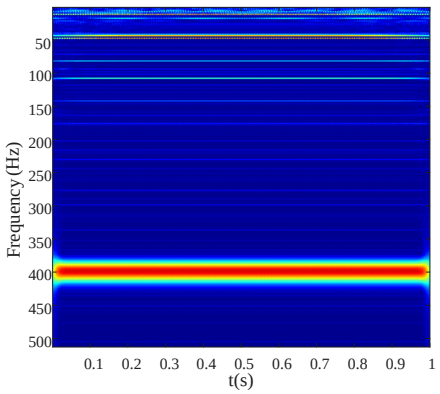

(c) Noise component 3

Fig. 3: Time-frequency diagram of noise components

The results show that the frequency characteristics of each separated noise signal are extracted after separating the mixed conducted EMI noise based on In fomax-WT method, which makes the diagnosis result more accurate.

c) Verification experiment of conducted EMI noise diagnosis method based on Infomax-WT algorithm

The principle diagram of the conducted EMI noise diagnosis method verification experiment is shown in Fig. 4. The resistance values of R1, R2, R3, and R4 are all 50Ω, the capacitance values of C1 and C2 are both 0.1μF. The LISN RF output port is composed of capacitors C1, C2 and R1 and R2. R3, R4 and signal generators V1 and V2 constitute an analog noise source.

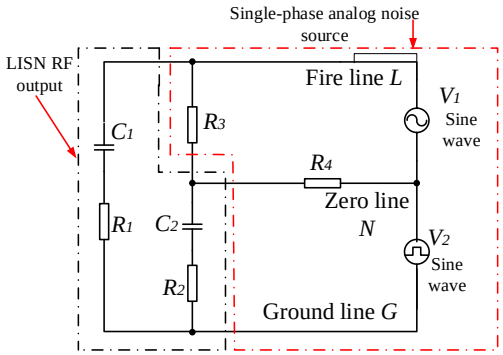

Fig. 4: The principle diagram of the conducted EMI noise diagnosis method verification experiment

*V1*generates a sine wave, and V2 generates a square wave with an amplitude of 4V and frequency of 200kHz and 400kHz, respectively. The noise voltage on the live wire L is the mixed conduction noise of *V1* and *V2*, extracted by resistance R1. The waveform of mixed conducted noise measured by the oscilloscope is shown in Fig. 5.

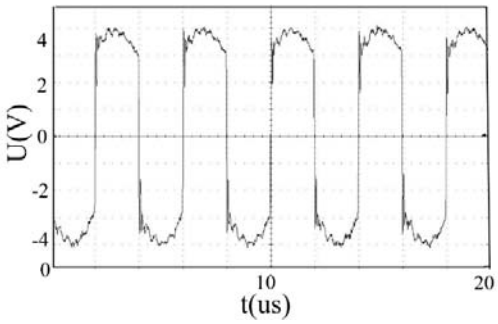

Fig. 5: The waveform of mixed conducted noise

The extracted mixed conducted noise is separated into two noise components by the infomax algorithm, as shown in Fig. 6 (a) and Fig. 6 (b). Compared with the analog conducted noise signal waveform shown in Fig. 5, it can be seen that the waveform characteristics of the two are the same. The frequency characteristics of the separated signal are extracted by wavelet transform, and the time-frequency diagram is obtained. As shown in Fig. 7, the frequency

of the separated signal is 200kHz and 400kHz, respectively, which is consistent with the noise signal frequency simulated by the signal generator. Therefore, it can be determined that the conducted EMI noise sources are *V1* and *V2*.

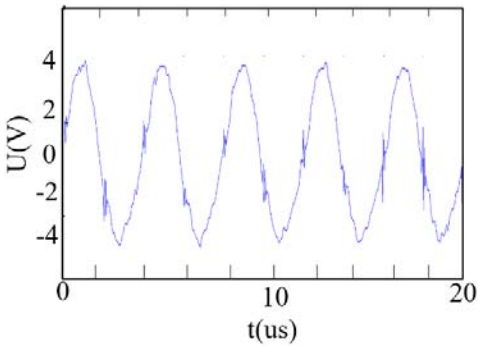

(a) Separated signal 1

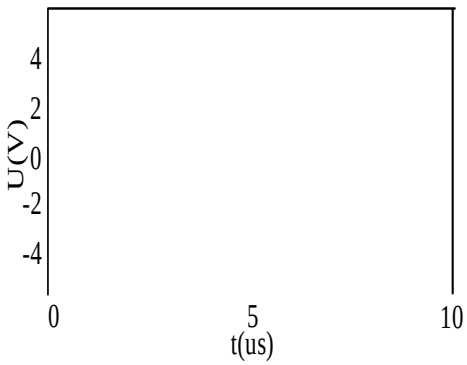

(b) Separated signal 2

Fig. 6: Conducted EMI noise separated by Infomax-WT

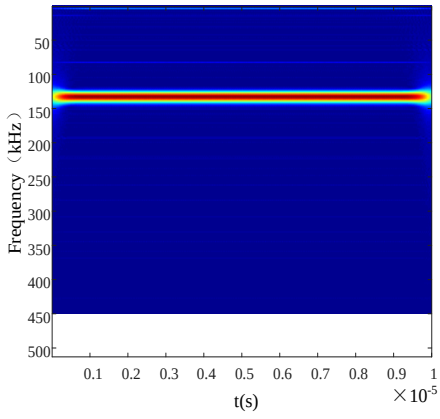

(a)

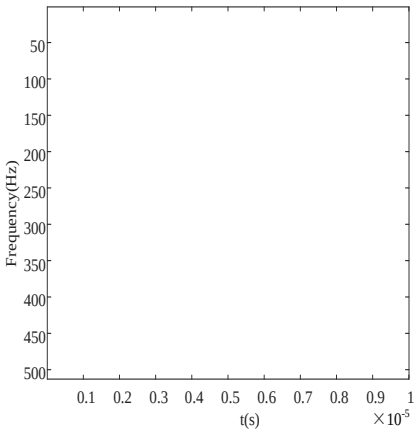

(b)

Fig. 7: Conducted EMI noise diagnosed by Infomax-WT
(a) Signal 1 (b) Signal 2

The experimental results show that the conducted EMI noise diagnosis method based on the Infomax-WT algorithm can accurately diagnose and identify the conducted noise sources with different waveforms and frequencies, which verifies the feasibility and effectiveness of this method.

III. Application of Infomax-WT Algorithm in Conducted EMI Noise Diagnosis and Suppression

a) Problem Description

The test results of the conducted EMI noise of a type of anorectal therapy instrument are shown in Fig. 8. According to the medical equipment industry-standard YY 0505-2012 class B standard, the noise exceeds the standard seriously at 1.9 MHz frequency point.

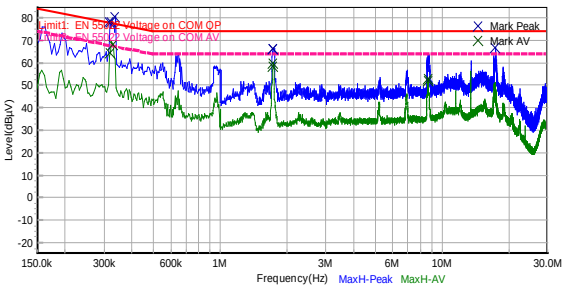

Fig. 8: Conducted EMI noise before rectification

b) Cause analysis and suppression measures

There is a power conversion chip with a high frequency of 2MHZ on the main circuit board. It is preliminarily predicted that the power conversion chip is the main reason for the excessive conducted noise.

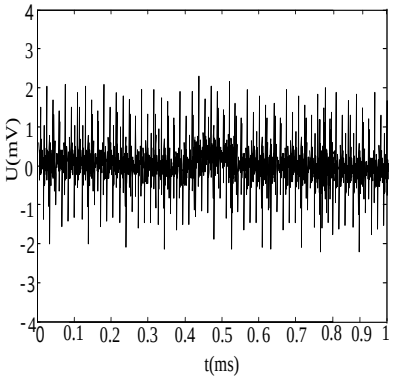

(a) Mixed time-domain signal

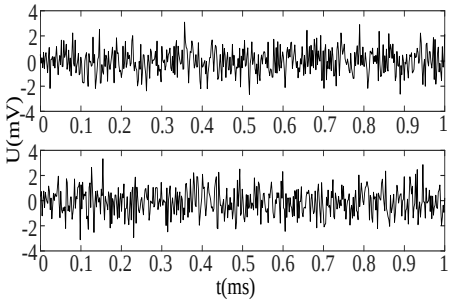

(b) Separated signals

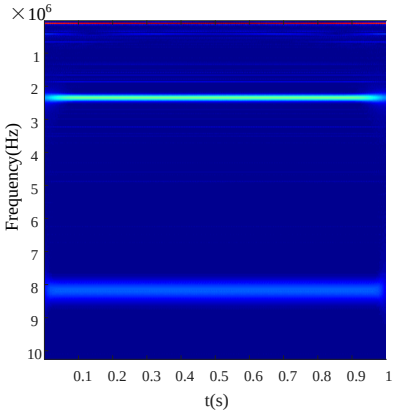

(c)Time-frequency diagram of separated signal 1

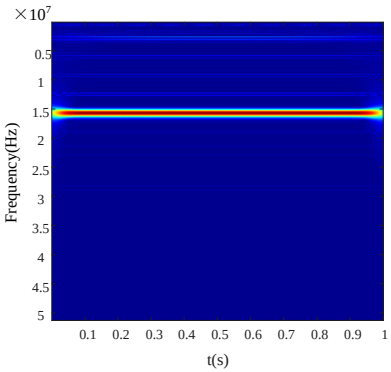

(d)Time-frequency diagram of separated signal 2

Fig. 9: Diagnosis of conducted noise based on Infomax-WT algorithm

To accurately diagnose the noise source with excessive conducted EMI noise, the Infomax-WT algorithm is used to analyze the conducted EMI of the equipment. The time-domain noise is collected by the conducted EMI noise diagnosis system, and the waveform is shown in Fig. 9 (a). The signal characteristics of the separated signals are separated and extracted by the Infomax-WT algorithm, as shown in Fig. 9 (b), 9 (c), and 9 (d), respectively. It can be known that the main noise component is 2MHz and its frequency doubles. Therefore, it can be determined that the 2MHz power conversion chip is the main reason for the excessive conducted noise of the equipment under test.

According to the above noise diagnosis results, the suppression measures are as follows:

1) A T-type EMI filter is connected in series at the entrance of the power line.
2) Clamp the magnetic ring on the signal line.
3) Improve the wiring, increase the distance between the AC power line and the DC power line, isolate the power line and the signal line, and separate the cables on the primary and secondary sides of the transformer.

c) Suppression result analysis

After the suppression measures are taken, the conducted EMI noise test is shown in Fig. 10. It is found that the noise of the equipment has been suppressed and has a safety margin, which meets the test standard.

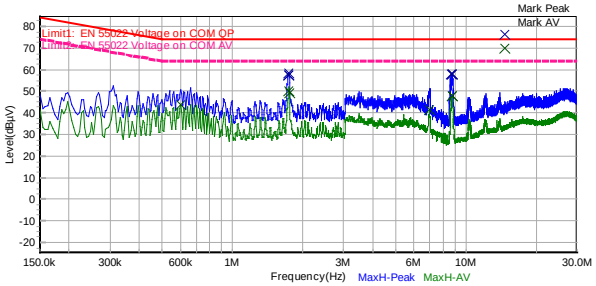

Fig. 10: Conducted EMI noise after rectification

IV. Conclusion

The conducted EMI noise diagnosis method based on the Infomax-WT algorithm effectively compensates for the defect that the infomax algorithm can only separate time-domain mixed conducted EMI noise signals and cannot reflect the frequency characteristics of noise signals. The simulation and experiment in Chapter 2 prove the effectiveness of this method in conducted EMI noise diagnosis.

This method is applied to the rectification of conducted EMI noise of anorectal therapy instrument. The Infomax-WT algorithm is used to diagnose and locate the noise source. The feasibility and engineering practicability of the method is verified.

References Références Referencias

1. Song Zhenfei. Detecting the number of EMI sources based on higher order statistics[C]. International Zurich Symposium on EMC. IEEE, 2009: 465-468.
2. Zhang Wenfa. A denoising adaptive blind separation algorithm based on Infomax[D]. Huazhong University of Science and Technology, 2008.
3. Wu Xiaopei, Ye Zhongfu, Shen Qian, Zhang Daoxin. On-line Infomax algorithm and its application in long recording EEG de-noising[J]. Journal of Circuits and Systems, 2005(05): 85-90.
4. Deng Feiyue. Research on feature extraction and diagnosis method of rolling bearing fault [D]. North China Electric Power University (Beijing), 2016.
5. Shang Haikun, Yuan Jinsha, Wang Yu, Jin Song. Partial discharge feature extraction based on cross wavelet transform and correlation coefficient matrix[J]. Journal of Electrotechnical Technology, 2014, 29(04): 274-281.
6. Duan Chendong, Gao Qiang, Xu Xianfeng. The application of frequency slice wavelet transform time-frequency analysis method in the fault diagnosis of generator set[J]. Proceedings of the CSEE, 2013, 33(32): 96-103+16.
7. Yuan Lifen, Sun Yesheng, He Yigang. An analog circuit fault feature extraction method based on wavelet packet optimization[J]. Transactions of the China Electrotechnical Society, 2018, 33(01): 158-165.
8. Xie Dong, Zhang Xing, Cao Renxian. Island detection technology based on wavelet transform and neural network[J]. Proceedings of the Chinese Society of Electrical Engineering, 2014, 34(04): 537-544.
9. Ge Zhizhi, Chen Zhongsheng. Time-frequency analysis technology of Matlab and its application [M]. People's Posts and Telecommunications Press, 2006: 2-8.

Global Journal of Science Frontier Research: a
Physics and Space Science
Volume 20 Issue 13 Version 1.0 Year 2020
Type : Double Blind Peer Reviewed International Research Journal
Publisher: Global Journals
Online ISSN: 2249-4626 & Print ISSN: 0975-5896

Electric Generators of Mende

By F. F. Mende

Abstract- In the article the survey of the existing constructions of high-voltage electrostatic generators is carried out. Are described the new types of the generators of Mende, the using laws of electrostatic induction and the tests of the experimental are carried out the models of such generators.

Keywords: *electrical induction, electromagnetic induction, dropper of calvin, generator of van de graaf, electro-form generator of wimshurst, dropper of mende, electrostatic generator of mende, parametric generator of mende, electro-form generator of mende, collectorless generator of mende.*

GJSFR-A Classification: *FOR Code: 040401*

Strictly as per the compliance and regulations of:

Electric Generators of Mende

F. F. Mende

Abstract- In the article the survey of the existing constructions of high-voltage electrostatic generators is carried out. Are described the new types of the generators of Mende, the using laws of electrostatic induction and the tests of the experimental are carried out the models of such generators.

Keywords: *electrical induction, electromagnetic induction, dropper of calvin, generator of van de graaf, electro-form generator of wimshurst, dropper of mende, electrostatic generator of mende, parametric generator of mende, electro-form generator of mende, collectorless generator of mende.*

I. Introduction

Three are today known basic of the type of the electrostatic generators, utilized for obtaining the high voltages. The work of these generators is based on the use of laws of electrostatic induction. These are the dropper of Calvin [1], generator of Van de Graaf[2] and the electro-form generator of Wimshurst [3].

The simplest electrostatic generator is dropper of Calvin, its diagram is represented in Fig. 1.

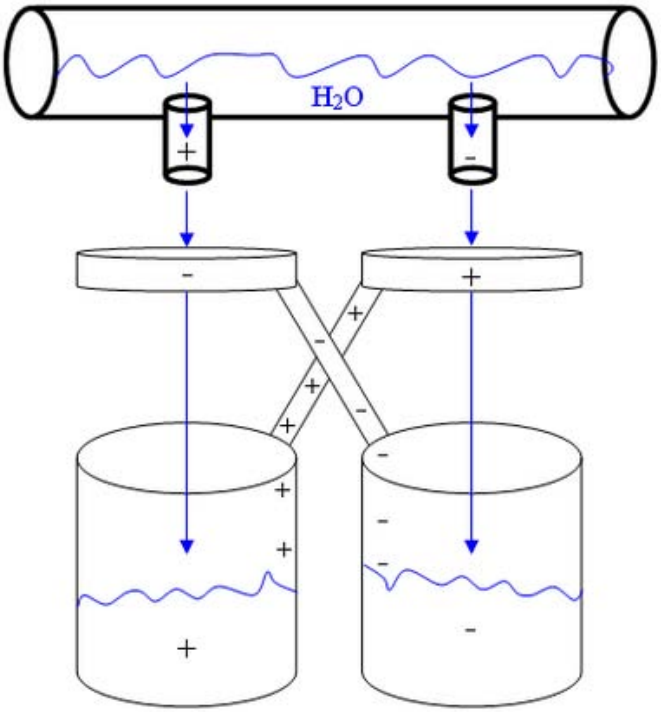

Fig. 1: Schematic of Calvin's dropper

Originally entire installation has neutral charge. It is unknown in view of the symmetry of installation and absence of charge, on which of the jars positive or negative charge will be accumulated. A small potential difference always is present because of different external actions between the left and right side of the installation, therefore the installation requires no starting charging of jars for the starting of system. By the force electrostatic induction ferrules direct in the reservoir with the water in that place, under which they are located, opposite charges. As a result a quantity of charges on the opposite edges of reservoir becomes different. After falling, drop they fall into the jar, which corresponds to its charge, thus increasing its charge, which creates still larger electric field near the rings, strengthening the separation of static charge and a potential difference between the banks it grows.

The electrical oscillator circuit of Van de Graaf is represented in Fig. 2.

Author: *e-mail: fedormende@gmail.com*

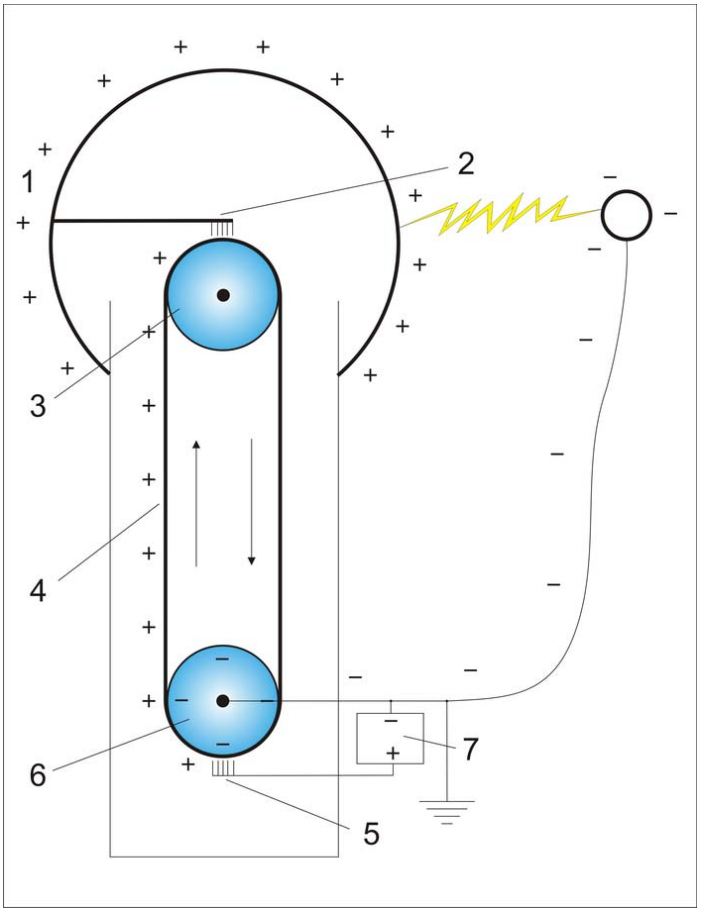

Ris. 2: Electrical oscillator circuit of Van de Graaf

Van de Graaf generator consists of the dielectric (silk or rubber) tape 4, of that revolving on the rollers 3 and 6, moreover upper roller dielectric, and lower metallic and is connected s by the earth. One it goes from the parts of the tape during the rotation of rollers in the metallic sphere 1. Two electrodes 2 and 5 in the form brushes are located at small distance from the tape on top and from below, moreover electrode 2 is connected with the internal surface of the sphere 1. Through the brush 5 air is ionized from the source of the high voltage 7. Resultant positive ions under the action Coulomb force they move to that grounded to roller they settle on the tape. The moving tape transfers charge inside the sphere, where it is removed by the brush, under the action Coulomb force charges are pushed out to the surface of sphere and field inside the sphere is created only by booster charge on the tape. Thus, on the external surface of sphere is accumulated electric charge. The possibility of obtaining the high voltage in this generator is limited by the corona discharge, appearing with the ionization air around the sphere.

Electro-form generator, developed by German scientist Wimshurst, is depicted in Fig. 3 and its name bears.

Fig. 3: Electro-form generator of Wimshurst

In the generator there are two revolving in the opposite direction disks, made from a good insulator. To the disks the conducting plates, which form capacitors, are stuck with the plates of opposite disk. In the process of rotating the disks the capacitance of these capacitors changes, since. the area of the overlap of the conducting plates changes. In the process of rotating the disks along the conducting plates the brushes, which connect the oppositely placed plates on both disks, slide. On both sides disks are two pairs of point electrodes, located on the appropriate holders. These electrodes during the rotation of disks do not concern the conducting plates, but charges on these electrodes appear with the electrical breakdown between the contacts and the conducting plates. On the electrodes indicated are collected the charges of the opposite signs, with the aid of which are charged high-voltage capacitors (Leyden jars). The holders of ball-shaped discharger are located on the Leyden jars.

II. Electric Generators of Mende

a) *Dropper of Mende*

If we on the electrolyte put the electric field (Fig. 3), thus it is polarized, in this case on the left side the baths will be collected anions, and in its right part cations will be collected. Charged anions produced through the openings in the lower part of the bath and cations fall into the separate baths, forming two battery terminals, which manufactures current, if we between these poles include load.

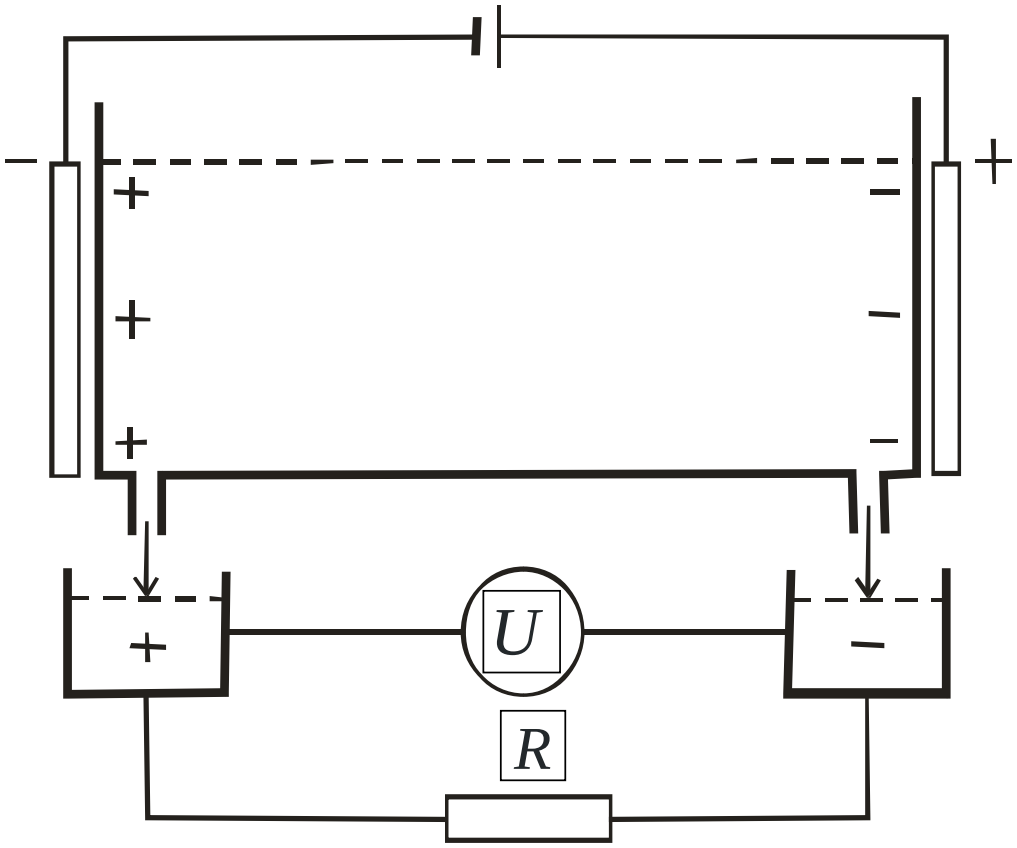

Fig. 3: Schematic dropper of Mende

A general view of the Mende dropper is shown in Fig. 4. Next to the dropper is an electroform generator, from which voltage is applied to the electrodes of the dropper.

Fig. 4: General view of the Mende dropper

b) The electrostatic generator of Mende

Generators for separation and accumulation examined above of charges are used the laws of electrostatic induction, and magnetic fields in these processes of participation do not assume. Hall's law is at the same time known, who gives the possibility to separate the moving charges [1].

In the simplest examination the Hall effect is represented in Fig. 5. Through that conducting plate in the normal direction passes magnetic field with the induction B and it flows through the same plate the electric current with the density j under the action voltage E. It will slant magnetic field charge carriers different signs to one of the faces of plate.

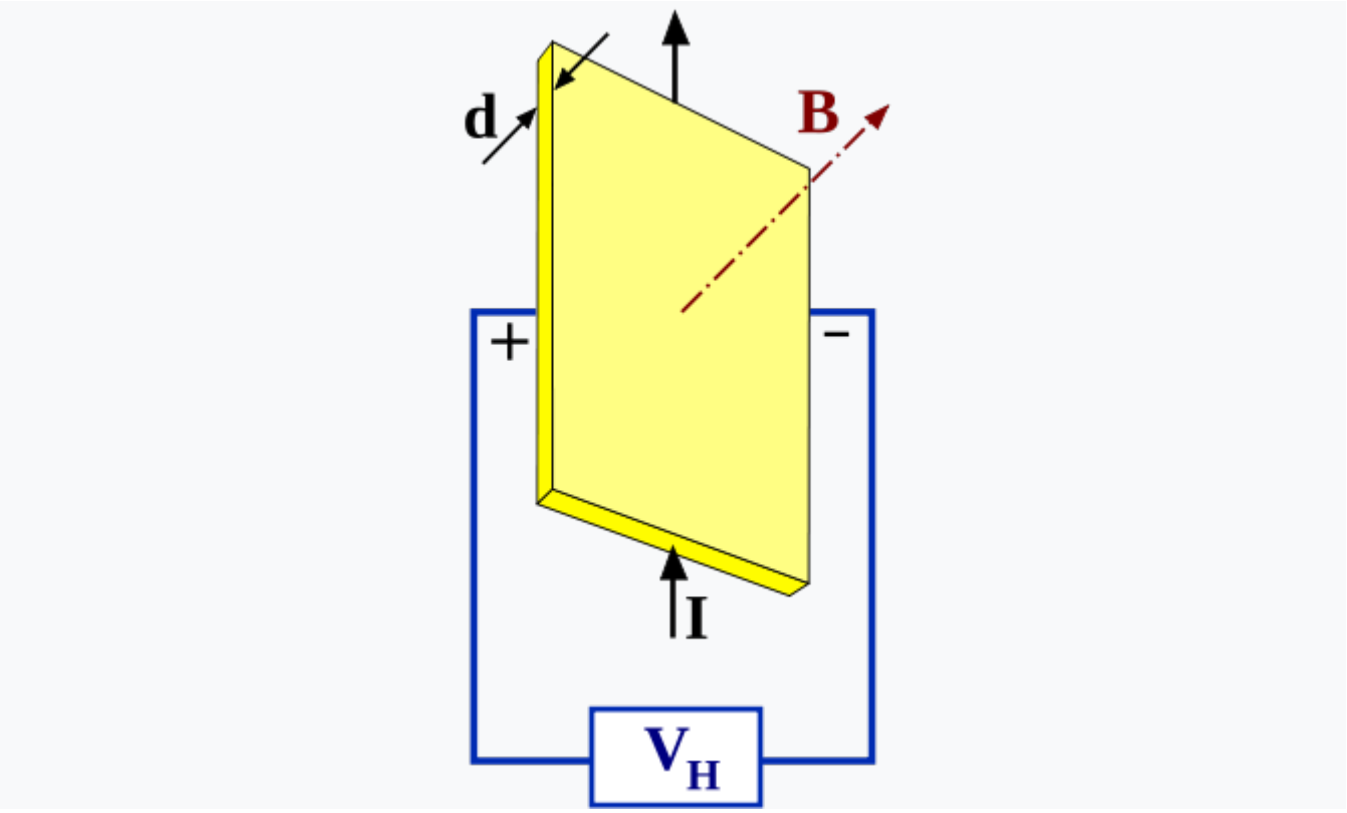

Fig. 5: Diagram of Hall effect

Thus, Lorentz force it will lead to the accumulation of negative charge near one face of plate, and positive- near the opposite face. The accumulation of charge will continue to those times, thus far arisen the electric field the charges E_1 it does not compensate for Lorentz force:

$$eE_1 = evB \text{ or } E_1 = vB,$$

where e - electric charge.

Usually Hall effect is used for measuring the magnetic field, but it can be used also for the separation of charges in the fluxion, for example to water. In the water there are always ions the dissolved in it salts. And it is possible to divide them with the aid of the Hall effect. If water will move normal to the direction magnetic field, then the ions of different signs will be accumulated on the different sides of flow. Dividing further flow to two parts, it is possible to obtain two separate flows, in which will be concentrated the ions of different signs. The circuit of separation of charges the method indicated is in Fig. 6.

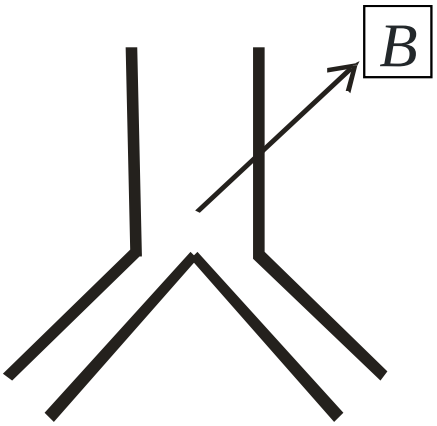

Fig. 6: Circuit of separation of charges with the magnetic separation

Gathering these flows into the different capacities, as is done in Calvin's dropper, it is possible to create the electrostatic generator (Fig. 7).

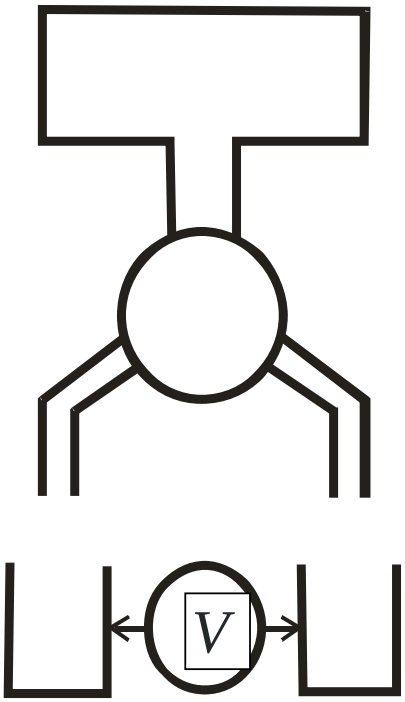

Fig. 7: Schematic of electrostatic generator with the magnetic separation of the charges

On the experimental installation with the use of two annular samarium magnets, between which magnetic induction composed 0,5T, was obtained a potential difference 50 kV.

The common form of electrostatic generator with the magnetic separation of charges is represented in Fig. 8.

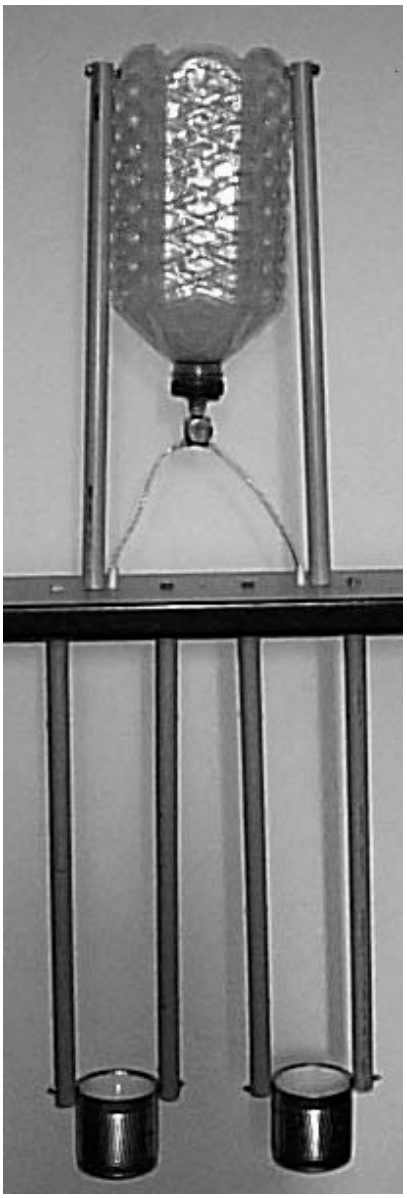

Fig. 8: The common form of electrostatic generator with the magnetic separation of the charges

c) Parametric generators of Mende

If there is a capacitor, whose capacity C, and this capacitor it is charged to a potential difference U, that the energy, accumulated in it, is determined by the relationship

$$W_C = \frac{1}{2} C U^2 \quad . \tag{2.1}$$

But charge Q, accumulated in the capacity, is equal

$$Q_{C,U} = CU \tag{2.2}$$

From relationship (2.1) it is evident that if the charge, accumulated in the capacity, remains constant, then voltage on it can be changed by changing the capacity. In this case is fulfilled the relationship

$$Q_{C,U}=CU=C_0U_0=const,$$

whereof and - instantaneous values, and and - initial values of these parameters.

The voltage on the capacity and the energy, accumulated in it, will be in this case determined by the relationships:

$$U=\frac{C_0U_0}{C}=KU_0, \quad (2.3)$$

$$W_C=\frac{1}{2}\frac{(C_0U_0)^2}{C}. \quad (2.4)$$

Coefficient

$$K=\frac{C_0}{C} \quad (2.5)$$

can be named by the multiplication factor (transformation) of the constant voltage.

The schematic of voltage transformer, realizing the principle examined, is represented in Fig. 9

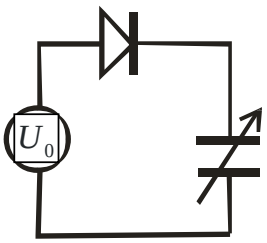

Fig. 9: Schematic of the transformer constant voltage

In this diagram to the variable capacitor by means of the diode the dc power supply is connected U_0

The incremental voltage, which can ensure this transformer, is determined from the relationship

$$\Delta U_C=\left(\frac{C_0}{C}-1\right)U_0 \quad (2.6)$$

As follows from the relationships (2.3) and (2.4) with the decrease of capacitance of capacitor on it increases not only voltage, but also the energy, accumulated in the Ger.

It should be noted that this transformer can work only in the regime of an increase in the voltage, since with the attempt to obtain the decrease of voltage across capacitor this cannot be made for that reason, that the diode the straight connection of the voltage source to the capacitor ensures and therefore voltage across capacitor decrease cannot.

An increase in the energy, accumulated in the capacitor, with a change in its capacity is determined from the relationship

$$\Delta W_C=\frac{1}{2}(C_0U_0)^2\left(\frac{1}{C}-\frac{1}{C_0}\right) \quad (2.7)$$

With a mechanical change in the capacitance of capacitor, the increase in the energy indicated ensures the spring mechanical energy source, Properties of the transformer of constant voltage is possible to use for creating the high-voltage source of the direct current, whose diagram is given in Fig. 10.

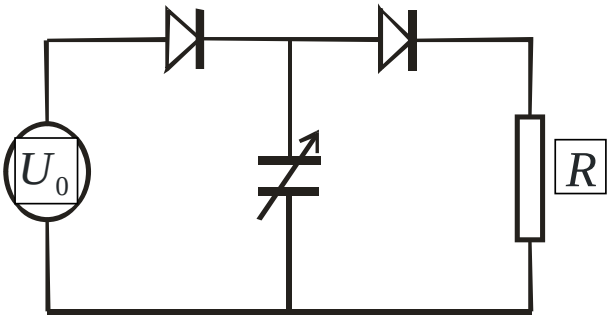

Fig. 10: Diagram of the high-voltage source of direct current

In this diagram is present still one diode and load resistance R.

In the initial state the capacitance of capacitor is equal C_0, and voltage on it equally U_0. At this time through the load resistance the current flows

$$I_0=\frac{U_0}{R}$$

In this case the energy, obtained by capacitor from the voltage source, comprises

$$W_0=\frac{1}{2}C_0U_0^2 \quad (2.8)$$

As soon as capacitance of capacitor will begin to decrease, the secondary voltage, assigned by the relationship will appear on it (2.5). This secondary voltage through the right diode enters the load resistance R. The additional energy, isolated in this case during the load resistance, is determined by the relationship (2.7).

The operating principle of the generator examined is such to the operating principle of the valve water pump, whose schematic is represented in Fig. 11.

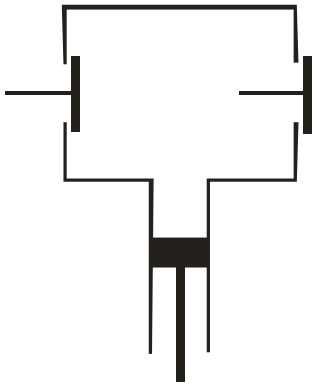

Fig. 11: Schematic of the valve water pump

With the displacement of piston downward left release valve is opened, and water is sucked in into the cavity of pump. With the displacement of piston upward the water through the right release valve is ejected outside.

The role of valves in the schematic of the described generator diodes play, while the role of cylinder with the being moved piston performs variable capacitor.

Hence it follows that the basic problem of the creation of the proposed generator is the development of the capacitor, whose capacity changes with mechanical method. In this case the capacitor must have the great significances of initial and final capacity and with the large relation of these values. This question can be solved by the way of using the technology of the creation of the ceramic capacitors, when titanate of barium, which has very large dielectric constant, is used as the dielectric between the capacitor plates. The construction of the generator, in which is used the principle indicated, it is shown in Fig. 12.

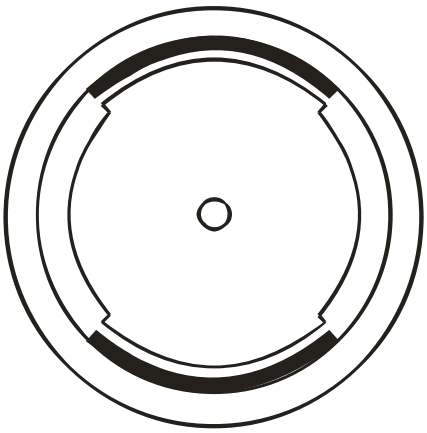

Fig. 12: The mechanical oscillator circuit, in which the inserts from titanate of barium are located on the internal surface of stator

In the given construction there is a figured rotor, and inserts from titanate of barium are located on the internal surface of cylindrical stator.

Let us calculate the practical construction of generator with the following parameters: the voltage of the voltage source $U_0 = 200\ V$, the diameter of the rotor $D = 0.5\ m$, clearance between the inserts of titanate of barium and the stator $d = 10\mu m$, the thickness of the inserts $25\ mm$, the depth of turnings on the rotor $25\ mm$, the speed of rotation of the rotor $n = 500\ \frac{1}{s}$ (this rotational speed it is characteristic for the gas turbines), the length of the generator $L = 1m$.

The power, manufactured by generator will comprise

$$P = \frac{\pi\varepsilon nKDLU_0^2}{2d}. \qquad (2.9)$$

During the record of this formula are taken into account the fact that in one revolution of rotor it occurs two cycles of a change in the capacity between the rotor and the stator.

The substitution of the assigned parameters into the formula (2.9) gives the power 34 kW.

The output voltage, which manufactures generator, calculated according to the formula (3.3) it will comprise $1\ MV$. This voltage will be developed between the stator-rotor unit when the capacity between them is minimum. In order in this case to avoid electrical breakdown, the internal cavity of generator must be filled with air or another gas under the high pressure.

None of the existing generators can ensure such high voltage without the use of the step-up transformers and rectifiers. Large simplicity of construction is the very great advantage of this generator.

The type of generator in the section is shown in Fig. 13.

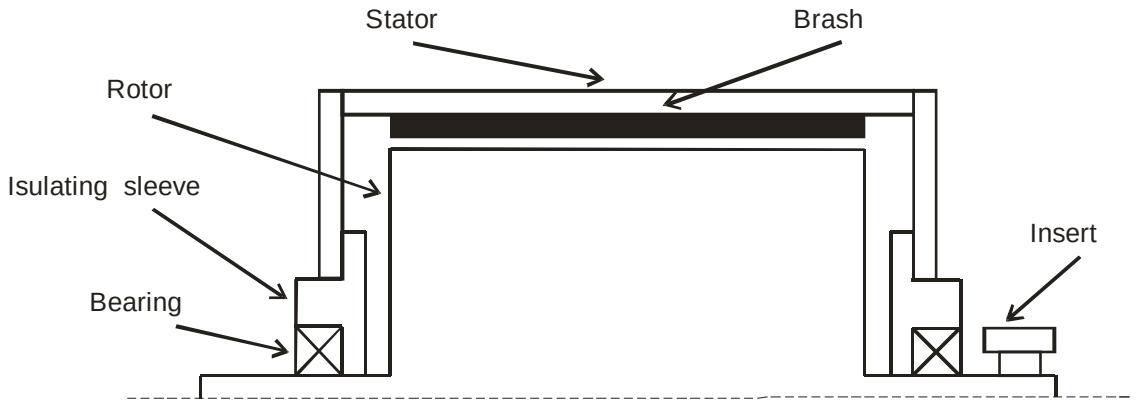

Fig. 13: Type of generator in the section

The insulating bush is located between the axis of rotor and the housing of stator. In this bushing the bearing is located. By lower its edge bushing slides along the axis of shaft, ensuring the vacuum seal between the internal cavity of generator and the atmosphere. The insert from titanate of barium is located on the internal part of the stator. The electrical contact between the axis of rotor and the external circuits brushes ensure.

d) Electro-form generator of Mende

The schematic of the work of elektro-form generator Mende is depicted in Fig. 14.

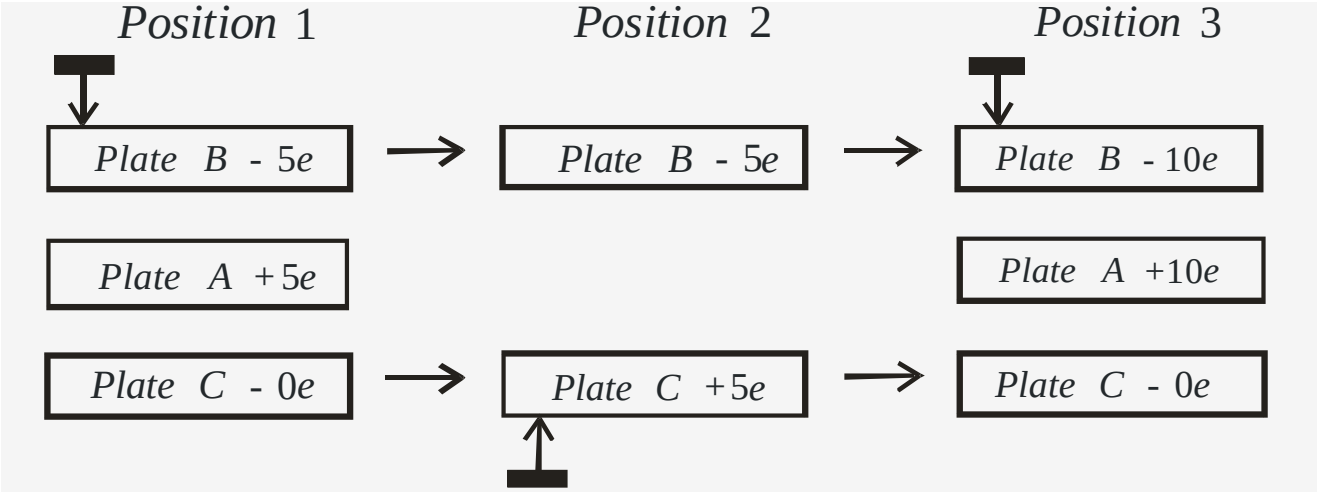

Fig. 14: Carry circuit and accumulation of charge in the generator

There are three plates of parallel-plate capacitor A, B and C, from which the plate B and C they can move in the direction, indicated with pointers, while average plate A it remains fixed.

In the position 1 the plate B by means of the contact sliding on it is connected with the earth. Plate C also by means of the sliding contact, which moves together with it, is connected with the plate A. On the plates there are designations, which indicate the instantaneous value of charges on them in the arbitrary units with the indication of the sign of charge. Initial magnitude of the charge can be other and depends on the the initial conditions.

Let us assume that in the initial position plate A bears on itself the charge +5e, and plates B and C begin to synchronously move to the right. In this case the plate v loses contact with the earth, and on it remains the charge – 5e.

In the position 2 the plate B preserves charge to -5e, and plate C acquires contact with the earth and on it is induced the charge +5e. After that, plates B and C continue to move in the direction indicated by the arrows.

In the position 3 of the platesCand A they are connected with the aid of the sliding contact, which moves together with the plate C, and plate B is connected to the earth. In this case the charge +5e from the plate C overflows into the plate A and its charge it becomes equal +10e, and the charge of plate C becomes equal to zero. In this case the plate A, which received the booster charge +5e, induces in the plate into the charge -10e, i.e. in comparison with the position 1 the charges of plates A and B also in double.

It is evident that position 3 in the arrangement of plates and their connection differs in no way from the position 1, with the only difference that the magnitude of the charge of plates A also B in comparison with this position it was doubled, and the charge of the plate C it remained equal to zero. With the same following cycle the charges on the plates A and B also in again will be doubled and they will become respectively equal +20e and -20 e the doubling of charges with each subsequent cycle will continue. With this process of plate they will accumulate all increasing charge, which will lead to an increase in their potentials.

The automation of transfer and accumulation of charge thus can be realized, if capacitor plates are placed to the disks. The functional diagram of the automated transfer of charge is represented in Fig. 15.

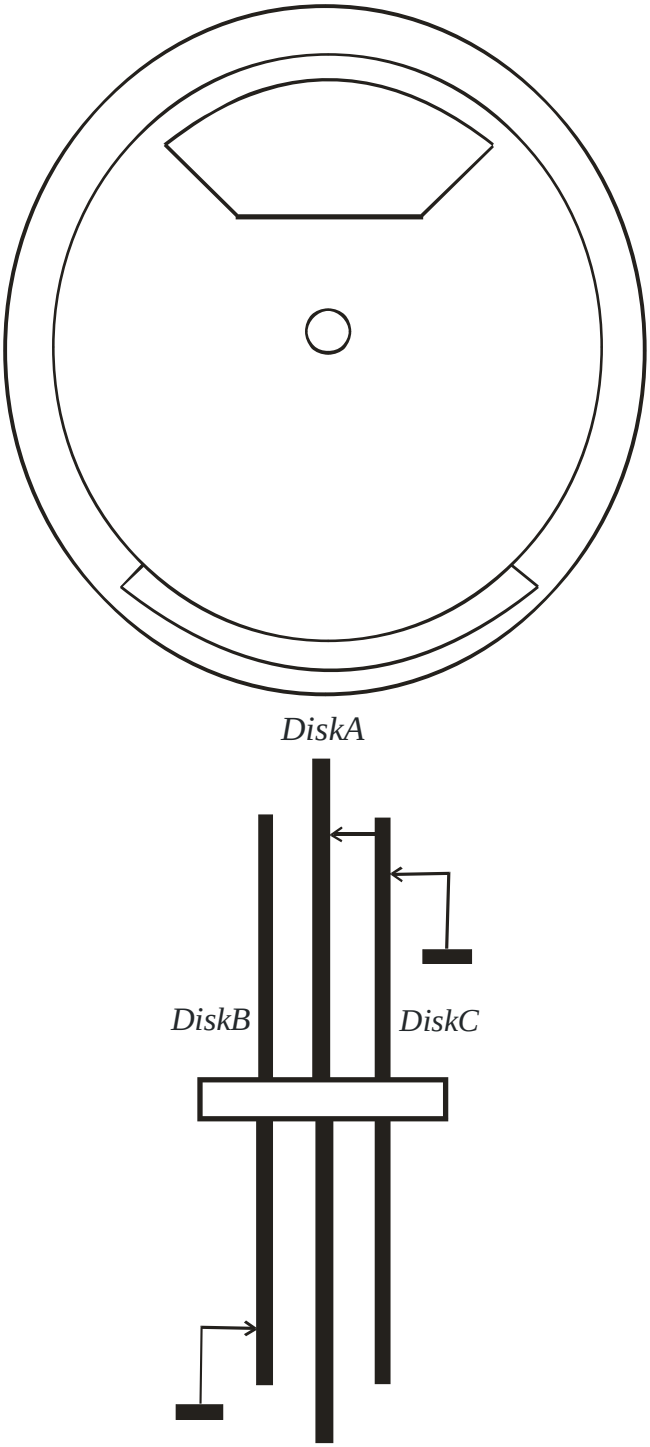

Fig. 15: The functional diagram of the automated transfer of the charge

Structurally the generator is executed in the form three disks, on which are stuck the current-conducting plates of capacitors. Two external disks B and C it is tightly planted on the axis, which ensures their synchronous rotation. Stator is the fixed central disk A, which is also established on the axis, but the diameter of its opening is more than its diameter, which ensures its easy-push fit. The fixation of the position of stator is achieved with the aid of the corner, which from one side is attached to the disk, and with another - to the platform, on which is established the generator. In the experimental mock-up of the generator with the diameters of lateral disks and central disk of 250mm and 300 mm examined respectively, is obtained a potential difference 20 kV.

Design a difference in the generator from the generator examined Wimshurst lies in the fact that lateral disks revolve in one direction, and central disk is fixed, appearing by stator, while in the generator Wimshurst lateral disks they revolve in the different directions, and there is no fixed central disk.

A general view of the Mende electroform generator is shown in the following photo.

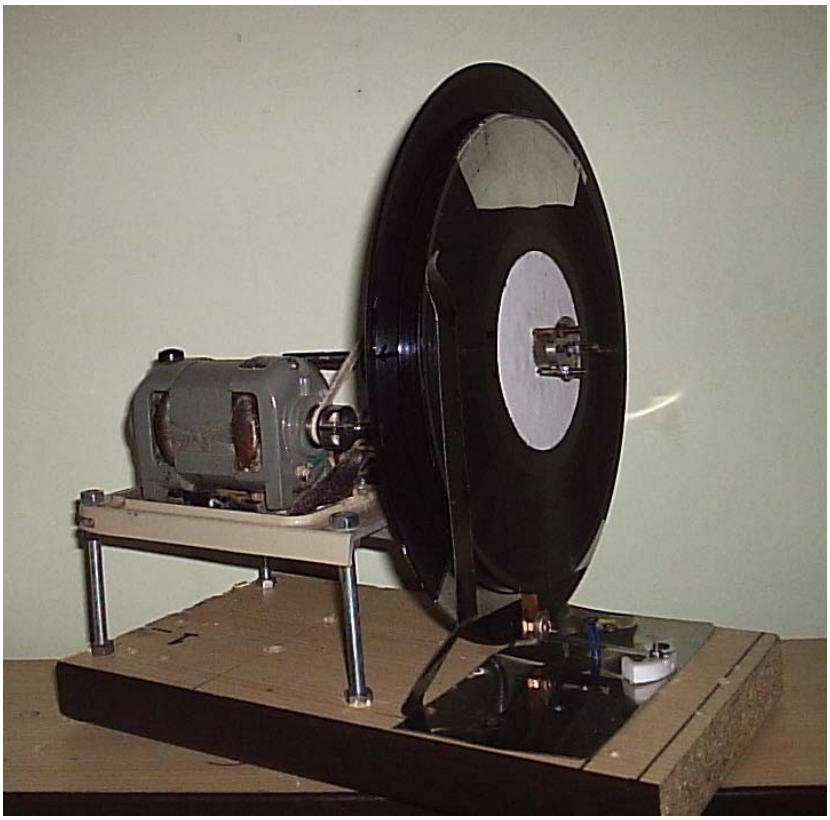

III. Conclusion

In the article the survey of the existing constructions of high-voltage electrostatic generators is carried out. Are described the new types of the generators of Mende, the using laws of electrostatic induction and the tests of the experimental are carried out the models of such generators.

References Références Referencias

1. Калашников С. Г., Электричество, М., ГИТТЛ, 1956.
2. Darryl J. Leiter. Van de Graaff, Robert Jemison // A to Z of Physicists. — 2003. — С. 312.
3. http://hypertextbook.com/facts/2005/kelvin.shtml.
4. Ф. Ф. Менде, А. С. Дубровин. Особые свойства реактивных элементов и потоков заряженных частиц. Инженернаяфизика, №11, 2016, с. 13-21.
5. F. F. Mende, New Properties of Reactive Elements and the Problem of Propagation of Electrical Signals in Long Lines, American Journal of Electrical and Electronic Engineering, Vol. 2, No. 5, (2014), p.141-145.
6. F. F. Mende. Induction and Parametric Properties of Radio-Technical Elements and Lines and Property of Charges and Their Flows, AASCIT Journal of Physics Vol.1, No. 3, Publication Date: May 21, 2015, p. 124-134.
7. Ф. Ф. Менде, А. С. Дубровин. Альтернативная идеология электродинамики. М.: Перо, 2016. - 198 с.
8. F. F. Mende. Mende Parametric Electric Generator. Global Journal of Science Frontier Research (A), Physics and Space Science, Volume 18, Issue 3, Version 1.0, Year 2018.

Global Journals Guidelines Handbook 2020

www.GlobalJournals.org

Memberships

Fellows/Associates of Science Frontier Research Council

FSFRC/ASFRC Memberships

Introduction

FSFRC/ASFRC is the most prestigious membership of Global Journals accredited by Open Association of Research Society, U.S.A (OARS). The credentials of Fellow and Associate designations signify that the researcher has gained the knowledge of the fundamental and high-level concepts, and is a subject matter expert, proficient in an expertise course covering the professional code of conduct, and follows recognized standards of practice. The credentials are designated only to the researchers, scientists, and professionals that have been selected by a rigorous process by our Editorial Board and Management Board.

Associates of FSFRC/ASFRC are scientists and researchers from around the world are working on projects/researches that have huge potentials. Members support Global Journals' mission to advance technology for humanity and the profession.

FSFRC

Fellow of Science Frontier Research Council

FELLOW OF SCIENCE FRONTIER RESEARCH COUNCIL is the most prestigious membership of Global Journals. It is an award and membership granted to individuals that the Open Association of Research Society judges to have made a 'substantial contribution to the improvement of computer science, technology, and electronics engineering.

The primary objective is to recognize the leaders in research and scientific fields of the current era with a global perspective and to create a channel between them and other researchers for better exposure and knowledge sharing. Members are most eminent scientists, engineers, and technologists from all across the world. Fellows are elected for life through a peer review process on the basis of excellence in the respective domain. There is no limit on the number of new nominations made in any year. Each year, the Open Association of Research Society elect up to 12 new Fellow Members.

Benefit

To the institution

Get letter of appreciation

Global Journals sends a letter of appreciation of author to the Dean or CEO of the University or Company of which author is a part, signed by editor in chief or chief author.

Exclusive Network

Get access to a closed network

A FSFRC member gets access to a closed network of Tier 1 researchers and scientists with direct communication channel through our website. Fellows can reach out to other members or researchers directly. They should also be open to reaching out by other.

Career | Credibility | Exclusive | Reputation

Certificate

Receive a print ed copy of a certificate

Fellows receive a printed copy of a certificate signed by our Chief Author that may be used for academic purposes and a personal recommendation letter to the dean of member's university.

Career | Credibility | Exclusive | Reputation

Designation

Get honored title of membership

Fellows can use the honored title of membership. The “FSFRC” is an honored title which is accorded to a person’s name viz. Dr. John E. Hall, Ph.D., FSFRC or William Walldroff, M.S., FSFRC.

Career | Credibility | Exclusive | Reputation

Recognition on the Platform

Better visibility and citation

All the Fellow members of FSFRC get a badge of "Leading Member of Global Journals" on the Research Community that distinguishes them from others. Additionally, the profile is also partially maintained by our team for better visibility and citation. All fellows get a dedicated page on the website with their biography.

Career | Credibility | Reputation

Future Work

Get discounts on the future publications

Fellows receive discounts on future publications with Global Journals up to 60%. Through our recommendation programs, members also receive discounts on publications made with OARS affiliated organizations.

Career | Financial

GJ Internal Account

Unlimited forward of Emails

Fellows get secure and fast GJ work emails with unlimited forward of emails that they may use them as their primary email. For example,
john [AT] globaljournals [DOT] org.

Career | Credibility | Reputation

Premium Tools

Access to all the premium tools

To take future researches to the zenith, fellows and associates receive access to all the premium tools that Global Journals have to offer along with the partnership with some of the best marketing leading tools out there.

Financial

Conferences & Events

Organize seminar/conference

Fellows are authorized to organize symposium/seminar/conference on behalf of Global Journal Incorporation (USA). They can also participate in the same organized by another institution as representative of Global Journal. In both the cases, it is mandatory for him to discuss with us and obtain our consent. Additionally, they get free research conferences (and others) alerts.

Career | Credibility | Financial

Early Invitations

Early invitations to all the symposiums, seminars, conferences

All fellows receive the early invitations to all the symposiums, seminars, conferences and webinars hosted by Global Journals in their subject.

Exclusive

Publishing Articles & Books

Earn 60% of sales proceeds

Fellows can publish articles (limited) without any fees. Also, they can earn up to 60% of sales proceeds from the sale of reference/review books/literature/ publishing of research paper. The FSFRC member can decide its price and we can help in making the right decision.

Exclusive | Financial

Reviewers

Get a remuneration of 15% of author fees

Fellow members are eligible to join as a paid peer reviewer at Global Journals Incorporation (USA) and can get a remuneration of 15% of author fees, taken from the author of a respective paper.

Financial

Access to Editorial Board

Become a member of the Editorial Board

Fellows may join as a member of the Editorial Board of Global Journals Incorporation (USA) after successful completion of three years as Fellow and as Peer Reviewer. Additionally, Fellows get a chance to nominate other members for Editorial Board.

Career | Credibility | Exclusive | Reputation

And Much More

Get access to scientific museums and observatories across the globe

All members get access to 5 selected scientific museums and observatories across the globe. All researches published with Global Journals will be kept under deep archival facilities across regions for future protections and disaster recovery. They get 10 GB free secure cloud access for storing research files.

ASSOCIATE OF SCIENCE FRONTIER RESEARCH COUNCIL

ASSOCIATE OF SCIENCE FRONTIER RESEARCH COUNCIL is the membership of Global Journals awarded to individuals that the Open Association of Research Society judges to have made a 'substantial contribution to the improvement of computer science, technology, and electronics engineering.

The primary objective is to recognize the leaders in research and scientific fields of the current era with a global perspective and to create a channel between them and other researchers for better exposure and knowledge sharing. Members are most eminent scientists, engineers, and technologists from all across the world. Associate membership can later be promoted to Fellow Membership. Associates are elected for life through a peer review process on the basis of excellence in the respective domain. There is no limit on the number of new nominations made in any year. Each year, the Open Association of Research Society elect up to 12 new Associate Members.

Benefit

To the institution

Get letter of appreciation

Global Journals sends a letter of appreciation of author to the Dean or CEO of the University or Company of which author is a part, signed by editor in chief or chief author.

Exclusive Network

Get access to a closed network

A ASFRC member gets access to a closed network of Tier 1 researchers and scientists with direct communication channel through our website. Associates can reach out to other members or researchers directly. They should also be open to reaching out by other.

Career | Credibility | Exclusive | Reputation

Certificate

Receive a print ed copy of a certificate

Associates receive a printed copy of a certificate signed by our Chief Author that may be used for academic purposes and a personal recommendation letter to the dean of member's university.

Career | Credibility | Exclusive | Reputation

Designation

Get honored title of membership

Associates can use the honored title of membership. The “ASFRC” is an honored title which is accorded to a person’s name viz. Dr. John E. Hall, Ph.D., ASFRC or William Walldroff, M.S., ASFRC.

Career | Credibility | Exclusive | Reputation

Recognition on the Platform

Better visibility and citation

All the Associate members of ASFRC get a badge of "Leading Member of Global Journals" on the Research Community that distinguishes them from others. Additionally, the profile is also partially maintained by our team for better visibility and citation. All associates get a dedicated page on the website with their biography.

Career | Credibility | Reputation

Future Work

Get discounts on the future publications

Associates receive discounts on the future publications with Global Journals up to 60%. Through our recommendation programs, members also receive discounts on publications made with OARS affiliated organizations.

Career | Financial

GJ Internal Account

Unlimited forward of Emails

Associates get secure and fast GJ work emails with unlimited forward of emails that they may use them as their primary email. For example,
john [AT] globaljournals [DOT] org.

Career | Credibility | Reputation

Premium Tools

Access to all the premium tools

To take future researches to the zenith, fellows receive access to almost all the premium tools that Global Journals have to offer along with the partnership with some of the best marketing leading tools out there.

Financial

Conferences & Events

Organize seminar/conference

Associates are authorized to organize symposium/seminar/conference on behalf of Global Journal Incorporation (USA). They can also participate in the same organized by another institution as representative of Global Journal. In both the cases, it is mandatory for him to discuss with us and obtain our consent. Additionally, they get free research conferences (and others) alerts.

Career | Credibility | Financial

Early Invitations

Early invitations to all the symposiums, seminars, conferences

All associates receive the early invitations to all the symposiums, seminars, conferences and webinars hosted by Global Journals in their subject.

Exclusive

Publishing Articles & Books

Earn 30-40% of sales proceeds

Associates can publish articles (limited) without any fees. Also, they can earn up to 30-40% of sales proceeds from the sale of reference/review books/literature/publishing of research paper.

Exclusive | Financial

Reviewers

Get a remuneration of 15% of author fees

Associate members are eligible to join as a paid peer reviewer at Global Journals Incorporation (USA) and can get a remuneration of 15% of author fees, taken from the author of a respective paper.

Financial

And Much More

Get access to scientific museums and observatories across the globe

All members get access to 2 selected scientific museums and observatories across the globe. All researches published with Global Journals will be kept under deep archival facilities across regions for future protections and disaster recovery. They get 5 GB free secure cloud access for storing research files.

Associate	Fellow	Research Group	Basic
$4800 **lifetime designation**	$6800 **lifetime designation**	$12500.00 **organizational**	APC **per article**
Certificate, LoR and Momento **2** discounted publishing/year **Gradation** of Research **10** research contacts/day **1 GB** Cloud Storage **GJ** Community Access	**Certificate,** LoR and Momento **Unlimited** discounted publishing/year **Gradation** of Research **Unlimited** research contacts/day **5 GB** Cloud Storage **Online Presense** Assistance **GJ** Community Access	**Certificates,** LoRs and Momentos **Unlimited** free publishing/year **Gradation** of Research **Unlimited** research contacts/day **Unlimited** Cloud Storage **Online Presense** Assistance **GJ** Community Access	**GJ** Community Access

Preferred Author Guidelines

We accept the manuscript submissions in any standard (generic) format.

We typeset manuscripts using advanced typesetting tools like Adobe In Design, CorelDraw, TeXnicCenter, and TeXStudio. We usually recommend authors submit their research using any standard format they are comfortable with, and let Global Journals do the rest.

Alternatively, you can download our basic template from https://globaljournals.org/Template.zip

Authors should submit their complete paper/article, including text illustrations, graphics, conclusions, artwork, and tables. Authors who are not able to submit manuscript using the form above can email the manuscript department at submit@globaljournals.org or get in touch with chiefeditor@globaljournals.org if they wish to send the abstract before submission.

Before and during Submission

Authors must ensure the information provided during the submission of a paper is authentic. Please go through the following checklist before submitting:

1. Authors must go through the complete author guideline and understand and *agree to Global Journals' ethics and code of conduct,* along with author responsibilities.
2. Authors must accept the privacy policy, terms, and conditions of Global Journals.
3. Ensure corresponding author's email address and postal address are accurate and reachable.
4. Manuscript to be submitted must include keywords, an abstract, a paper title, co-author(s') names and details (email address, name, phone number, and institution), figures and illustrations in vector format including appropriate captions, tables, including titles and footnotes, a conclusion, results, acknowledgments and references.
5. Authors should submit paper in a ZIP archive if any supplementary files are required along with the paper.
6. Proper permissions must be acquired for the use of any copyrighted material.
7. Manuscript submitted *must not have been submitted or published elsewhere* and all authors must be aware of the submission.

Declaration of Conflicts of Interest

It is required for authors to declare all financial, institutional, and personal relationships with other individuals and organizations that could influence (bias) their research.

Policy on Plagiarism

Plagiarism is not acceptable in Global Journals submissions at all.

Plagiarized content will not be considered for publication. We reserve the right to inform authors' institutions about plagiarism detected either before or after publication. If plagiarism is identified, we will follow COPE guidelines:

Authors are solely responsible for all the plagiarism that is found. The author must not fabricate, falsify or plagiarize existing research data. The following, if copied, will be considered plagiarism:

- Words (language)
- Ideas
- Findings
- Writings
- Diagrams
- Graphs
- Illustrations
- Lectures

- Printed material
- Graphic representations
- Computer programs
- Electronic material
- Any other original work

Authorship Policies

Global Journals follows the definition of authorship set up by the Open Association of Research Society, USA. According to its guidelines, authorship criteria must be based on:

1. Substantial contributions to the conception and acquisition of data, analysis, and interpretation of findings.
2. Drafting the paper and revising it critically regarding important academic content.
3. Final approval of the version of the paper to be published.

Changes in Authorship

The corresponding author should mention the name and complete details of all co-authors during submission and in manuscript. We support addition, rearrangement, manipulation, and deletions in authors list till the early view publication of the journal. We expect that corresponding author will notify all co-authors of submission. We follow COPE guidelines for changes in authorship.

Copyright

During submission of the manuscript, the author is confirming an exclusive license agreement with Global Journals which gives Global Journals the authority to reproduce, reuse, and republish authors' research. We also believe in flexible copyright terms where copyright may remain with authors/employers/institutions as well. Contact your editor after acceptance to choose your copyright policy. You may follow this form for copyright transfers.

Appealing Decisions

Unless specified in the notification, the Editorial Board's decision on publication of the paper is final and cannot be appealed before making the major change in the manuscript.

Acknowledgments

Contributors to the research other than authors credited should be mentioned in Acknowledgments. The source of funding for the research can be included. Suppliers of resources may be mentioned along with their addresses.

Declaration of funding sources

Global Journals is in partnership with various universities, laboratories, and other institutions worldwide in the research domain. Authors are requested to disclose their source of funding during every stage of their research, such as making analysis, performing laboratory operations, computing data, and using institutional resources, from writing an article to its submission. This will also help authors to get reimbursements by requesting an open access publication letter from Global Journals and submitting to the respective funding source.

Preparing your Manuscript

Authors can submit papers and articles in an acceptable file format: MS Word (doc, docx), LaTeX (.tex, .zip or .rar including all of your files), Adobe PDF (.pdf), rich text format (.rtf), simple text document (.txt), Open Document Text (.odt), and Apple Pages (.pages). Our professional layout editors will format the entire paper according to our official guidelines. This is one of the highlights of publishing with Global Journals—authors should not be concerned about the formatting of their paper. Global Journals accepts articles and manuscripts in every major language, be it Spanish, Chinese, Japanese, Portuguese, Russian, French, German, Dutch, Italian, Greek, or any other national language, but the title, subtitle, and abstract should be in English. This will facilitate indexing and the pre-peer review process.

The following is the official style and template developed for publication of a research paper. Authors are not required to follow this style during the submission of the paper. It is just for reference purposes.

Manuscript Style Instruction (Optional)

- Microsoft Word Document Setting Instructions.
- Font type of all text should be Swis721 Lt BT.
- Page size: 8.27" x 11'", left margin: 0.65, right margin: 0.65, bottom margin: 0.75.
- Paper title should be in one column of font size 24.
- Author name in font size of 11 in one column.
- Abstract: font size 9 with the word "Abstract" in bold italics.
- Main text: font size 10 with two justified columns.
- Two columns with equal column width of 3.38 and spacing of 0.2.
- First character must be three lines drop-capped.
- The paragraph before spacing of 1 pt and after of 0 pt.
- Line spacing of 1 pt.
- Large images must be in one column.
- The names of first main headings (Heading 1) must be in Roman font, capital letters, and font size of 10.
- The names of second main headings (Heading 2) must not include numbers and must be in italics with a font size of 10.

Structure and Format of Manuscript

The recommended size of an original research paper is under 15,000 words and review papers under 7,000 words. Research articles should be less than 10,000 words. Research papers are usually longer than review papers. Review papers are reports of significant research (typically less than 7,000 words, including tables, figures, and references)

A research paper must include:

a) A title which should be relevant to the theme of the paper.
b) A summary, known as an abstract (less than 150 words), containing the major results and conclusions.
c) Up to 10 keywords that precisely identify the paper's subject, purpose, and focus.
d) An introduction, giving fundamental background objectives.
e) Resources and techniques with sufficient complete experimental details (wherever possible by reference) to permit repetition, sources of information must be given, and numerical methods must be specified by reference.
f) Results which should be presented concisely by well-designed tables and figures.
g) Suitable statistical data should also be given.
h) All data must have been gathered with attention to numerical detail in the planning stage.

Design has been recognized to be essential to experiments for a considerable time, and the editor has decided that any paper that appears not to have adequate numerical treatments of the data will be returned unrefereed.

i) Discussion should cover implications and consequences and not just recapitulate the results; conclusions should also be summarized.
j) There should be brief acknowledgments.
k) There ought to be references in the conventional format. Global Journals recommends APA format.

Authors should carefully consider the preparation of papers to ensure that they communicate effectively. Papers are much more likely to be accepted if they are carefully designed and laid out, contain few or no errors, are summarizing, and follow instructions. They will also be published with much fewer delays than those that require much technical and editorial correction.

The Editorial Board reserves the right to make literary corrections and suggestions to improve brevity.

Format Structure

It is necessary that authors take care in submitting a manuscript that is written in simple language and adheres to published guidelines.

All manuscripts submitted to Global Journals should include:

Title

The title page must carry an informative title that reflects the content, a running title (less than 45 characters together with spaces), names of the authors and co-authors, and the place(s) where the work was carried out.

Author details

The full postal address of any related author(s) must be specified.

Abstract

The abstract is the foundation of the research paper. It should be clear and concise and must contain the objective of the paper and inferences drawn. It is advised to not include big mathematical equations or complicated jargon.

Many researchers searching for information online will use search engines such as Google, Yahoo or others. By optimizing your paper for search engines, you will amplify the chance of someone finding it. In turn, this will make it more likely to be viewed and cited in further works. Global Journals has compiled these guidelines to facilitate you to maximize the web-friendliness of the most public part of your paper.

Keywords

A major lynchpin of research work for the writing of research papers is the keyword search, which one will employ to find both library and internet resources. Up to eleven keywords or very brief phrases have to be given to help data retrieval, mining, and indexing.

One must be persistent and creative in using keywords. An effective keyword search requires a strategy: planning of a list of possible keywords and phrases to try.

Choice of the main keywords is the first tool of writing a research paper. Research paper writing is an art. Keyword search should be as strategic as possible.

One should start brainstorming lists of potential keywords before even beginning searching. Think about the most important concepts related to research work. Ask, “What words would a source have to include to be truly valuable in a research paper?” Then consider synonyms for the important words.

It may take the discovery of only one important paper to steer in the right keyword direction because, in most databases, the keywords under which a research paper is abstracted are listed with the paper.

Numerical Methods

Numerical methods used should be transparent and, where appropriate, supported by references.

Abbreviations

Authors must list all the abbreviations used in the paper at the end of the paper or in a separate table before using them.

Formulas and equations

Authors are advised to submit any mathematical equation using either MathJax, KaTeX, or LaTeX, or in a very high-quality image.

Tables, Figures, and Figure Legends

Tables: Tables should be cautiously designed, uncrowned, and include only essential data. Each must have an Arabic number, e.g., Table 4, a self-explanatory caption, and be on a separate sheet. Authors must submit tables in an editable format and not as images. References to these tables (if any) must be mentioned accurately.

Figures

Figures are supposed to be submitted as separate files. Always include a citation in the text for each figure using Arabic numbers, e.g., Fig. 4. Artwork must be submitted online in vector electronic form or by emailing it.

Preparation of Eletronic Figures for Publication

Although low-quality images are sufficient for review purposes, print publication requires high-quality images to prevent the final product being blurred or fuzzy. Submit (possibly by e-mail) EPS (line art) or TIFF (halftone/ photographs) files only. MS PowerPoint and Word Graphics are unsuitable for printed pictures. Avoid using pixel-oriented software. Scans (TIFF only) should have a resolution of at least 350 dpi (halftone) or 700 to 1100 dpi (line drawings). Please give the data for figures in black and white or submit a Color Work Agreement form. EPS files must be saved with fonts embedded (and with a TIFF preview, if possible).

For scanned images, the scanning resolution at final image size ought to be as follows to ensure good reproduction: line art: >650 dpi; halftones (including gel photographs): >350 dpi; figures containing both halftone and line images: >650 dpi.

Color charges: Authors are advised to pay the full cost for the reproduction of their color artwork. Hence, please note that if there is color artwork in your manuscript when it is accepted for publication, we would require you to complete and return a Color Work Agreement form before your paper can be published. Also, you can email your editor to remove the color fee after acceptance of the paper.

Tips for Writing a Good Quality Science Frontier Research Paper

Techniques for writing a good quality Science Frontier Research paper:

1. Choosing the topic: In most cases, the topic is selected by the interests of the author, but it can also be suggested by the guides. You can have several topics, and then judge which you are most comfortable with. This may be done by asking several questions of yourself, like "Will I be able to carry out a search in this area? Will I find all necessary resources to accomplish the search? Will I be able to find all information in this field area?" If the answer to this type of question is "yes," then you ought to choose that topic. In most cases, you may have to conduct surveys and visit several places. Also, you might have to do a lot of work to find all the rises and falls of the various data on that subject. Sometimes, detailed information plays a vital role, instead of short information. Evaluators are human: The first thing to remember is that evaluators are also human beings. They are not only meant for rejecting a paper. They are here to evaluate your paper. So present your best aspect.

2. Think like evaluators: If you are in confusion or getting demotivated because your paper may not be accepted by the evaluators, then think, and try to evaluate your paper like an evaluator. Try to understand what an evaluator wants in your research paper, and you will automatically have your answer. Make blueprints of paper: The outline is the plan or framework that will help you to arrange your thoughts. It will make your paper logical. But remember that all points of your outline must be related to the topic you have chosen.

3. Ask your guides: If you are having any difficulty with your research, then do not hesitate to share your difficulty with your guide (if you have one). They will surely help you out and resolve your doubts. If you can't clarify what exactly you require for your work, then ask your supervisor to help you with an alternative. He or she might also provide you with a list of essential readings.

4. Use of computer is recommended: As you are doing research in the field of science frontier then this point is quite obvious. Use right software: Always use good quality software packages. If you are not capable of judging good software, then you can lose the quality of your paper unknowingly. There are various programs available to help you which you can get through the internet.

5. Use the internet for help: An excellent start for your paper is using Google. It is a wondrous search engine, where you can have your doubts resolved. You may also read some answers for the frequent question of how to write your research paper or find a model research paper. You can download books from the internet. If you have all the required books, place importance on reading, selecting, and analyzing the specified information. Then sketch out your research paper. Use big pictures: You may use encyclopedias like Wikipedia to get pictures with the best resolution. At Global Journals, you should strictly follow here.

6. Bookmarks are useful: When you read any book or magazine, you generally use bookmarks, right? It is a good habit which helps to not lose your continuity. You should always use bookmarks while searching on the internet also, which will make your search easier.

7. Revise what you wrote: When you write anything, always read it, summarize it, and then finalize it.

8. Make every effort: Make every effort to mention what you are going to write in your paper. That means always have a good start. Try to mention everything in the introduction—what is the need for a particular research paper. Polish your work with good writing skills and always give an evaluator what he wants. Make backups: When you are going to do any important thing like making a research paper, you should always have backup copies of it either on your computer or on paper. This protects you from losing any portion of your important data.

9. Produce good diagrams of your own: Always try to include good charts or diagrams in your paper to improve quality. Using several unnecessary diagrams will degrade the quality of your paper by creating a hodgepodge. So always try to include diagrams which were made by you to improve the readability of your paper. Use of direct quotes: When you do research relevant to literature, history, or current affairs, then use of quotes becomes essential, but if the study is relevant to science, use of quotes is not preferable.

10. Use proper verb tense: Use proper verb tenses in your paper. Use past tense to present those events that have happened. Use present tense to indicate events that are going on. Use future tense to indicate events that will happen in the future. Use of wrong tenses will confuse the evaluator. Avoid sentences that are incomplete.

11. Pick a good study spot: Always try to pick a spot for your research which is quiet. Not every spot is good for studying.

12. Know what you know: Always try to know what you know by making objectives, otherwise you will be confused and unable to achieve your target.

13. Use good grammar: Always use good grammar and words that will have a positive impact on the evaluator; use of good vocabulary does not mean using tough words which the evaluator has to find in a dictionary. Do not fragment sentences. Eliminate one-word sentences. Do not ever use a big word when a smaller one would suffice.

Verbs have to be in agreement with their subjects. In a research paper, do not start sentences with conjunctions or finish them with prepositions. When writing formally, it is advisable to never split an infinitive because someone will (wrongly) complain. Avoid clichés like a disease. Always shun irritating alliteration. Use language which is simple and straightforward. Put together a neat summary.

14. Arrangement of information: Each section of the main body should start with an opening sentence, and there should be a changeover at the end of the section. Give only valid and powerful arguments for your topic. You may also maintain your arguments with records.

15. Never start at the last minute: Always allow enough time for research work. Leaving everything to the last minute will degrade your paper and spoil your work.

16. Multitasking in research is not good: Doing several things at the same time is a bad habit in the case of research activity. Research is an area where everything has a particular time slot. Divide your research work into parts, and do a particular part in a particular time slot.

17. Never copy others' work: Never copy others' work and give it your name because if the evaluator has seen it anywhere, you will be in trouble. Take proper rest and food: No matter how many hours you spend on your research activity, if you are not taking care of your health, then all your efforts will have been in vain. For quality research, take proper rest and food.

18. Go to seminars: Attend seminars if the topic is relevant to your research area. Utilize all your resources.

19. Refresh your mind after intervals: Try to give your mind a rest by listening to soft music or sleeping in intervals. This will also improve your memory. Acquire colleagues: Always try to acquire colleagues. No matter how sharp you are, if you acquire colleagues, they can give you ideas which will be helpful to your research.

20. Think technically: Always think technically. If anything happens, search for its reasons, benefits, and demerits. Think and then print: When you go to print your paper, check that tables are not split, headings are not detached from their descriptions, and page sequence is maintained.

21. Adding unnecessary information: Do not add unnecessary information like "I have used MS Excel to draw graphs." Irrelevant and inappropriate material is superfluous. Foreign terminology and phrases are not apropos. One should never take a broad view. Analogy is like feathers on a snake. Use words properly, regardless of how others use them. Remove quotations. Puns are for kids, not grunt readers. Never oversimplify: When adding material to your research paper, never go for oversimplification; this will definitely irritate the evaluator. Be specific. Never use rhythmic redundancies. Contractions shouldn't be used in a research paper. Comparisons are as terrible as clichés. Give up ampersands, abbreviations, and so on. Remove commas that are not necessary. Parenthetical words should be between brackets or commas. Understatement is always the best way to put forward earth-shaking thoughts. Give a detailed literary review.

22. Report concluded results: Use concluded results. From raw data, filter the results, and then conclude your studies based on measurements and observations taken. An appropriate number of decimal places should be used. Parenthetical remarks are prohibited here. Proofread carefully at the final stage. At the end, give an outline to your arguments. Spot perspectives of further study of the subject. Justify your conclusion at the bottom sufficiently, which will probably include examples.

23. Upon conclusion: Once you have concluded your research, the next most important step is to present your findings. Presentation is extremely important as it is the definite medium though which your research is going to be in print for the rest of the crowd. Care should be taken to categorize your thoughts well and present them in a logical and neat manner. A good quality research paper format is essential because it serves to highlight your research paper and bring to light all necessary aspects of your research.

Informal Guidelines of Research Paper Writing

Key points to remember:

- Submit all work in its final form.
- Write your paper in the form which is presented in the guidelines using the template.
- Please note the criteria peer reviewers will use for grading the final paper.

Final points:

One purpose of organizing a research paper is to let people interpret your efforts selectively. The journal requires the following sections, submitted in the order listed, with each section starting on a new page:

The introduction: This will be compiled from reference matter and reflect the design processes or outline of basis that directed you to make a study. As you carry out the process of study, the method and process section will be constructed like that. The results segment will show related statistics in nearly sequential order and direct reviewers to similar intellectual paths throughout the data that you gathered to carry out your study.

The discussion section:

This will provide understanding of the data and projections as to the implications of the results. The use of good quality references throughout the paper will give the effort trustworthiness by representing an alertness to prior workings.

Writing a research paper is not an easy job, no matter how trouble-free the actual research or concept. Practice, excellent preparation, and controlled record-keeping are the only means to make straightforward progression.

General style:

Specific editorial column necessities for compliance of a manuscript will always take over from directions in these general guidelines.

To make a paper clear: Adhere to recommended page limits.

Mistakes to avoid:

- Insertion of a title at the foot of a page with subsequent text on the next page.
- Separating a table, chart, or figure—confine each to a single page.
- Submitting a manuscript with pages out of sequence.
- In every section of your document, use standard writing style, including articles ("a" and "the").
- Keep paying attention to the topic of the paper.
- Use paragraphs to split each significant point (excluding the abstract).
- Align the primary line of each section.
- Present your points in sound order.
- Use present tense to report well-accepted matters.
- Use past tense to describe specific results.
- Do not use familiar wording; don't address the reviewer directly. Don't use slang or superlatives.
- Avoid use of extra pictures—include only those figures essential to presenting results.

Title page:

Choose a revealing title. It should be short and include the name(s) and address(es) of all authors. It should not have acronyms or abbreviations or exceed two printed lines.

Abstract: This summary should be two hundred words or less. It should clearly and briefly explain the key findings reported in the manuscript and must have precise statistics. It should not have acronyms or abbreviations. It should be logical in itself. Do not cite references at this point.

An abstract is a brief, distinct paragraph summary of finished work or work in development. In a minute or less, a reviewer can be taught the foundation behind the study, common approaches to the problem, relevant results, and significant conclusions or new questions.

Write your summary when your paper is completed because how can you write the summary of anything which is not yet written? Wealth of terminology is very essential in abstract. Use comprehensive sentences, and do not sacrifice readability for brevity; you can maintain it succinctly by phrasing sentences so that they provide more than a lone rationale. The author can at this moment go straight to shortening the outcome. Sum up the study with the subsequent elements in any summary. Try to limit the initial two items to no more than one line each.

Reason for writing the article—theory, overall issue, purpose.

- Fundamental goal.
- To-the-point depiction of the research.
- Consequences, including definite statistics—if the consequences are quantitative in nature, account for this; results of any numerical analysis should be reported. Significant conclusions or questions that emerge from the research.

Approach:

- Single section and succinct.
- An outline of the job done is always written in past tense.
- Concentrate on shortening results—limit background information to a verdict or two.
- Exact spelling, clarity of sentences and phrases, and appropriate reporting of quantities (proper units, important statistics) are just as significant in an abstract as they are anywhere else.

Introduction:

The introduction should "introduce" the manuscript. The reviewer should be presented with sufficient background information to be capable of comprehending and calculating the purpose of your study without having to refer to other works. The basis for the study should be offered. Give the most important references, but avoid making a comprehensive appraisal of the topic. Describe the problem visibly. If the problem is not acknowledged in a logical, reasonable way, the reviewer will give no attention to your results. Speak in common terms about techniques used to explain the problem, if needed, but do not present any particulars about the protocols here.

The following approach can create a valuable beginning:

- Explain the value (significance) of the study.
- Defend the model—why did you employ this particular system or method? What is its compensation? Remark upon its appropriateness from an abstract point of view as well as pointing out sensible reasons for using it.
- Present a justification. State your particular theory(-ies) or aim(s), and describe the logic that led you to choose them.
- Briefly explain the study's tentative purpose and how it meets the declared objectives.

Approach:

Use past tense except for when referring to recognized facts. After all, the manuscript will be submitted after the entire job is done. Sort out your thoughts; manufacture one key point for every section. If you make the four points listed above, you will need at least four paragraphs. Present surrounding information only when it is necessary to support a situation. The reviewer does not desire to read everything you know about a topic. Shape the theory specifically—do not take a broad view.

As always, give awareness to spelling, simplicity, and correctness of sentences and phrases.

Procedures (methods and materials):

This part is supposed to be the easiest to carve if you have good skills. A soundly written procedures segment allows a capable scientist to replicate your results. Present precise information about your supplies. The suppliers and clarity of reagents can be helpful bits of information. Present methods in sequential order, but linked methodologies can be grouped as a segment. Be concise when relating the protocols. Attempt to give the least amount of information that would permit another capable scientist to replicate your outcome, but be cautious that vital information is integrated. The use of subheadings is suggested and ought to be synchronized with the results section.

When a technique is used that has been well-described in another section, mention the specific item describing the way, but draw the basic principle while stating the situation. The purpose is to show all particular resources and broad procedures so that another person may use some or all of the methods in one more study or referee the scientific value of your work. It is not to be a step-by-step report of the whole thing you did, nor is a methods section a set of orders.

Materials:

Materials may be reported in part of a section or else they may be recognized along with your measures.

Methods:

- Report the method and not the particulars of each process that engaged the same methodology.
- Describe the method entirely.
- To be succinct, present methods under headings dedicated to specific dealings or groups of measures.
- Simplify—detail how procedures were completed, not how they were performed on a particular day.
- If well-known procedures were used, account for the procedure by name, possibly with a reference, and that's all.

Approach:

It is embarrassing to use vigorous voice when documenting methods without using first person, which would focus the reviewer's interest on the researcher rather than the job. As a result, when writing up the methods, most authors use third person passive voice.

Use standard style in this and every other part of the paper—avoid familiar lists, and use full sentences.

What to keep away from:

- Resources and methods are not a set of information.
- Skip all descriptive information and surroundings—save it for the argument.
- Leave out information that is immaterial to a third party.

Results:

The principle of a results segment is to present and demonstrate your conclusion. Create this part as entirely objective details of the outcome, and save all understanding for the discussion.

The page length of this segment is set by the sum and types of data to be reported. Use statistics and tables, if suitable, to present consequences most efficiently.

You must clearly differentiate material which would usually be incorporated in a study editorial from any unprocessed data or additional appendix matter that would not be available. In fact, such matters should not be submitted at all except if requested by the instructor.

Content:

- Sum up your conclusions in text and demonstrate them, if suitable, with figures and tables.
- In the manuscript, explain each of your consequences, and point the reader to remarks that are most appropriate.
- Present a background, such as by describing the question that was addressed by creation of an exacting study.
- Explain results of control experiments and give remarks that are not accessible in a prescribed figure or table, if appropriate.
- Examine your data, then prepare the analyzed (transformed) data in the form of a figure (graph), table, or manuscript.

What to stay away from:

- Do not discuss or infer your outcome, report surrounding information, or try to explain anything.
- Do not include raw data or intermediate calculations in a research manuscript.
- Do not present similar data more than once.
- A manuscript should complement any figures or tables, not duplicate information.
- Never confuse figures with tables—there is a difference.

Approach:

As always, use past tense when you submit your results, and put the whole thing in a reasonable order.

Put figures and tables, appropriately numbered, in order at the end of the report.

If you desire, you may place your figures and tables properly within the text of your results section.

Figures and tables:

If you put figures and tables at the end of some details, make certain that they are visibly distinguished from any attached appendix materials, such as raw facts. Whatever the position, each table must be titled, numbered one after the other, and include a heading. All figures and tables must be divided from the text.

Discussion:

The discussion is expected to be the trickiest segment to write. A lot of papers submitted to the journal are discarded based on problems with the discussion. There is no rule for how long an argument should be.

Position your understanding of the outcome visibly to lead the reviewer through your conclusions, and then finish the paper with a summing up of the implications of the study. The purpose here is to offer an understanding of your results and support all of your conclusions, using facts from your research and generally accepted information, if suitable. The implication of results should be fully described.

Infer your data in the conversation in suitable depth. This means that when you clarify an observable fact, you must explain mechanisms that may account for the observation. If your results vary from your prospect, make clear why that may have happened. If your results agree, then explain the theory that the proof supported. It is never suitable to just state that the data approved the prospect, and let it drop at that. Make a decision as to whether each premise is supported or discarded or if you cannot make a conclusion with assurance. Do not just dismiss a study or part of a study as "uncertain."

Research papers are not acknowledged if the work is imperfect. Draw what conclusions you can based upon the results that you have, and take care of the study as a finished work.

- You may propose future guidelines, such as how an experiment might be personalized to accomplish a new idea.
- Give details of all of your remarks as much as possible, focusing on mechanisms.
- Make a decision as to whether the tentative design sufficiently addressed the theory and whether or not it was correctly restricted. Try to present substitute explanations if they are sensible alternatives.
- One piece of research will not counter an overall question, so maintain the large picture in mind. Where do you go next? The best studies unlock new avenues of study. What questions remain?
- Recommendations for detailed papers will offer supplementary suggestions.

Approach:

When you refer to information, differentiate data generated by your own studies from other available information. Present work done by specific persons (including you) in past tense.

Describe generally acknowledged facts and main beliefs in present tense.

The Administration Rules

Administration Rules to Be Strictly Followed before Submitting Your Research Paper to Global Journals Inc.

Please read the following rules and regulations carefully before submitting your research paper to Global Journals Inc. to avoid rejection.

Segment draft and final research paper: You have to strictly follow the template of a research paper, failing which your paper may get rejected. You are expected to write each part of the paper wholly on your own. The peer reviewers need to identify your own perspective of the concepts in your own terms. Please do not extract straight from any other source, and do not rephrase someone else's analysis. Do not allow anyone else to proofread your manuscript.

Written material: You may discuss this with your guides and key sources. Do not copy anyone else's paper, even if this is only imitation, otherwise it will be rejected on the grounds of plagiarism, which is illegal. Various methods to avoid plagiarism are strictly applied by us to every paper, and, if found guilty, you may be blacklisted, which could affect your career adversely. To guard yourself and others from possible illegal use, please do not permit anyone to use or even read your paper and file.

Criterion for Grading a Research Paper (Compilation) by Global Journals

Please note that following table is only a Grading of "Paper Compilation" and not on "Performed/Stated Research" whose grading solely depends on Individual Assigned Peer Reviewer and Editorial Board Member. These can be available only on request and after decision of Paper. This report will be the property of Global Journals.

Topics	Grades		
	A-B	**C-D**	**E-F**
Abstract	Clear and concise with appropriate content, Correct format. 200 words or below	Unclear summary and no specific data, Incorrect form Above 200 words	No specific data with ambiguous information Above 250 words
Introduction	Containing all background details with clear goal and appropriate details, flow specification, no grammar and spelling mistake, well organized sentence and paragraph, reference cited	Unclear and confusing data, appropriate format, grammar and spelling errors with unorganized matter	Out of place depth and content, hazy format
Methods and Procedures	Clear and to the point with well arranged paragraph, precision and accuracy of facts and figures, well organized subheads	Difficult to comprehend with embarrassed text, too much explanation but completed	Incorrect and unorganized structure with hazy meaning
Result	Well organized, Clear and specific, Correct units with precision, correct data, well structuring of paragraph, no grammar and spelling mistake	Complete and embarrassed text, difficult to comprehend	Irregular format with wrong facts and figures
Discussion	Well organized, meaningful specification, sound conclusion, logical and concise explanation, highly structured paragraph reference cited	Wordy, unclear conclusion, spurious	Conclusion is not cited, unorganized, difficult to comprehend
References	Complete and correct format, well organized	Beside the point, Incomplete	Wrong format and structuring

Index

Global Journal of Science Frontier Research

Visit us on the Web at www.GlobalJournals.org | www.JournalofScience.org
or email us at helpdesk@globaljournals.org

ISSN 9755896